

# Applications of Machine Learning in Real-time Brain Tissue Strain Estimation

A Dissertation  
Submitted to the Faculty of  
WORCESTER POLYTECHNIC INSTITUTE  
In Partial Fulfillment of the Requirements for the Degree of  
DOCTOR OF PHILOSOPHY  
in Biomedical Engineering

Summer 2021

By

Kianoosh Ghazi

Approved by:

---

Songbai Ji

Professor, Advisor  
Biomedical Engineering, Mechanical  
Engineering  
Worcester Polytechnic Institute

---

Karen Troy

Professor  
Biomedical Engineering, Mechanical  
Engineering  
Worcester Polytechnic Institute

---

Dirk Albrecht

Associate Professor  
Biomedical Engineering, Biology and  
Bio technology  
Worcester Polytechnic Institute

---

Nima Rahbar

Associate Professor  
Civil and Environmental Engineering,  
Mechanical Engineering  
Worcester Polytechnic Institute

---

Steve Rowson

Associate Professor  
Biomedical Engineering and Mechanics  
Virginia Polytechnic Institute and State  
University (Virginia Tech)

## **Acknowledgements:**

Thank you to my wonderful advisor, Dr. Songbai Ji for your mentorship over the past four years. I am grateful for the opportunity to work alongside you on this project, and for your continuous support and guidance, encouragement and patience. Working with you has been an experience that taught me independence and resilience and I appreciate your hard work in helping me learn and succeed. I would also like to thank the members of my dissertation committee, Dr. Karen Troy, Dr. Dirk Albrecht, Dr. Nima Rahbar, and Dr. Steve Rowson for their insight in developing this dissertation.

I would like to thank all past and present members of Ji Lab. Especially I am grateful to Wei Zhao for his generous guidance and help along the way and Shaoju Wu for sharing his insight and knowledge. Working alongside you has been instructive and encouraging and I am grateful to be teammates and friends with you.

Further, I thank the WPI faculty for their role as role models and support for students. I am particularly thankful to Dr. Marsha Rolle for her help and guidance during my time as a Ph.D. student.

I want to thank Megan Chrobak for her mentorship during my internship. Thank you for your patience and being an exemplar. I learned so much from you and I am grateful to you.

I am thankful to all WPI graduate students whose friendship and company made this experience all the more enjoyable. Particularly I am thankful to Elizabeth English and Kate Mistretta for their friendship.

Lastly, I would like to thank my wonderful friends, especially Sam Bagheri, Hooman Pilevar Abrisham, and Aria Masoomi. A special thank you to my wonderful mother Marjan Mollabeirami, for her endless love and support for me. This would not be possible without you.

# Table of Contents

## Contents

Table of Contents.....	3
Table of Figures .....	8
Table of Tables .....	15
Abstract.....	17
Chapter 2: Background .....	22
Clinical Significance.....	22
Methods of diagnosis.....	23
Symptomatic diagnosis .....	23
Kinematic metrics.....	24
Finite Element.....	27
Worcester Head Injury Model (WHIM) .....	39
WHIM Model Validation .....	40
Limitations of FE head models .....	41
Mapping to other simpler functions .....	42
Pre-Computed Brain Response Atlas (pcBRA) .....	42
Use of Machine Learning in conjunction with pre-computation .....	44
Machine Learning Background.....	45

Alternative Approaches to FE modeling.....	53
Roadmap.....	53
Chapter 3: Converting a head injury model implemented in Abaqus into LS-DYNA for impact simulation.....	56
Introduction .....	56
Methods .....	57
Results .....	59
Discussion and Conclusion.....	61
Chapter 4: Aim 1: Assessment of a CNN based approach to obtain real-time element-wise strain prediction for the entire brain directly from impact profile .....	64
Introduction .....	64
Methods .....	68
CNN Training Data.....	68
CNN Architecture .....	69
CNN Estimation Performance .....	71
Injury Prediction .....	72
Data Analysis .....	74
Results .....	74
Discussion.....	78
Potential Applications.....	79
Limitations and further developments.....	80

CNN architecture and estimation performance.....	82
Conclusion.....	85
Acknowledgments.....	86
Funding Information.....	86
Chapter 5: Aim 2: Feasibility assessment of the functionality of simplified “effective kinematics” to map complex profiles to equivalent simple profiles while maintaining brain strain map. ....	87
Introduction.....	87
Methods.....	91
Workflow Overview.....	91
Impact dataset.....	92
Strain responses from idealized impacts in a pcBRA.....	92
Effective peak rotational velocity magnitude to preserve peak MPS.....	94
Effective kinematic triplets to preserve elementwise MPS.....	95
CNN model to derive effective impact kinematics directly.....	97
Data Analysis:.....	99
Results.....	100
Effective peak rotational velocity magnitudes about the three anatomical axes.....	100
Effective kinematic triplets to preserve elementwise MPS.....	103
Discussion.....	105
Effective peak rotational velocity magnitude to preserve peak MPS.....	106

Effective peak rotational velocity magnitude to preserve elementwise MPS.....	107
Idealized head impact mode .....	110
Limitations .....	110
Acknowledgements: .....	111
Chapter 6: Aim 3: Football helmet comparison based on strain-based and kinematics-based metrics .....	112
Introduction .....	112
Methodology.....	116
Roadmap .....	116
STAR Methodology and Helmet Impact Database .....	118
Instantaneous brain strain estimation using a CNN-based brain injury model .....	121
Range of helmet injury mitigation capabilities using brain strain.....	121
Statistical Analysis .....	123
Results .....	124
CNN Performance in Brain Strain Generation .....	124
Comparison between CNN and simulation in injury metrics .....	124
Strain-based uncertainty in helmet concussion mitigation capability.....	125
Investigation of Significance of Impact Directionality in Helmet Injury Mitigation	
Performance using an Impact location-based comparison .....	126
Discussion.....	128
Disparities between strain-based helmet safety performances.....	129

Potential of CNN to facilitate helmet testing and iterative design.....	130
Limitations .....	131
Conclusion .....	133
Chapter 7: Conclusions and future directions.....	134
Chapter 8: References.....	141

# Table of Figures

**Figure 1:** Worcester Head Injury Model (WHIM) mesh and anatomical regions (a and b). (c) Shows the injury relevant deep white matter regions of the brain and (d) shows the white matter fibers in the model.....40

**Figure 2:** (a) Example of an idealized 3DOF impact rotational velocity profile; (b) the corresponding kinematics triplet ( $v_{rotp}$ ,  $\theta$ ,  $\alpha$ ) is represented by a vector emanating from the head center of gravity characterizing the impact kinematic magnitude and directionality in the WHIM coordinate system. For a given impact severity (denoted by rotational velocity peak:  $v_{rotp}$ ), traversing the end point of the vector in space would generate a hemisphere shown in (c). In the middle hemisphere, the discretized ( $\theta$ ,  $\alpha$ ) pairs are also shown as grid on the hemisphere. ....43

**Figure 3:** Schematic Representation of a fully connected artificial neural network with 3 input values, four hidden neurons, and one output. The weights of each connection as well as the biases for each node are shown in  $w$  and  $b$  respectively. The values of each neuron is based on all the preceding neurons *via* the internally optimized weights and biases. ....49

**Figure 4:** An illustration of the use of fully connected neural networks. An illustrative 4 channel signal is “flattened” before being fed into the network. The data “flattening” necessary in the pre-processing neglects the temporal relationship between the signals.....52

**Figure 5:** A flowchart of the aims in this dissertation. Aim1 focuses on developing an alternative to FE modeling to improve efficiency. Aim 2 addresses the gap between kinematics metrics and FE modeling by proposing a strain-driven kinematics (Effective Kinematics). Aim 3 is a real-world application of the aim 1 where a number of helmets are compared in terms of strains and

the Summation of Tests for the Analysis of Risk (STAR) to provide context about the implications of using strain in helmet injury mitigation capabilities.....55

**Figure 6:** Cumulative maximum principal strain from C3D8I with an anisotropic material model (a), C3D8R with anisotropic material and high SFs (b), optimized isotropic material with GM/WM heterogeneity using C3D8R and high SFs (c), and same isotropic materials converted into LS-DYNA (d). .....62

**Figure 7:** Histograms of peak resultant rotational velocity (a; vrot) and acceleration (b; arot) for the entire training sample (n = 5661). The real-world impacts are overlaid. Regions between the two vertical lines are considered “in range.” The starred cases are explained in more detail in **Fig. 10**. The blue bars are a subset of the database we used as independent validation data (scaled by 10 for visibility). This process is detailed in the following sections. ....69

**Figure 8:** Flow chart showing preprocessing of a head impact kinematic profile (top) and an empirically optimized convolutional neural network (CNN) architecture (bottom) to predict the distribution of peak maximum principal strain (MPS) of the entire brain. The preprocessed vrot profile (after transforming to its “conjugate rotational axis,” and if needed, shifting, and padding (Wu, Zhao, Ghazi, *et al.*, 2019)) is combined with the corresponding pre-processed and scaled arot profile (effectively, with a unit of 100 rad/sec<sup>2</sup> after scaling). The resulting two-dimensional [2D] image representation serves as the CNN input.....71

**Figure 9:** Histograms of peak resultant rotational velocity (a; vrot) and acceleration (b; arot) for a subset of data (n = 3064) used to train and test on an independent National Football League (NFL) data set (n = 53), which is overlaid (number of occurrences multiplied by 10 to improve visualization). .....73

**Figure 10:** Summary of k and r when comparing convolutional neural network (CNN)-estimated and directly simulated maximum principal strain (MPS) distributions using a 10-fold cross-

validation, using either the entire (a) or a subset of (b) the impact data set focusing on “in-range” impacts (after removing “outliers”). The shaded area represents impact cases of sufficient accuracy (i.e.,  $0.9 < k < 1.1$  and  $r > 0.9$ ). The k and r axes are capped to improve visualization. The identified four cases in (a) are further illustrated in **Fig. 10**.....75

**Figure 11:** Representative impact cases showing impact vrot and arot profiles with the convolutional neural network (CNN)-estimated (eest) and directly simulated (esim) maximum principal strain (MPS) distributions for a successful prediction (a) or “failed” cases resulting from (1) out-of-range vrot peak magnitude (b); (2) out-of-range arot peak magnitude together with a large initial vrot value (c); and (3) a large initial vrot value (d). The four cases correspond to cases 1–4 identified in **Fig. 6**. .....76

**Figure 12:** Summary of k and r for convolutional neural network (CNN)-estimated ( $\epsilon_{est}$ ) and directly simulated ( $\epsilon_{sim}$ ) maximum principal strain (MPS) distribution for an independent National Football League (NFL) impact data set (a; shaded area represents impacts of sufficient estimation accuracy, i.e.,  $0.9 < k < 1.1$  and  $r > 0.9$ ). Three representative impacts are selected to show a successful estimation (b; purposefully chosen to represent an r toward the threshold value for success) and two “failed” cases (c and d). The latter two cases only failed “marginally”; that is, their corresponding k and r were rather close to their success threshold values. ....77

**Figure 13:** Comparison of estimation performance using the previous convolutional neural network (CNN) architecture (a; with the size of the last output layer changed to 55 k to match the number of brain elements for response prediction<sup>39</sup>) and the one updated in this study (b). Their convergence behaviors in terms of root mean squared error (RMSE) between the two distributions versus epochs are also compared (c). All performance measures reported here are

based on the previous impact data set ( $n = 3069$ ) using  $v_{rot}$  profiles alone as CNN input, without the addition of  $a_{rot}$  profiles. ....84

**Figure 14:** Illustration of a National Football League (NFL) concussive head impact (a; Case125HD0243) and another head impact from the HF data set (b; no injury diagnosis available). Even though their  $v_{rot}$  peak magnitudes are significantly larger than the targeted range (61.4 rad/sec and 78.4 rad/sec, respectively, vs. 40 rad/sec as the upper bound of the targeted range; corresponding to the two cases identified in **Fig. 6a**), the convolutional neural network (CNN)-estimated strains were sufficiently accurate. Note, strain in (a) is higher than that in (b), even though its  $v_{rot}$  peak magnitude is lower, because of its significant deceleration, which is lacking in the recorded profile in (b). ....85

**Figure 15:** Flowchart of the study to translate an arbitrary head impact into effective impact kinematics to preserve either peak MPS or spatially detailed MPS. Elementwise MPS of the brain for an arbitrary head impact is first obtained and compared with the pcBRA library to identify an idealized impact. With a CNN, this process is automated without the need for actual costly impact simulation. pcBRA: pre-computed brain response atlas. ....91

**Figure 16:** (a) Example of an idealized three-degree-of-freedom (3DOF) impact rotational velocity profile; (b) the corresponding kinematics triplets ( $v_{rotp}, \theta, \alpha$ ) represented by a vector emanating from the head center of gravity to characterize the peak velocity magnitude and directionality in the WHIM coordinate system. For a given  $v_{rotp}$ , traversing the vector end point in space would generate a hemisphere shown in (c). In the middle hemisphere, the discretized ( $\theta, \alpha$ ) pairs are also shown as grid on the hemisphere. ....93

**Figure 17:** (a) Histogram distribution of peak MPS for the  $N=3069$  impacts. (b) Peak MPS values corresponding to the same anatomical axis from the pcBRA are grouped to fit a constrained third order polynomial. The MPS of each impact is used to identify the

corresponding  $vrot_x$ ,  $vrot_y$ ,  $vrot_z$  along the three anatomical axes. The two dashed lines on the far right show the extent of  $vrot_p$  extrapolation range deemed of sufficient accuracy. For the same  $vrot_p$ , an axial rotation produces a considerably higher MPS than a coronal or a sagittal rotation. The red line shows an unsuccessful case that did not coincide with the X and Y polynomials within the allowed margin for extrapolation. ....95

**Figure 18:** (a) Illustration to identify nearest neighbors in the pcBRA parametric space for an arbitrary head impact based on brain strain. The rotational axis is weight averaged and then fixed to interpolate a number of brain strains for a range of  $vrot_p$  values based on the pcBRA. Their corresponding  $k$  values as regressed against simulated elementwise MPS for a given impact are used to generate a constrained third order polynomial fitting (b). The effective  $vrot_p$  is finally determined by intersecting a horizontal line with  $k$  of 1.0. ....97

**Figure 19:** The CNN architecture used in this study, which shares the architecture with the one in aim 1 with the exception of the final layer. ....98

**Figure 20:** (a) shows the definition of angular and magnitude errors. Angular error is represented by  $\beta$ . ....99

**Figure 21:** A scatterplot between the peak MPS and peak effective rotational velocity and the nominal counterparts are shown along X, Y, and Z ((a) through (c)). Comparison between effective and nominal peak rotational velocity and acceleration along the x, y, and z axis (coronal, sagittal, and axial directions, respectively, as defined in Fig. 15) in ((d) through (f)) and ((g) through (i)).....102

**Figure 22:** (Left) shows the scatterplot of CNN prediction of effective peak rotational velocity magnitude against the label counterpart for all three axes. (Right) shows the scatterplot of CNN predictions translated to MPS compared against the ground-truth MPS.....103

**Figure 23:** (a) Summary of element-wise Pearson correlation coefficient ( $r$ ) with the most similar idealized impact in the pcBRA database when the linear regression slope ( $k$ ) was forced to be 1.0 by adjusting the effective  $vrot_p$  (those with  $r > 0.9$  were considered “successfully matched”). (b) a comparison of effective  $vrot_p$  and the nominal counterparts for the successfully matched impacts; (c) and (d) illustration of example cases showing their actual and idealized impact profiles, together with the corresponding elementwise MPS.....104

**Figure 24:** The histograms of error in terms of “angular” and “ $V_{rot}$  percentage magnitude” errors respectively using a 10-fold cross validation. The relative error in (a) is the percentage of the absolute magnitude error. The unsuccessful impacts are shown in red. For clarity, data points outside the shown range on the subfigure on the left were shown on the border.....105

**Figure 25:** An example of a biphasic impact in pcBRA format. The CNN from aim 1 is fully capable of predicting the strain distribution for this impact. ....109

**Figure 26:** A flowchart of the current study. Firstly we obtain the brain strain patterns from the CNN in aim 1 (Ghazi *et al.*, 2020). Based on the strain pattern, we calculate the injury metrics (peak MPS and CSDM). Using the collected injury metrics we run two experiments to answer the questions of this study.....116

**Figure 27:** The distribution of the peak linear (first row) and rotational (second row) accelerations as well as the peak rotational velocity (third row) of the STAR test dataset used in this study. The dashed lines show the data range that the CNN in aim 1 was trained on (an acceleration range of 793 to 6313  $\text{rad/s}^2$  and a velocity range of 2 to 40  $\text{rad/s}$ ).....119

**Figure 28:** An illustration of the voxel-wise comparison between the strain distribution obtained from FE simulations and the CNN estimations. (a) illustrates the performance in terms of  $k$  and  $r$  between the CNN estimation and corresponding simulations. (b) and (c) illustrate two example cases of the CNN predictions.....124

**Figure 29:** A scatter plot of the peak MPS (left) and CSDM (right) between each simulations and the corresponding CNN prediction. ....125

**Figure 30:** (a) shows the number of concussions between the best and the worst helmet based on each threshold value and regardless of helmet. The shaded area between the two curves shows the difference between the best and the worst helmet given each threshold. (b) Illustrates the same properties for CSDM. In both figures, the red and blue line illustrate the helmets ranked the poorest among all helmets. The dashed line in both sub-figures represents the injury mitigation difference between the best and the worst helmet in each threshold value. ....126

**Figure 33:** Box plot of the peak MPS (top) and CSDM (bottom) across helmets in each scenario. Helmets V and W (shown in green and yellow respectively) had the lowest STAR score yet performed average in terms of strain metrics. Helmet M (shown in red) generated large strains in the front boss direction, but perform close to the average in other directions.  $\tau$  denotes the kendall's tau value between the ranking in each scenario and the STAR ranking of the helmets. ....127

**Figure 34:** An illustration of the strain pattern difference between two impacts that have a low correlation. These two cases belong to the impact condition with  $\theta = 90^\circ$  and the Front Boss impact location, and the helmets O and P ("Schutt F7 LTD" and "Schutt F7" corresponding to the left and right figure respectively).....130

## Table of Tables

<b>Table 1:</b> A general overview of the symptoms of concussion on a group-wise basis. ....	23
<b>Table 2:</b> A summary of selected head injury models and their characteristics (Giudice <i>et al.</i> , 2019). ....	28
<b>Table 3:</b> Summary of the discretizing variables, their ranges, step sizes, and number of samples for the idealized head impact rotational profiles used to establish the pcBRA. Peak rotational acceleration ( <i>arotp</i> ) and peak rotational velocity ( <i>vrotp</i> ) are equivalent when the impulse duration, $\Delta t$ is constant. ....	43
<b>Table 4:</b> Summary of six simulation steps to convert the baseline WHIM using anisotropic brain material properties in Abaqus into LS-DYNA counterpart with isotropic properties. ....	58
<b>Table 5:</b> Summary of the results from the experiments. ....	60
<b>Table 6:</b> The number and the depth of trees, (N, D), used in RF depended on whether RF was used for feature selection (FS) or classification (CL), as shown below. ....	74
<b>Table 7:</b> Summary of injury prediction performances in terms of accuracy, sensitivity, specificity and AUC using CNN-estimated (“CNN”) or directly simulated (“WHIM”) MPS distributions. Injuries are predicted using either SVM or RF with feature selection (specified in parenthesis) based on either F-score or RF “gini” importance ranking (Cai <i>et al.</i> , 2018). For comparison, baseline performances using peak MPS of the whole brain and logistic regression are also reported. All performances are evaluated <i>via</i> leave-one-out cross-validation for objective comparison. Using RF either for injury prediction or feature selection, 50 trials are used to account for the random initialization. Performances that are higher than the baseline are in bold ( $p < 0.05$ ; where appropriate). ....	77

**Table 8:** The helmets used for this aim. The starred (\*) helmets were randomly selected for direct simulations. ....117

**Table 9:** The exposures corresponding to each impact location and pendulum angle ( $\theta$ ) corresponding to the comparative likelihood of a representative impact being sustained (Virginia Tech Helmet Lab, 2020).....120

## Abstract

Mild Traumatic Brain Injury is a major health concern in the United States and around the world and is especially common in contact sports and is difficult to reliably diagnose as it is often diagnosed in a symptom-based fashion. This is problematic since the symptoms may take time to develop and the recognition of the symptoms could introduce some subjective bias. In addition, athletes are less likely to recognize, appreciate the significance of, or disclose symptoms in a competitive atmosphere such as that of contact sports. This is a contributing factor to the difficulty of diagnosis. Undiagnosed mTBI can cause more serious health complications such as neurodegenerative diseases. Hence, there is a significant need to reliably predict the risk of concussion, and prevent concussion using preventative equipment. One method that holds a great potential for such scenarios is FE modeling. Yet FE models are computationally expensive, making them infeasible in a side-line scenario. As a result there has been a recent shift to pre-computation based techniques to bypass the time consuming FE simulations. Yet, referring to the pre-simulated database to exploit the full potential of such methods is a challenge as a result of the complex nature of impact profiles. Here, we addressed this challenge by using deep learning based approaches, which are well-suited for modeling such complex scenarios with constant boundary conditions.

Here, we first identified a gap in the literature about the implications of the used software packages for FE simulation as a potential point of discrepancy in FE based TBI research. Hence, we established a bridge between Abaqus and LS-DYNA, which are two of the most widely-used software platforms currently used in FE modeling. We identified the differences between the two packages along the way to convert our Worcester Head Injury Model with material anisotropy, which was originally developed in Abaqus, into LS-DYNA format. We used the most reliable element type in Abaqus (C3D8I) as a benchmark, converted the WHIM with

C3D8I elements through a series of steps into an isotropic version with C3D8R elements that could be directly translated into LS-DYNA format, and translated the model into LS-DYNA format without any alterations. Then we compared the model with all the appropriate LS-DYNA model configurations to the Abaqus model. Then we identified the LS-DYNA configurations that perform the most similarly with Abaqus hence establishing a bridge between the two.

Further in the aims sections, with the assumption of limited time and computational power, we bridged the gap between FE based TBI research and utilization of such methods in real-world scenarios. We developed and assessed different machine learning based approaches with the goal of making different aspects of FE based injury assessment real-time. In the first aim, using a deep learning approach, we bypass FE based model simulations entirely and obtain the entire brain strain pattern directly from the impact profile. In the second aim, we developed a new, strain-based injury metric using an inverse approach to map brain strains into a simple kinematic profile. The advantage of this approach is that unlike all other available kinematic based injury metrics, it accounts for impact directionality. Finally in the third aim, we use our developed methods in a real-world scenario by investigating the effectiveness of a number of helmets based on the generated strains in the brain.

## Chapter 1: Introduction

With an estimated annual impact of 1.6 to 3.8 million cases, sports-related concussion or mild Traumatic Brain Injury (mTBI) is considered a major public health concern in the United States (Faul *et al.*, 2004). TBIs are often ignored by the athlete or under- or undiagnosed. Yet, late or lack of diagnosis of mTBI may lead to repetitive concussions, causing permanent neurocognitive impairment (Zhao and Ji, 2015). So, there is a need for a reliable method of TBI diagnosis on sports field.

Numerous statistically driven injury metrics were proposed to assess the risk of injury based on impact kinematic profile. Nevertheless, these metrics do not provide consistent injury predictions (Zhao and Ji, 2015). This may be because they are not directly based on brain tissue level mechanical responses which are thought to cause injury (Zhao, Kuo, *et al.*, 2017b). To address this shortcoming, Finite Element (FE) models play a significant role in providing the tissue level mechanical response (e.g. strain) which are otherwise difficult to measure in live human brain. Other methods to obtain such results include MR imaging, which is infeasible for on-field sports applications.

A significant barrier in the way of applying FE modeling in real world is its high computational cost, which makes it inapplicable for an on-field scenario. Hence, a methodology is needed to make the results from FE modeling, which requires high computational power, readily available for on field applications with limited computational capability (Zhao, Kuo, *et al.*, 2017b).

To address this problem, here we develop methodologies to provide real-time insight into brain tissue strains, strain-based injury metrics and the potential applications. These methodologies can help to assess concussion risk in real-time and reliably to avoid subsequent concussions and prevent injury aggravation. They can further be used to provide a tissue level

understanding on the effectiveness of injury mitigation equipment. This study aims to require minimal computational cost to be applicable with limited equipment. The achievement from this research bridges the gap between FE modeling of the brain and its on-field application to utilize the theoretical achievements of the computational brain models in real-world applications.

To that end we take advantage of the efficiency and versatility of machine learning methods to provide real-time methodologies for predicting brain tissue response and other injury metrics for any given impact collected from contact sports. This data will provide valuable information for assessment of injury risk on sports field as well as that of safety equipment in mitigating injury risk. The mentioned applications will be implemented by taking advantage of a number of simulated real-world sports impacts to train Convolutional Neural Networks (CNN) and subsequently using them in different contexts. We use our Worcester Head Injury FE model (WHIM) for this study, which has been verified extensively against cadaver and in-vivo relative brain-skull displacement as well as strain data, for all simulations.

**AIM 1: Assessment of a CNN based approach to obtain real-time element-wise strain prediction for the entire brain directly from impact profile.** Our first aim is to predict the cumulative MPS for the entire brain elements in our WHIM based on real-world simulated data using a Convolutional Neural Network (CNN). This aim is based on our previous study that took the same approach to obtain the peak MPS proved to perform very well ( $R^2 = 0.966$  when comparing predicted to the ground truth of simulated peak MPS (Wu, Zhao, Ghazi, *et al.*, 2019)).

**AIM 2: Feasibility assessment of the functionality of simplified “effective kinematics” to map complex profiles to equivalent simple profiles while maintaining brain strain map.** This aim matches MPS distribution pattern of a database of real-world impacts to a well-established “dictionary” of pre-simulated head impacts with simple impact profiles in a way that

maintains the brain MPS pattern. Then we train a CNN to predict the simplified profile given the real-world profile. The value of this approach, in our opinion, is that it translates complex real-world impacts into simple and intuitively understandable and comparable profiles based on the brain strains with minimal sacrifice in accuracy.

**AIM 3: Football helmet comparison based on strain-based and kinematics-based metrics.**

We use the CNN based approach from aim 1 to investigate the injury mitigation performance of a number of helmets based on brain tissue strain distribution and other commonly used FE based injury metrics. Most of the helmets in this aim are identically scored with the commercially used STAR rating system, which is a well-established rating system for helmet performance (Rowson and Duma, 2011).

## Chapter 2: Background

### Clinical Significance

With an estimated annual impact of between 1.6 and 3.8 million people, sports-related concussions, or mild traumatic brain injury (mTBI), is considered to be a major public health and socio-economic concern in the United States (Faul *et al.*, 2004). A large number of annual concussions occur in football and ice hockey (Thomas R. Frieden, Debra Houry, 2015).

The pathology as well as an exact definition of concussion is still being investigated. However, the current consensus is the fact that concussion is a pathophysiologic response of the brain to biomechanical forces that is functional rather than structural (Kutcher and Giza, 2014).

Given the potentially devastating effects of concussion, especially in contact sports, there has been an increasing focus on understanding the significance of concussion in the past 20-30 years. One of the earliest efforts was the publication of the first practice parameter document on sports concussion in 1997 by the American Academy of Neurology (AAN) (*American Academy of Neurology Report of the Quality Standards Subcommittee, Practice Parameter: The management of concussion in sports. Neurology*, 1997). This was a response to the surveillance of athletes revealing evidence of the potential long term effects of mTBI. Further, there was aggregating concerns over the dire consequences of repetitive head impacts that could cause serious health complications such as chronic traumatic encephalopathy (CTE), which is still an active area of research (Kutcher and Giza, 2014).

Yet, in an athletic atmosphere it is frequently under- or undiagnosed because the signs of cognitive changes may be unclear, masked, or unrecognized/ ignored by the athlete (McCrea *et al.*, 2004). Further, based upon the fact that diagnosis of concussion is frequently performed

based upon the symptoms, instant diagnosis of concussion is sometimes not possible, as the pathology that makes concussion diagnosis possible may take several hours to take place (Kutcher and Giza, 2014). This highlights the significance of predictive metrics in an on-field setting. Misdiagnosis of concussion could put the athlete at risk of sustaining subsequent impacts, if they were to return to the sports field after injury. Sustaining subsequent impacts to the head after concussion leads to permanent neurocognitive and neurophysiological impairments such as CTE (Kutcher and Giza, 2014). In addition, the athletes who sustain a first concussive impact are more likely to sustain another impact, which further highlights the necessity of timely diagnosis (Beckwith *et al.*, 2013). Hence, there is a need of a real-time method of on-field concussion diagnosis to remove the concussed athletes from practice to avoid subsequent impacts.

## Methods of diagnosis

### Symptomatic diagnosis

One of the most frequently used methods to diagnose concussion is based on the symptoms. These symptoms can be categorized into the following categories (Table 1). However, these symptoms cannot be reliably used to diagnose concussion on a sports field as they can take time (up to several hours) to develop (Kutcher and Giza, 2014).

**Table 1:** A general overview of the symptoms of concussion on a group-wise basis.

Physical	Headache, nausea/vomiting, photophobia, phonophobia, dizziness, slurred speech, blurred vision, incoordination.
Cognitive/Mental Status	Inattention, slowed thinking, amnesia, confusion, disorientation, vacant stare, loss of consciousness.

Affective	Emotional lability, depression, anxiety, mania.
Sleep	Increased latency, frequent waking, increased sleep time, decreased sleep time.

## Kinematic metrics

Numerous kinematics based injury metrics were developed over the last decades. The general idea behind kinematics metrics is to extract features from an impact to translate the impact into a scalar. These scalars are then used in conjunction with the available injury labeled impact data to develop a classification model to distinguish between concussive and non-concussive impacts. Some of these metrics aim to estimate risk of injury directly from the impact profile. The early metrics that aim to directly estimate injury risk based on the profile include basic metrics such as peak linear acceleration, peak rotational acceleration, or peak rotational velocity. However, later these metrics evolved into more complex metrics. Some of these metrics are as follows:

**Head Injury Criterion (HIC):** The most widely used injury criteria (*Part 571, Standard No. 202a–Head restraints.*, 2014), which is defined as follows:

$$HIC = \max\left\{\left[\frac{1}{t_2 - t_1} \int_{t_1}^{t_2} \|\vec{a}(t)\| dt\right]^{2.5} (t_2 - t_1)\right\} \quad (1)$$

Here,  $\|\vec{a}(t)\|$  is the resultant magnitude of linear acceleration with respect to time, and  $t_1$  and  $t_2$  are time boundaries chosen to maximize the value of HIC so that  $t_2 - t_1 < 15 \text{ ms}$  for  $HIC_{15}$  and  $t_2 - t_1 < 36 \text{ ms}$  for  $HIC_{36}$ .

**Severity index (SI):** This metric is also known as Gadd Severity Index (GSI) and is given as follows (Beckwith, Greenwald and Chu, 2012):

$$SI = \int \|\vec{a}(t)\|^{2.5} dt \quad (2)$$

**Rotational Injury Criterion (RIC):** The rotational equivalent of the HIC, is defined as follows:

$$RIC = \max \left\{ \left[ \frac{1}{t_2 - t_1} \int_{t_1}^{t_2} \|\vec{\alpha}(t)\| dt \right]^{2.5} (t_2 - t_1) \right\} \quad (3)$$

**Brain Injury Criterion (BrIC):** This metric was developed by National Highway Traffic Safety Administration. It is based on Cumulative Strain Damage Measure (CSDM), which is derived from a Finite Element head model.

$$BrIC = \frac{\vec{\omega}_{peaks}}{\vec{\omega}_{cr}} \quad (4)$$

Where  $\vec{\omega}_{peaks}$  is the vector containing the peak velocities in each anatomical direction and  $\vec{\omega}_{cr}$  is a vector of critical values derived from the FE model (E. G. G. Takhounts *et al.*, 2013).

**Diffuse Axonal Multi-Axis General Evaluation (DAMAGE):** This metric is based on mapping the MPS obtained from an FE simulation onto the equations of motion of a three-degree-of-freedom, coupled 2nd-order system. It is obtained as follows:

$$DAMAGE = \beta \max_t \{ |\vec{\delta}(t)| \} \quad (5)$$

Here,  $\beta$  is a scale factor relating the maximum resultant displacement of the systems to the MPS value from the FE brain model and  $|\vec{\delta}(t)|$  is a vector containing the displacement time (t) histories of the three coupled masses in the second order system model (Lee F. Gabler, Crandall and Panzer, 2018).

**STAR Injury Risk Function:** This statistically driven, logistic based metric is used to assess the injury risk possessed by an impact based on the peak linear and rotational acceleration values. It is defined as follows:

$$R(a, \alpha) = \frac{1}{1 + e^{-(-10.2 + 0.0433*a + 0.000873*\alpha - 0.000000920*a\alpha)}}$$

Where  $\alpha$  and  $a$  denote the peak rotational (rad/s) and linear accelerations (g) (Tyson and Rowson, 2018).

However, despite years of endeavor, kinematic metrics have major drawbacks that introduce inconsistencies in injury risk prediction (Ji and Zhao, 2015). One of the reasons for the discrepancies could be that these metrics are dependent on the database, which could introduce bias in either direction in terms of the number of concussive vs. non-concussive impacts. Further, since these metrics are statistically driven, if they are developed on a “simple” database, they could perform worse for more complicated databases. For instance the BrIC metric performs well in the study performed by Takhounts et al. ( $R^2 = 0.98$  when compared to the MPS from the related head model), yet the performance decreases in (Lee F. Gabler, Crandall and Panzer, 2018) when used on a different dataset ( $R^2 = 0.85$ ).

Further, translating a temporal 3-Degree-of-Freedom impact profile into a scalar value neglects the impact directionality, which plays a significant role in the generated strains in the brain tissue, which causes injury (Zhao, Kuo, *et al.*, 2017b). Finally, another possible reason for the discrepancy between kinematic metrics is perhaps due to their limitation in providing insight into tissue mechanical responses, most notably strain pattern (Ji and Zhao, 2015).

## Finite Element

FE models play a unique role in providing brain tissue mechanical response to an impact to the head. FE models are valuable since they can provide insight into mechanics of injury based on the brain tissue mechanical responses to the impact (e.g. strains), which are the most probable cause of injury (Post and Hoshizaki, 2012). Consequently, there has been various endeavors for implementation of Finite Element models of the human brain, most of which were conducted in the recent years (Hardy *et al.*, 2001, 2007; Ji, Zhao, *et al.*, 2014).

In comparison to kinematic metrics, FE models have proven to perform more accurately, which is expected since they are based on the tissue level strain response which is closely related to injury. For this reason, they are believed to withhold great potential in understanding the mechanics of injury (Wu, Zhao, Rowson, *et al.*, 2019).

Another unique capability of FE models, is their ability to provide various features of the strain response, which may be closely correlated with injury. For instance, strains along white matter fiber directions (instead of isotropic maximum principal strains) is one of such measurable features. When using this response, the consistency between model- estimation and neuroimaging findings significantly improves in terms of the spatial distribution and group-wise extent of potential white matter damage. (Bazarian *et al.*, 2012; Ji *et al.*, 2015a)

Numerous efforts were made to create accurate FE models of the human head. These efforts have resulted in an increase in the model sophistication (Wu, Zhao, Rowson, *et al.*, 2019). Nonetheless, researchers have not reached consensus on the “correct” properties to model the brain. For instance optimizing brain material properties (Zhao, Choate and Ji, 2018) and enhancing the quality of brain mesh (Giudice *et al.*, 2019; Zhao and Ji, 2019b) are only a few of these brain model parameters, which are open areas of research. The following

subsections will provide more detail into the characteristics that separate FE models available to date.

Characteristics

FE models play a crucial role in providing insight into how impact kinematics can be converted to regional brain tissue level response. These responses are not available by any other means as they cannot be obtained in vivo. This lends strength to the significance of FE models in studying concussion. FE head models in general can be regarded as functions to translate physical boundary conditions (e.g. acceleration or velocity) into tissue responses, such as strain, pressure, or stress (Van Dommelen, Hrapko and Peters, 2010). Several studies have been dedicated to using FE models in various contexts using FE models (e.g. in American football based on impact reconstruction (Zhang, Yang and King, 2004; Marjoux *et al.*, 2008; Ji *et al.*, 2015a), pedestrian and motorcycle accidents (Willinger and Baumgartner, 2004), and instrumented helmets from collegiate football players (Takhounts *et al.*, 2008)). A list of some of the human head FE models used today is presented in **table 2** (Giudice *et al.*, 2019).

**Table 2:** A summary of selected head injury models and their characteristics (Giudice *et al.*, 2019).

	KTH (Kleiven and Von Holst, 2002)	THUMS (Hideyuki <i>et al.</i> , 2006)	SIMon (Takhounts <i>et al.</i> , 2004)	GHBMC (Jin <i>et al.</i> , 2013)	WHIM V1 (Ji <i>et al.</i> , 2015b)
Head Elm. No.	21k	50k	46k	270k	115k
Mean Resolution	3.9 mm	3.8 mm	3.2 mm	2.5 mm	3.3 mm

Elm. Type	Hexahedral Quadrilateral	Hexahedral Quadrilateral	Hexahedral Quadrilateral	Hexahedral Quadrilateral Triangular Pentahedral Tetrahedral	Hexahedral Quadrilateral
Elm. Formulation	Selectively Reduced	Constant Stress	Constant Stress	Constant Stress	Constant Stress
Anisotropy	No	No	No	No	No
Viscoelasticity	No	Yes	Yes	Yes	Yes
Hyperelasticity	Yes	No	No	No	No
Hourglass Control	N/A	Viscous	Viscous	Viscous	Enhanced
Geometry	Visible Human Database	50 <sup>th</sup> Percentile Male	50 <sup>th</sup> Percentile Male	50 <sup>th</sup> Percentile Male	Subject- specific (male)
Solver	LS-DYNA	LS-DYNA	LS-DYNA	LS-DYNA	Abaqus

The models mentioned above were specifically developed for investigating the biomechanics of TBI, and have been validated to different extents using brain deformation (Hardy *et al.*, 2001, 2007) and intracranial pressure (Nahum, Randall and Ward, 1977; Trosseille *et al.*, 1992). They are each unique in their numerical implementations such as mesh

type, number of elements, mesh size, element formulation, hourglass formation, and the FE solver software package. The following sections will discuss the differences between the model specifications across the mentioned models to provide a background on the FE model characteristics.

### Meshing

To begin with, an obvious and crucial discordance between the previously mentioned head models is meshing. Meshing is a crucial component to FE modeling since it is directly related to the complexity of the model. Not surprisingly, with the advancement of computational capacity of computers, human head FE models are growing more sophisticated in the recent studies--e.g. (Fernandes *et al.*, 2018; Zhao and Ji, 2019a). Meshing has two major components, which are, mesh type and mesh size.

#### *Mesh Element Type*

The most common three dimensional element type is hexahedral elements (Giudice *et al.*, 2019). This preference is expected because of the computational efficiency, accuracy, and the high rate of convergence in hexahedral elements (Tadepalli, Erdemir and Cavanagh, 2011). Further characteristics lending strength to the precedence of this element type are their stability and capacity to compute accurate solutions in highly non- linear applications that involve large deformation and material incompressibility, such as that of the brain (Bonet and Burton, 1998; Tadepalli, Erdemir and Cavanagh, 2011).

However, the downside of hexahedral elements is that the mesh generation process includes a large portion of manual labor (Giudice *et al.*, 2019). This can make the process

increasingly arduous as the shape geometry grows more convoluted, such as the gyri and sulci in the brain (Yang *et al.*, 2014). Further, maintaining the quality of the mesh could be challenging while modeling geometric details such as gyri and sulci, hence such details are often compromised in favor of mesh quality. This is the reason why no hexahedral- based brain model contains such details (Giudice *et al.*, 2019). Another shortfall of hexahedral elements is their vulnerability to unrealistic hourglass deformation modes which are explained in more detail in the next chapters (Giudice *et al.*, 2019).

Voxel elements are a subset of hexahedral elements with some fundamental differences in terms of characteristics compared to regular hexahedral elements. These elements were implemented in several recent brain FE models (Ho, Von Holst and Kleiven, 2009; Chen and Ostoja-Starzewski, 2010; Miller, Urban and Stitzel, 2016; Ghajari, Hellyer and Sharp, 2017). These models can be automatically generated (as opposed to manually in regular hexahedral element type) based on MR images of the brain, where each voxel of the MR image is converted to a cubic hexahedral element and construct the whole model in this fashion. This method paves the way for creating subject specific models (Ho, Von Holst and Kleiven, 2009). These models benefit from the accuracy and stability of the hexahedral elements, as well as the ability to take into account the anatomical features of the brain at the fine resolution of MR images, hence in the absence of smoothing the elements are perfect cubes with a length of 1—2 mm (depending on the resolution of the utilized image) (Giudice *et al.*, 2019).

Yet, voxel based models are unable to compensate for discretization error at curved interfaces (e.g. brain and cortical Cerebrospinal Fluid (CSF) interface or White Matter and Grey Matter interfaces) (Guldberg, Hollister and Charras, 1998; Ho, Von Holst and Kleiven, 2009). To alleviate this problem, smoothing algorithms were proposed. Yet, these algorithms affect the quality of the elements negatively (Taubin, 2000; Boyd and Müller, 2006; Chen and Ostoja-

Starzewski, 2010). Element quality becomes increasingly important when modeling soft incompressible materials, such as that of the brain. Consequently, the elements of poor quality, especially where the model is experiencing large shearing deformations (such as the interface of the brain and CSF), will result in unrealistically large strains compared to the neighboring elements with better quality (Panzer *et al.*, 2012; Panzer, Myers and Bass, 2013). To measure element quality, Scaled Jacobian is the metric often used to measure the deviation of a hexahedral element from a perfect cubic element. The range of Scaled Jacobian is from -1 to 1, which indicates the position of the centroid with respect to the element, hence first order tetrahedral elements have an irrevocable Jacobian of 1. A lot of FE solvers will not solve the model if the Scaled Jacobian is less than zero, which in the model means that the centroid of the element is falling outside of the element volume. Same as all models with hexahedral element type, voxel FE models are prone to hourglass energy formation, hence using hourglass control while utilizing them is necessary (Giudice *et al.*, 2019).

In contrast to most hexahedral elements, tetrahedral elements can be generated automatically, and are suitable for complex geometries such as that of the brain. They further do not exhibit hourglass deformation modes. For these reasons, tetrahedral elements have been used in several studies examining the influence of gyri and sulci on brain deformation such as (Yang *et al.*, 2014; Fernandes *et al.*, 2018).

However, tetrahedron elements are overly stiff for this application (Zeng and Liu, 2018) and prone to a numerical phenomenon called volume locking when modeling incompressible materials such as that of the brain tissue (Tadepalli, Erdemir and Cavanagh, 2011). Volume locking is a result of the reduced degrees-of-freedom in tetrahedral elements (Hallquist, 1986). This can be alleviated, to some extent, through mesh refinement or by using higher-order tetrahedral elements. For instance Singapore model (Yang *et al.*, 2014) has 1.17 million

elements compared to hexahedral models, for which the element count is in the order of thousands. However, each of the mentioned options greatly increases computational cost of the FE solution.

### *Mesh size*

Mesh size is one of the most important factors in finite element modeling. The nature of meshing is discretizing a continuum, hence the finer the mesh is, the more accurately it will mimic the behavior of the original continuum, and the better it will perform (Giudice *et al.*, 2019). Meshes are almost never uniformly distributed (with an exception of the voxel models that were described earlier), and the mesh size is usually not reported in the literature (Giudice *et al.*, 2019). The closest one can get to the mesh resolution is based on the number of elements and the estimated size of the brain (1275 cm<sup>3</sup>) (Scahill *et al.*, 2009). A finer mesh also allows for modeling more details within the brain such as the anatomical boundaries between different regions within the brain. Another benefit of increasing the mesh resolution is that a more refined mesh is less prone to hourglass deformation modes (Hallquist, 1986).

However, increasing the mesh resolution is a tradeoff of accuracy and computational cost. In order to find a reasonable point in this tradeoff a mesh convergence studies are performed to determine the proper mesh resolution. In a study using the Worcester Head Injury Model (WHIM), it was concluded that there is a convergence point of approximately 200,000 elements for meshing the brain, after which point the results from finer meshes do not significantly differ (Zhao and Ji, 2019b). Typically a mesh is considered to have “converged” if the outputs do not vary by more than 5% with increasing the mesh resolution (Tadepalli, Erdemir and Cavanagh, 2011). Another method of assessing the convergence of a mesh is the Grid Convergence Index (GCI). This method is one that qualitatively assesses the model’s

discretization convergence, provides an estimation of the discretization error, and estimates the exact value of the converged solution (Roache, 1994). Despite the importance of a mesh convergence behavior study, the existing models rarely prove their mesh quality through a mesh convergence study (Giudice *et al.*, 2019). Aside from the WHIM, some studies focused on the pressure while reporting convergence behavior, but not strain (Kleiven and Von Holst, 2002; Mao, Gao, *et al.*, 2013). A different study only reported averaged strains of the whole brain in mesh convergence behavior (Garimella and Kraft, 2017).

### Element Formulation

Another important model characteristic that contributes to the disparity between different models is element formulation (or integration scheme). Element formulation indicates the shape functions as well as the integration scheme to compute finite element problems. In a more general way, element formulation indicates the mathematical equations that are to be made use of to solve the FE simulation. The shape functions are the functions used to interpolate the directly calculated results on the nodes to yield the field variables in all the points in an element (Hughes, 2012). Shape functions are predominantly linear functions in each dimension. An exception is elements which incorporate nodal rotation degrees of freedom where higher order formulations are utilized. Based on this element formulation, the number of integration points varies. With an increase in the number of the integration points, the computation cost will increase (often exponentially). To illustrate, a single element with C3D8I formulation (Fully Integrated Hexahedral Element, which has 8 integration points), requires 25 times more computational power than the equivalent C3D8R (constant- stress hexahedral also referred to as reduced integrated hexahedral element) (Hallquist, 1986). Selectively-reduced hexahedral elements (referred to as S/R in LS-DYNA (J. O. Hallquist, 2007) equivalent to C3D8 in Abaqus

(Abaqus, 2016)), are considered somewhere in between reduced integrated and fully integrated elements in terms of cost. Due to their low computational cost and their ability to maintain their integrity under large shear forces, the constant- stress hexahedral are generally preferred in FE modeling of the brain (Giudice *et al.*, 2019).

For the application of FE modeling of the brain, the brain material, which is a nearly incompressible material due to its high water content, undergoes large shear deformations in case of an impact (Libertiaux, Pascon and Cescotto, 2011; Alshareef *et al.*, 2018a). Hence, choosing an element formulation is a trade-off between their pros and cons. For instance, fully-integrated elements, which are considered to be the most accurate element types (Abaqus, 2016), tend to be stiffer compared to the constant stress elements and vulnerable to volumetric locking when used with nearly incompressible materials and to shear locking when the aspect ratio of the element is large (Hallquist, 1986; Hughes, 2012). To address a part of these issues, selectively reduced elements were designed to compensate for the volumetric locking that the fully integrated elements are prone to. Yet, they still suffer from the same shear locking problem (J. O. Hallquist, 2007).

The downside of constant- stress elements is their vulnerability to Hourglass deformation modes. Hourglassing is an unrealistic, zero-energy deformation mode for the mesh that yields zero stress and strain (Belytschko *et al.*, 1984). Hourglassing can lead to numerical instabilities and model failure in constant stress hexahedral elements. The fully integrated and selectively reduced elements do not have Hourglass deformation modes. Hence, while using constant stress elements for simulations, models must have a form of hourglass control embedded in them, which is an important aspect of the model (Giudice *et al.*, 2019).

Tetrahedral elements are not suitable for the application of modeling a soft nearly incompressible material such as that of the brain as they result in little to no deformation in the

brain, and are clearly prone to volumetric locking (Giudice *et al.*, 2019). Further, selectively Reduced Tetrahedral elements and 10 –node composite tetrahedron elements were shown to be unstable and fail to terminate normally in the literature. Which leads to the conclusion that tetrahedral elements in general are unrealistically stiff or unstable to be utilized in brain biomechanical modeling and they are prone to volumetric locking (Giudice *et al.*, 2019).

### Hourglass deformation and Formulations

One shortfall of using constant- stress hexahedral element formulation is their potential error due to formation of hourglass deformation modes. Hourglass deformation is an unrealistic deformation in finite element analysis due to reduced stiffness of the elements introduced by using reduced integration. Each software package has a way of artificially compensate for such deformations to make the simulations more realistic. Hourglass deformation modes are especially problematic while modeling soft, nearly incompressible materials such as that of the Brain (Giudice *et al.*, 2019).

To address this issue, Hourglass control algorithms were developed to prevent these modes to an extent. Hourglass control is mandatory for every simulation which uses constant stress hexahedral elements. Furthermore, the hourglass energy decreases with higher mesh quality and increases with higher mesh size. Hence, increasing mesh resolution is a way of tackling this issue, yet it comes at the expense of higher computational cost (Abaqus, 2016). As a result, normally a lower mesh density along with hourglass control algorithm is used to maintain computational efficiency.

Hourglass control algorithms are numerical ways of overcoming unrealistic, zero energy deformations resulted from Hourglass deformation modes. In a very high level, the general idea

of these methods is that the solver applies small internal nodal forces to nullify the zero energy deformation modes that are inherent to constant– stress elements. The determination of the amount of this force divides hourglass controls into three general groups. These algorithms either use a stiffness formulation, or a viscous formulation (Flanagan and Belytschko, 1981) or a combination of these (Abaqus, 2016). Different hourglass types proved to have significant implications in the solution and the stability of the FE simulation (Giudice *et al.*, 2019).

Hourglass control algorithms are crucial when using constant- stress elements. However, all of these approaches to hourglass control make the elements stiffer. This is to some extent expected due to the fact that they aim to increase their resistance to non-physical deformation modes.

In a deeper perspective, when using stiffness Hourglass control formulations, the previously mentioned internal forces correspond to the displacement of the nodes due to hourglass modes. Hence, they are recommended for the applications with a low rate loading (Hallquist, 1986). Algorithms that fall under this category are effective in reducing hourglass energy, yet they should be closely monitored to insure that the final results are not overly affected by the Hourglass control algorithm. In other words, if employed incorrectly, these methods could make the model excessively stiff (Takhounts *et al.*, 2004).

In contrast, the internal forces in viscous hourglass control algorithms are closely related to the velocity of the model nodes, which makes them suitable for applications in which the loading conditions are of a high velocity and high strain rate (Hallquist, 1986). Thus, it is not surprising that in brain modeling viscous models are predominantly used (Hideyuki *et al.*, 2006; Takhounts *et al.*, 2008; Jin *et al.*, 2013). Yet, Hourglass control algorithms are not well reported in the literature, which makes a thorough investigation of different models challenging since it can cause significant effect in the results (Giudice *et al.*, 2019).

Hourglass control algorithms, introduce external work to the system to counteract the hourglass deformation modes. This work is reported as “Hourglass Energy”, which is not accounted for in the global energy calculations in an FE simulation. Hence, Hourglass control drains real energy from the system (Hallquist, 1986). The extent of this drained energy can be monitored through the Hourglass energy ratio (Takhounts *et al.*, 2004). The literature suggests maintaining this ratio below 10% ensures that this energy is not affecting the results extensively. The same guideline was originally pursued for brain modeling (Flanagan and Belytschko, 1981; Belytschko and Tsay, 1983; Belytschko and Bindeman, 1993). However, it was later expanded to ratios 2.0-3.0 for human brain modeling (Takhounts *et al.*, 2004).

To name some of the alternate methods of addressing the hourglass energy formation, there is the solution of increasing the number of elements, and element quality, which of course comes at the price of increased computational cost because of the increased elements. Another solution to address hourglass control is using tetrahedral elements, which are not prone to Hourglass deformation modes. However as discussed previously, these element types are overly stiff to be able to mimic the behavior of a soft nearly incompressible material such as the brain.

### Software package

As observed in the previous sections, there are quite a few properties within each software package affecting the final accuracy of a computational analysis. However, as the implementation of these methods may not be conducted identically in different software packages, the use of different software packages also introduces inherent disparities to results from the simulation. A majority of the previously mentioned head models use the LS-DYNA platform. Yet, another widely used platform is Abaqus, which was used for the Worcester Head

Injury Model (WHIM). To address these discrepancies, we conduct a study in the chapter 3 where we translate our WHIM model from Abaqus to LS-DYNA to characterize the differences between these two software packages.

### Material Anisotropy within Software Packages

To mimic the behavior of the brain material, some FE models include the material anisotropy of the white matter. The implementation of anisotropy, however, is a point of discrepancy across FE head models. For instance, WHIM incorporates material anisotropy modeled by Holzapfel-Gasser-Ogden (HGO), an example of an anisotropic material in Abaqus (Abaqus, 2016). Yet, this material model is absent from LS-DYNA and hence cannot be implemented in models that use the LS-DYNA platform.

## **Worcester Head Injury Model (WHIM)**

The Worcester Head Injury Model (WHIM) V1 was used for obtaining strain distributions generated in the brain tissue. The FE mesh of the WHIM was constructed based on the MR images of an individual male athlete. It uses the reduced integrated (C3D8R) element type in Abaqus software package with optimized configurations (to mimic the behavior of C3D8I which the most accurate element type in Abaqus, while using less computational power). There are ~55k brain elements in WHIM V1 while distinguishing the white matter and gray matter material properties. To mimic the behavior of the brain tissue more closely, WHIM uses white matter anisotropy. The hyper-viscoelastic materials were used to mimic the brain material properties along with the enhanced hourglass control settings, which is recommended by Abaqus for this material c. WHIM can provide entire brain strain distributions (element-wise or voxel-wise strain

distribution), strains distribution in specific regions of interest within the brain, and strains along the white matter fibers (Zhao *et al.*, 2016; Zhao, Cai, *et al.*, 2017a) (**Figure 1**).

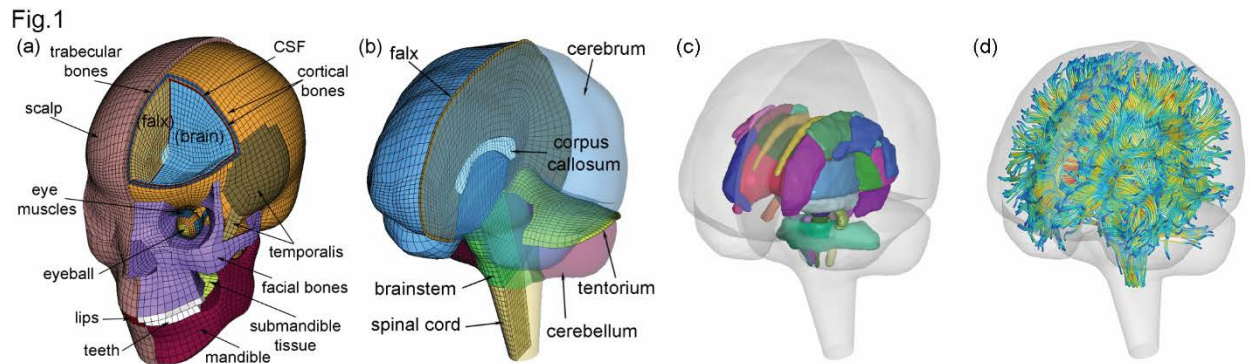


**Figure 1:** Worcester Head Injury Model (WHIM) mesh and anatomical regions (a and b). (c) Shows the injury relevant deep white matter regions of the brain and (d) shows the white matter fibers in the model.

## WHIM Model Validation

The biofidelity of a head injury model is insured by validation of a head injury model. However, there is a debate on the validation data used for FE model validation. In a nutshell, even the “validated” head models using current techniques exhibit significant differences in terms of generated brain strains when simulating the same impact. These differences suggest that the current validation methods need improvements to become more discriminating among models.

One point of debate in model validation is available data. For example, a majority of FE models (Yang *et al.*, 2006; Mao, Zhang, *et al.*, 2013; Ji *et al.*, 2015b; Giordano and Kleiven, 2016; Miller, Urban and Stitzel, 2016; Garimella and Kraft, 2017) were validated against relative brain-skull displacement. However, the spatial gradient of such displacements result in

injury, not the displacements directly (King *et al.*, 2003). So brain-skull displacements have been deemed not specifically suitable for FE model validation.

Another point of debate is the injury relevance of the available data. As discussed before, most models have been validated by high-rate cadaveric impacts. This database generally has more severe impacts than those typically seen in contact sports (Hardy, 2007; Hardy *et al.*, 2007). Another available database is *in vivo* strains that are lower in terms of generated strains and are related to subconcussion (Sabet *et al.*, 2008; Knutsen *et al.*, 2014; Atsumi *et al.*, 2018; Lu *et al.*, 2019). A recent dataset is focused on the mid-rate range which is more aligned with the impact magnitudes experienced on sports fields (Alshareef *et al.*, 2017; Guettler, 2017; Guettler *et al.*, 2018), compared to the high rate and low rate impacts.

To address these inconsistencies, a recent study investigate the validity of the WHIM and proposed a standard way of model validation with currently available baseline experiment data. In this study, WHIM was further validated across a wide range of impacts, including high-rate cadaveric impacts, mid-rate cadaveric pure rotations simulating impacts in contact sports, and *in vivo* head rotation/extension tests as discussed above (Zhao and Ji, 2020a).

## **Limitations of FE head models**

As discussed in the sections above, FE models are computationally expensive. Further, accuracy of FE models is a tradeoff with the computational cost that they incur. Yet, in a sideline setting there is limited computational power available compared to a lab setting (A personal laptop vs. a high-end computer cluster). Even with the available resources in a lab setting, simulating a single impact could take hours to complete (Ji and Zhao, 2015). Hence, using FE modeling directly in a sport setting is simply unfeasible.

To address this issue, there has been various methods to mitigate the computational costs of FE modeling while taking advantage of the valuable insight into the brain tissue. Some of these methods map FE simulations into a simpler, less computationally costly method for faster strain prediction. Another group of such methods provide an estimation of the FE simulation based on a database of completed simulations. The following sections provides some background for some of these methods.

## **Mapping to other simpler functions**

Gabler et al. (Lee F. Gabler, Crandall and Panzer, 2018) proposes an innovative way to model the MPS generated by the strain map from a frequently used head model into a second-order spring dashpot system for rapid estimation of MPS. While this method performs well in predicting the peak MPS generated in the brain in an impact, it remains incapable of predicting the strain patterns of the brain.

Another example of such methods is the BrIC method that was mentioned in the previous sections. This method also suffers from the same limitation as DAMAGE. Further, as mentioned before, it is database dependent and performs less accurately with more “complex” impact data.

## **Pre-Computed Brain Response Atlas (pcBRA)**

Another method to mitigate the time needed for FE simulations is pre computation. Pre computation is using simulations that are already complete. The Pre-computed Brain Response Atlas (pcBRA) is an FE based pre-computation technique to reduce the expensive

computational cost of FE simulation to make FE models usable on the sports field. The pcBRA consists of a dataset of pre-defined simplified impacts with various directionalities and impact magnitudes. These impacts only have a rotational component, as it is known that rotation is the most major contributor to generated brain strains. The severity of these impacts is defined using the peak resultant rotational velocity of the impacts, while the directionality was defined by the azimuth and elevation angle of the rotational axis (**Fig. 2**). The duration of these single impacts was shown to not have a significant effect on the strain generated in the brain by the impact for this specific tear of impacts related to contact sports and was hence set to be 10ms (Ji and Zhao, 2015; Zhao, Kuo, *et al.*, 2017b). **Table 3** illustrates the step-size in the three values defining the impact. **Fig. 2** shows a visual illustration of the pcBRA.

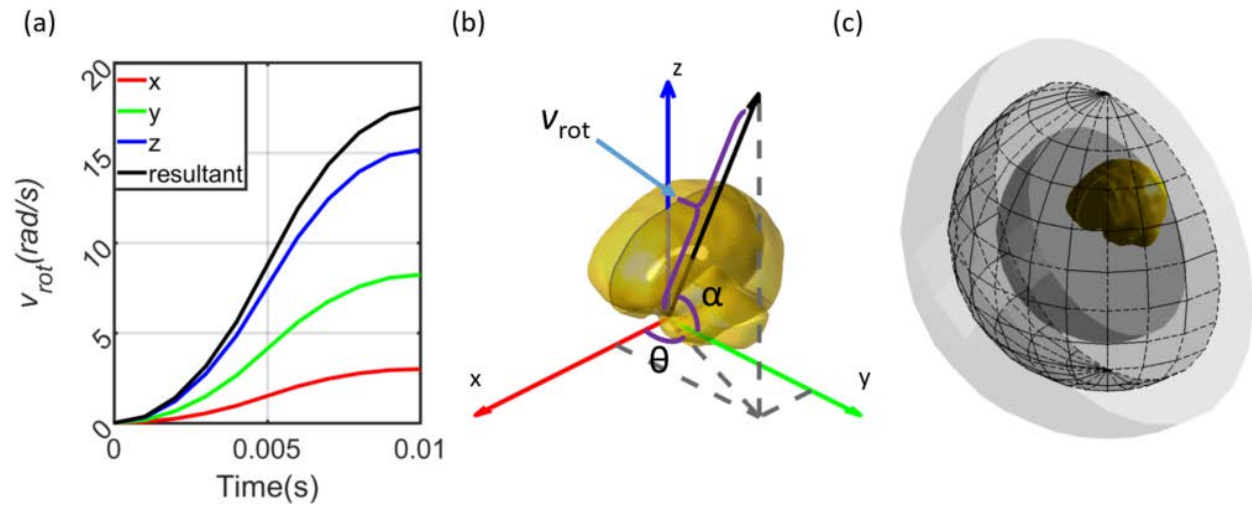


**Figure 2:** (a) Example of an idealized 3DOF impact rotational velocity profile; (b) the corresponding kinematics triplet  $(v_{rot}^p, \theta, \alpha)$  is represented by a vector emanating from the head center of gravity characterizing the impact kinematic magnitude and directionality in the WHIM coordinate system. For a given impact severity (denoted by rotational velocity peak:  $v_{rot}^p$ ), traversing the end point of the vector in space would generate a hemisphere shown in (c). In the middle hemisphere, the discretized  $(\theta, \alpha)$  pairs are also shown as grid on the hemisphere.

**Table 3:** Summary of the discretizing variables, their ranges, step sizes, and number of samples for the idealized head impact rotational profiles used to establish the pcBRA. Peak rotational acceleration ( $a_{rot}^p$ ) and peak rotational velocity ( $v_{rot}^p$ ) are equivalent when the impulse duration,  $\Delta t$  is constant.

Variable	$\alpha_{rot}^p$ (rad/s <sup>2</sup> )	$v_{rot}^p$ (rad/s)	$\theta$ (°)	$\alpha$ (°)	$\Delta t$ (ms)
Range	[1500 7500]	[7.5 37.5]	[-90 90]	[-90 90]	10
Step size	750	3.75	15	15	N/A
# of samples	9	9	13	13	1

While this method can provide a reasonably well estimation of the brain strain pattern as well as the peak MPS, its performance diminishes when confronted by more complex impacts. This is due to the simplicity of the pre-defined impacts as shown in (Zhao, Kuo, *et al.*, 2017b).

Despite the fact that studies such as (Ji and Zhao, 2015; Zhao, Kuo, *et al.*, 2017b) pave the way in using the pre-computation technique, they rely heavily on empirical observations to use the pre-computed database. Yet, the nature of contact sports-related impacts is complex. While empirical observations gain some insight into the strain generation mechanism, they have room for fine-tuning and improvement. For instance, Zhao *et al.* relies on the peak rotational velocity of the entire impact to predict the brain strain distribution. This assumption loses accuracy with more complex impacts. For instance, velocity reversals in impact profiles introduces a large error to the pcBRA (Zhao, Kuo, *et al.*, 2017b). This suggests that pre-computation, while promising, requires a more versatile technique for implementation on complex real-world impacts.

## Use of Machine Learning in conjunction with pre-computation

Recently a number of studies have shifted focus to applications of machine learning in biomedical application. The attraction of machine learning techniques is in that they have

proven to be extremely adaptive to different scenarios, such as diagnosis (Chong *et al.*, 2015; Mitra *et al.*, 2016), biomedical signal processing, and even modeling (Wu, Zhao, Ghazi, *et al.*, 2019; Zhan *et al.*, 2020).

For the purpose of modeling, machine learning is particularly attractive because it has the potential to reduce the time required to obtain brain strains and strain-based metrics drastically. A number of approaches have been proposed to predict the peak MPS of the brain using a set of complex, real-world impacts (Wu, Zhao, Ghazi, *et al.*, 2019; Zhan *et al.*, 2020). These methods, compared to the empirically based pre-computation methods, provide a more sophisticated approach to pre-computation. This grants the method considerable versatility compared to analytical techniques. Further, as they are based on real-world impacts, they “learn” to function well with real-world impacts that possess a higher level of complexity compared to idealized impacts. The following sections provide a deeper background as well as a more detailed description of machine learning based methods in TBI as they pertain to this dissertation.

## **Machine Learning Background**

Machine learning (ML) methods are a set of data-driven statistical methods for statistical tasks using available data (Mitchell, 1997). This method has been used extensively for different applications including in the biomedical field (Wu *et al.*, 2018) . Generally speaking, these methods are based on optimizing some of loss function to perform a prediction task based on a set of features (which themselves can be engineered to increase training performance (Masoomi *et al.*, 2020)). There are several methods of optimizing these loss functions, each of which are suitable for certain scenarios. They can differ in many aspects such as types of input

and output, model level of complexity, scalability, and time required to train the model. Two of the most predominant applications of ML are classification and regression tasks.

### Classification

Classification tasks are scenarios where we desire to determine the class of a data point based on previously classified data. These classifications could be binary classifications, as well as multi-class classifications. For instance in case of brain biomechanics, given an impact, whether or not an impact would result in an injury (such as that in (Cai *et al.*, 2018)). There are several methods that can provide an injury probability in such a scenario. The most simplistic method is Logistic Regression (Cai *et al.*, 2018). This method uses a logistic function to differentiate between the two or more classes. Another method includes Support Vector Machines, which function by finding the best border line between different classes of data. Once the line is determined, it classifies any new data point using the regions that are separated by the borderlines (Cai *et al.*, 2018).

Machine Learning based classification techniques have proven to be effective in TBI injury assessment (Cai *et al.*, 2018). While simple methods, such as logistic regression can provide a crude comparison of impacts with a high risk of injury compared to those with a low risk, more sophisticated methods are emerging that are capable of outperforming the other methods. For instance, (Wu, Zhao, Rowson, *et al.*, 2019) uses a network-based response feature matrix as a brain injury metric, where a matrix is used to represent specific regions of the gray matter as well as the white matter interconnections between the gray matter regions. This metric consistently outperformed conventional scalar metrics including peak maximum principal strain of the whole brain (MPS), peak linear/rotational acceleration, and peak rotational velocity across different performance measures, showing great promise for this approach.

## Regression

Another popular application of machine learning is for regression tasks. Regression tasks follow a similar concept to classification tasks, however they predict a desired value as opposed to a class. An example of a regression task would be to predict the peak MPS of the brain in case of an impact (such as that in (Wu, Zhao, Ghazi, *et al.*, 2019)). Linear Regression models are the most basic models used for regression tasks. Regression models find the best function that relates two sets of data to each other (e.g. peak velocity magnitude and peak MPS). Then given a new data point in one dataset, they predict the corresponding value in the second dataset using the fitted line.

Regression models provide great value to FE based TBI research. Once trained, these methods can predict FE based injury metrics directly and accurately, which effectively bypasses the time-consuming simulation step in FE modeling. These methods can also be designed and trained to predict the desired FE based injury metric directly, which can save unnecessary computational cost. In other words, machine learning based regression methods can approximate the non-linear relationship between a given impact profile and the corresponding FE based results and represent them in real-time, making them a promising option for making the FE based research more accessible without necessitating substantial computational power. As a result, they hold the potential to making FE based injury assessment into a usable method for sideline applications as well as providing easy access for TBI researchers in general.

### Support Vector Machines

Support Vector Machines (SVMs also known as Support Vector Networks (Cortes and Vapnik, 1995)) are supervised learning methods developed and used for both regression and classification tasks. This method is based on mapping data into points in a high dimensional space and finding a hyperplane or a set of hyperplanes boundary between different classes of data that maximizes the margin between different classes (Hastie, Tibshirani and Friedman, 2017). To further expand the versatility of this method and increase the sophistication, it can be used in conjunction with different kernel functions. Kernel functions are functions that help determine a higher order hyperplane for classification, while not introducing the significant computational cost of calculation in the higher dimensions (Chen and Lin, 2006). Recent studies have shifted towards using SVMs based on both Kinematic metrics (Hernandez *et al.*, 2015) and strains (Cai *et al.*, 2018).

### Artificial Neural Networks

A highly versatile machine learning method that has been successfully used in both classification and regression tasks is Artificial Neural Networks (ANNs) (Cai *et al.*, 2018). ANN is an iterative method that is based on the interaction of mathematical nodes (called “neuron” or “perceptron”) to optimize a loss function. This method is designed to mimic the behavior of the neurons in a biological brain. The nodes in this model interact with each other using weights and biases. The schematic representation of a neural network is presented in **Fig. 3**.

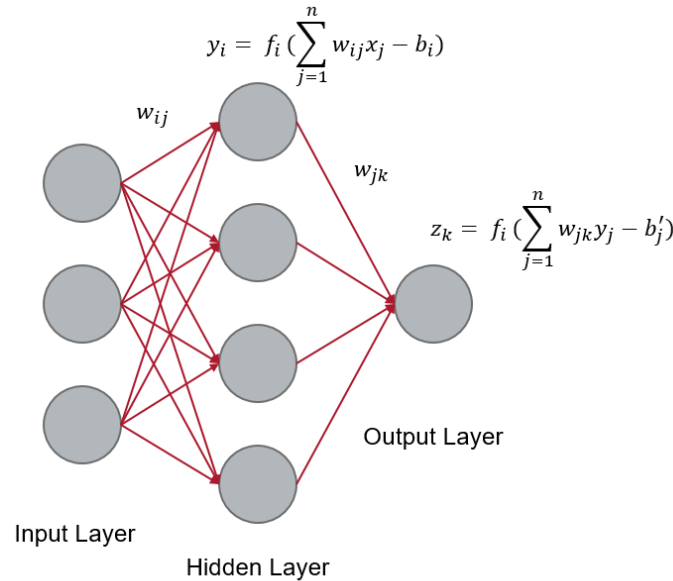


**Figure 3:** Schematic Representation of a fully connected artificial neural network with 3 input values, four hidden neurons, and one output. The weights of each connection as well as the biases for each node are shown in  $w$  and  $b$  respectively. The values of each neuron is based on all the preceding neurons *via* the internally optimized weights and biases.

In the training process, based on the desired outputs (referred to as “labels”), the network iteratively adjusts the weights and biases to result in a prediction that is as close as possible to the labels. This iterative approach is a high dimensional gradient based optimization called “error back propagation”. As the name suggests, in error back propagation, the final error of the predicted values compared to the labels is traced back through the entire network, resulting in an individualized adjustment for each node weight and bias.

The upside of these networks is their versatility and their minimal need for operator adjustment. As a result, with an application appropriate architecture, ANNs can achieve substantially better results compared to other methods. However, depending on the architecture of the network, there is a need for a large number of data to train the network and reach the full

potential (Wu, Zhao, Ghazi, *et al.*, 2019). The crudest architecture for ANNs is the fully connected sequential networks, which requires all inputs to be inputted in one vector.

### Convolutional Neural Networks

A drawback of fully connected ANNs is that they lose the spatial features of the input, as the input is “flattened” into a vector (Wu, Zhao, Ghazi, *et al.*, 2019). This reduces the performance of ANNs with tasks such as image processing as the relative spatial positioning of the pixels has a high importance. To address this, Convolutional Neural Networks (CNNs) were developed to account for the spatial positioning of features. CNNs are deep learning architectures inspired by the natural perception mechanism of living creatures (Hubel and Wiesel, 1968) and consider the spatial positioning of the input into account through a set of two dimensional filters (Gu *et al.*, 2018).

### Model Validation

While machine learning algorithms are powerful tools in for a vast variety of research topics, they are prone to errors associated with data-driven approaches. Two of the most common problems with data-driven approaches are under-fitting and over-fitting. Under-fitting occurs when either the model is not trained for enough iterations or it is “too simplistic” for representing the relationship between the inputs and the outputs for the application. Over-fitting, on the other hand, occurs when the network performs well on the data used for training but poorly on any other independent dataset. In other words the network “memorizes” the training data as opposed to “learning” the trends (Van Der Aalst *et al.*, 2010). Model validation is a way to avoid both of these scenarios.

A common practice for validation is to have three sets of data: a training set, a validation set, and a testing set. The model is trained based on the training set, and then evaluated on the validation set. Based on the comparison of these two performances, the operator can alter the model hyper-parameters to maximize the model performance on both the training and the validation dataset (Gareth *et al.*, 2013). However, the final product can also be tested on an independent testing dataset to ensure that the hyper-parameters were not chosen in a fashion that would “over-fit” the training and validation data (Wu, Zhao, Ghazi, *et al.*, 2019).

When using one large database for training testing and validation cross validation is often used. In this method, the data is broken down into separate portions for training, validation, and testing. To ensure that the grouping of data is not introducing any bias to the model, k-fold cross validation is used. In this method, the data is broken down into k-folds. The network is trained a number of times in a systematic way where k-2 folds of the data are used for training the network, while the remaining two are reserved for validation and testing. Then the process repeats until all the data-points had a chance to take part in training and validation. The extreme version of k-fold validation is the leave-one-out cross validation. As the name suggests, this cross validation method uses the entire database but one data-point to train, retaining the one data-point for validation. Effectively, this is a k-fold cross validation where k equals the number of data-points in the database. The leave-one-out cross validation method is desirable for situations where data is sparse (Gareth *et al.*, 2013).

### *Applications of ANNs in TBI Research: Strain Prediction*

The most basic networks are Sequential fully connected networks, where all neurons in one layer are connected to all neurons to the adjacent layer. Zhan et al. in (Zhan *et al.*, 2020) uses a fully connected network to estimate the entire brain deformation based on the impact

rotational profiles in three dimensions. They input an 8 channel signal constructed by  $(\alpha_x, \alpha_y, \alpha_z, \alpha_{res.}, \omega_x, \omega_y, \omega_z, \omega_{res.})$  where the x, y, and z are the anatomical directions and “res.” is the resultant value from all three directions. While this method achieves acceptable results, it does not take the relation between these channels into account. This means that the effects of impact directionality (which is obtained from the relative magnitude of the impact in the x, y, and z directions) are not directly surveyed (**Fig. 4**).

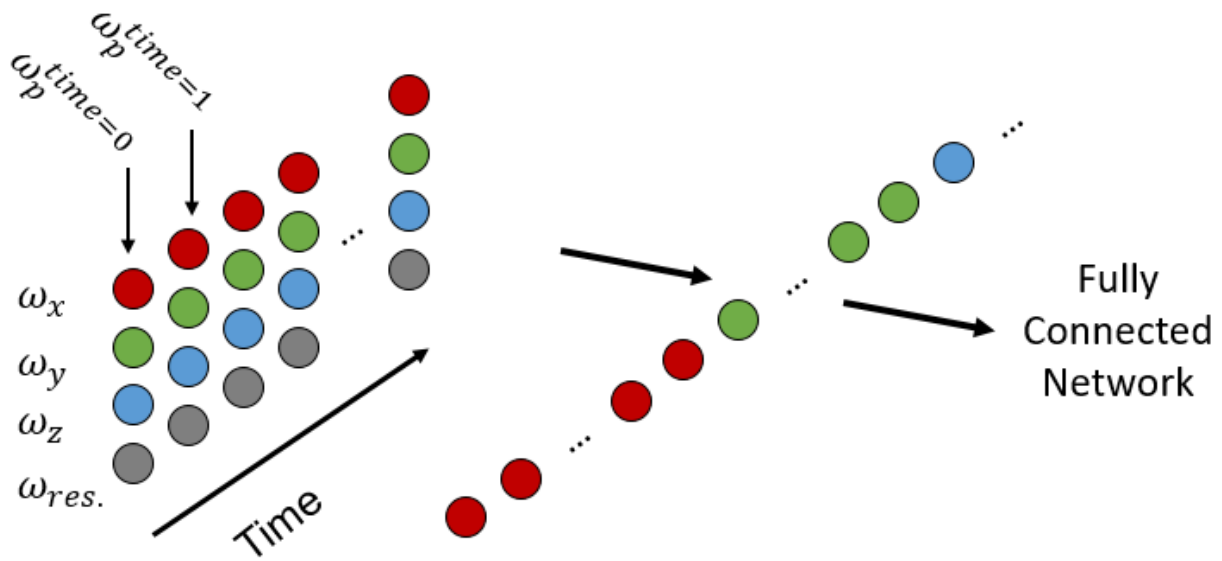


**Figure 4:** An illustration of the use of fully connected neural networks. An illustrative 4 channel signal is “flattened” before being fed into the network. The data “flattening” necessary in the pre-processing neglects the temporal relationship between the signals.

This is a known fact about the fully connected architecture. To combat that, Convolutional Neural Networks (CNNs) are designed in a way that can account for the spatial features in two dimensional inputs (Wu, Zhao, Ghazi, *et al.*, 2019). This makes them into a well suited candidate for 2D data such as images. Wu et al. takes advantage of this characteristic of the CNNs by translating the impact profile into a 2D image via pre-processing (Wu, Zhao, Ghazi, *et al.*, 2019). Then they train a Convolutional Neural Network using the produced image

data to predict the peak MPS. This approach takes the temporal relationship between the profile components into account and thereby accounts for the impact directionality.

However, while this approach is instant and accurate in predicting the peak MPS, it does not provide a full brain strain pattern, which results in an under sampling of the simulation in just one number. Thus, it is a logical next step to extend this approach to include whole brain strain pattern, which is discussed in more detail in aim 1.

## **Alternative Approaches to FE modeling**

While the Lagrangian finite element methods are utilized most frequently to model the brain, there are some alternate solutions for modeling the brain. (Ganpule *et al.*, 2017; Marques *et al.*, 2017) To illustrate the John Hopkins university (JHU) model takes advantage of a material point method (MPM) which is a meshless technique. In this technique the model is represented by material nodal points, where the equations of motion, boundary conditions and material properties are applied. A stable and non-deformable grid is used to solve the equations of motion, while shape functions are used to compute a continuous field response (Ganpule *et al.*, 2017). The downside of these approaches is that they are computationally inefficient and validation and assessment for the specific purpose of brain modeling is yet to be done (Więckowski, 2004).

## **Roadmap**

Understanding the exact mechanics of mild traumatic brain injury is an active field of research (Bailey *et al.*, 2020). Yet, it is known that strain plays a significant role in the mechanics of mTBI (Zhao, Kuo, *et al.*, 2017b). As a result, many studies have focused on developing a predictive head injury model (Svein Kleiven, 2002; Takhounts *et al.*, 2004; Fernandes *et al.*, 2018). However, there are a number of hurdles on the way of using FE

modeling for injury risk prediction. Firstly, as discussed in detail in the previous sections, obtaining the strains from an FE model is computationally expensive. Secondly, there is no clear way of relating whole brain strain patterns obtained from an FE model to injury risk. Many studies use the peak MPS or CSDM as benchmarks from FE models (E. G. G. Takhounts *et al.*, 2013; Lee F. Gabler, Crandall and Panzer, 2018). For instance, (Lee F. Gabler, Crandall and Panzer, 2018) uses a second order system to rapidly and accurately estimate the peak MPS of the entire brain. However, peak MPS and CSDM have shortcomings. Peak MPS samples the high strain values across the entire brain without attention to where the high strain region occurs. In other words, the same peak MPS value could result from high strain values in completely different regions of the brain. This could potentially result in injury to a different part of the brain or a different injury risk altogether. Similarly, CSDM samples the volume of the brain that exceeds a certain threshold. Yet, it provides no indication of the extent to which the threshold is surpassed. Further, just like peak MPS, it does not indicate the regions of the brain where the strain exceeds the threshold. These shortcomings signify the need to take a holistic approach to the brain strain distribution.

In aims 1 and 2 of this dissertation, we provide two methodologies to address this problem. In the first aim we develop a deep learning model as an alternative to FE modeling. This results in a significant improvement in terms of computational efficiency. Yet, despite the accumulating evidence of the significance of tissue level brain responses (Cai *et al.*, 2018), kinematics-based metrics (Hernandez *et al.*, 2015) continue to be used for injury prediction (Fahlstedt *et al.*, 2021). This is potentially problematic as the relationship between impact kinematics and tissue-level responses is non-linear, hence the kinematics cannot directly relate to such responses. To address that, in the second aim, we developed a strain-based simplified kinematics to provide intuitive understanding of tissue-level strains as well as the ability to easily

compare head impacts in terms of simple kinematics as opposed to complex real-world impact profiles, which are not directly comparable.

One of the applications of the methods developed in aim 1 and 2 are in the design cycle of injury mitigation instruments, such as helmets. Hence, in aim 3 we use the deep learning model from aim 1 in a real-world application scenario. We compare the widely used strain-based injury metrics (MPS and CSDM) to a well-accepted kinematics-based injury mitigation assessment method known as the Summation of Tests for the Analysis of Risk (STAR) method. We provide context for implications of potential differences between the two and provide suggestions on ways to improve the injury mitigation capability of helmets.

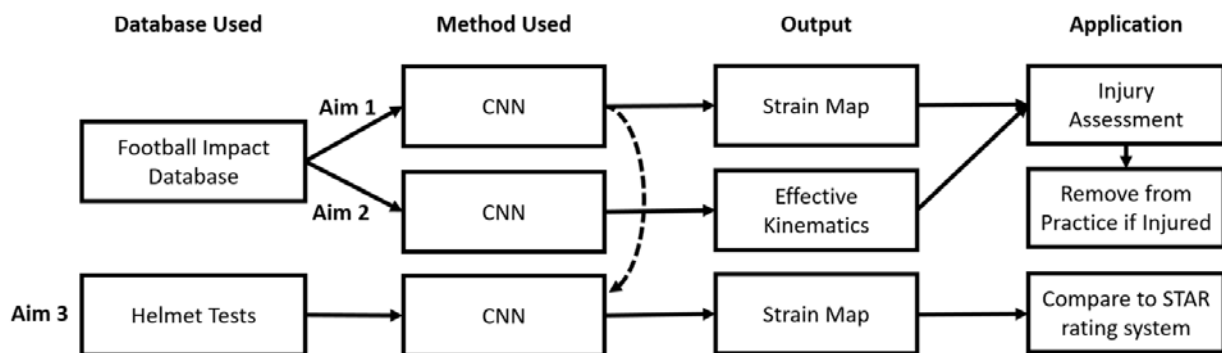


**Figure 5:** A flowchart of the aims in this dissertation. Aim1 focuses on developing an alternative to FE modeling to improve efficiency. Aim 2 addresses the gap between kinematics metrics and FE modeling by proposing a strain-driven kinematics (Effective Kinematics). Aim 3 is a real-world application of the aim 1 where a number of helmets are compared in terms of strains and the Summation of Tests for the Analysis of Risk (STAR) to provide context about the implications of using strain in helmet injury mitigation capabilities.

# **Chapter 3: Converting a head injury model implemented in Abaqus into LS-DYNA for impact simulation**

## **Introduction**

Traumatic brain injury, including sports-related concussion occurring in 1.6 to 3.8 million athletes, is considered to be a major health problem in the United States. This necessitates accurate and reliable prediction of brain injury. In the past, head impact kinematics including peak magnitudes of linear or rotational accelerations have been extensively used as injury predictors. Lately, efforts to employ finite element (FE) models of the human head are increasing. FE models translate impacts into tissue strains and hold substantial promise to improve injury prediction performance over kinematic metrics.

Numerous efforts exist to improve FE models of the human head, including optimizing brain material properties, enhancing the quality of brain meshes, etc. These characteristic differences have been identified as causes of model result disparity. However, a significant yet less studied disparity between the various human head injury models is their platform software packages. Two of the most widely used FE software packages are Abaqus and LS-DYNA. This difference contributes to model response differences that may preclude a meaningful comparison between their simulation results and injury analyses.

In this chapter, we converted our anisotropic Worcester Head Injury Model (WHIM) V2 originally developed in Abaqus into LS-DYNA format. The reason WHIM V2 was used for this portion of the study is that this model has been optimized through a mesh convergence study, which eliminates the variable of mesh size from our comparisons in this portion. Yet, the WHIM V1 with 55k elements was used in the subsequent aims as performs better in validation and hence is more biofidelic (Zhao and Ji, 2020b).

The conversion process in this study allowed us to understand the differences between these two most commonly used software packages in brain injury studies. This would facilitate the comparisons between models developed in these two packages in the future.

## Methods

The WHIM V2 with white matter anisotropy served as a baseline for model conversion. The model uses a re-meshed brain (202.8 k high-quality hexahedral elements of the brain (Zhao and Ji, 2019b)) and implements brain material property anisotropy in Abaqus using the HGO hyperelastic model coupled with viscoelasticity (Zhao and Ji, 2018). It was successfully validated against a range of impact and *in vivo* scenarios (Zhao and Ji, 2018). Unfortunately, LS-DYNA currently does not have an equivalent anisotropic material to that used in the WHIM V2 (Holzapfel-Gasser-Ogden (HGO) anisotropic material as introduced in the previous chapter). Therefore, a material optimization scheme was conducted to convert the Abaqus HGO anisotropic material model into an isotropic model in LS-DYNA while minimizing differences between model simulation responses. To that end, it was necessary to model the gray matter (GM) and white matter (WM) separately in order to preserve their response differences arising from brain material anisotropy.

Specifically, we started with the baseline WHIM V2 based on fully integrated elements with incompatible modes (C3D8I) in Abaqus. This type of element often serves as a benchmark in simulation that is free from shear locking, immune to hourglass deformation, and with minimal volumetric locking (Abaqus, 2016; Zhao and Ji, 2019b). However, this element is computationally expensive. Therefore, we next converted the model into reduced integrated elements (C3D8R) using relax stiffness hourglass control (HG) with a high scaling factor (SF) of

200 for GM and 100 for WM to maximize model simulation efficiency as suggested by (Zhao and Ji, 2019b) to mimic the C3D8I elements.

Next, an Ogden isotropic hyper-viscoelastic model was selected to approximate the anisotropic strain distribution from the previous step. The initial shear modulus in the Ogden model ( $G_0$ ) was determined *via* iterative adjustment so that a linear regression slope between the maximum principal strain distribution across all brain elements (GM and WM regions) obtained from the isotropic and the anisotropic model was within  $1.00\pm 0.05$ .

Then, using the obtained  $G_0$  value for the entire brain as a new starting point, the  $G_0$  values were separately altered in an iterative manner for the GM and WM so that the linear regression slope between the strain distribution in both GM and WM regions were within  $1.00\pm 0.05$ .

Next, the two isotropic GM and WM material models were directly converted into LS-DYNA format without any further alteration. As there were many integration schemes available in LS-DYNA, we identified the most compatible option by maximizing the match between simulation results with respect to that from Abaqus. All the tested element types examined were the selectively reduced integration (S/R; element types 2, -1, and -2) as well as all of the reduced integration schemes in LS-DYNA, enumerating each hourglass control type (HG) with three hourglass coefficients (QM) (0.01, 0.1 (default), and 1), with a maximum QM of 1 to avoid unstable simulations. **Table 4** summarizes the overall procedure of this study, including the type of material properties and element types used in each step.

**Table 4:** Summary of six simulation steps to convert the baseline WHIM using anisotropic brain material properties in Abaqus into LS-DYNA counterpart with isotropic properties.

Step	Software	Hourglass Control (HG)	Elm. Type	Material
1	Abaqus	Not needed	C3D8I	Anisotropic
2	Abaqus	Relaxed stiffness WM SF of 100 GM SF of 200	C3D8R	Anisotropic
3	Abaqus	Relaxed stiffness WM SF of 100 GM SF of 200	C3D8R	Isotropic (same for GM/WM)
4	Abaqus	Relaxed stiffness WM SF of 100 GM SF of 200	C3D8R	Isotropic (with GM/WM heterogeneity)
5	LS-DYNA	Not needed for S/R	{2, -1, 2}	Isotropic (with GM/WM heterogeneity)
6	LS-DYNA	Type{1 to 7, 9, 10}/QM of 0.001, 0.01, 0.1, 1	1	Isotropic (with GM/WM heterogeneity)

## Results

After converting the baseline WHIM (step 1 in **Table 4**) into isotropic and heterogeneous GM/WM with C3D8R (step 4 in **Table 4**), element-wise comparisons led to the following linear regression slopes ( $k$ ) and Pearson correlation coefficients ( $r$ ):  $k_{WM} = 0.91$  and  $r_{WM} = 0.71$  for the 50 WM ROIs;  $k_{GM} = 0.96$  and  $r_{GM} = 0.86$  for the 54 GM ROIs. Step-wise comparisons are reported in **Table 5**. Converting anisotropy into isotropy mostly affected the WM (a low  $r_{WM}$  of

0.78), as expected. These results suggested that the reduced integration scheme was able to preserve the simulation accuracy while maximizing computational efficiency (2h 24 min versus 38 min on a computer cluster: 15 CPUs + 2 GPUs). **Fig.5** (a, b, c) compares their fringe plots of accumulated maximum principal strain.

**Table 5:** Summary of the results from the experiments.

Reference	Target	GM		WM	
		$k_{GM}$	$r_{GM}$	$k_{WM}$	$r_{WM}$
Anisotropic/ C3D8I	Anisotropic/ C3D8R	0.97	0.92	0.93	0.95
Anisotropic/ C3D8R	Isotropic/ C3D8R	0.99	0.92	0.98	0.78
Isotropic/ C3D8R	LS-DYNA HG = 1	0.93	0.88	0.98	0.85
Anisotropic/ C3D8I	LS-DYNA HG = 1	0.89	0.87	0.89	0.64

When further converting into LS-DYNA, results from the S/R integration (element types 2, -1, -2; step 4 in **Table 4**) did not match the Abaqus counterpart (e.g.,  $k_{WM} = 1.12$ ,  $r_{WM} = 0.42$  and  $k_{GM} = 1.32$ ,  $r_{GM} = 0.72$  with element type 2). The closest response was obtained using reduced integration with HG types 1, 2, or 3 with the default QM of 0.1 (e.g., step 6 in **Table 4**;

**Fig. 5d).** A QM of 1 led to unstable simulations in most cases. Results from HG type 6, 9 and 10 were always unstable regardless of the QM (type 8 for shell elements was not applicable here).

These findings were further re-affirmed by simulating a separate impact case (self-reported concussion case (Hernandez *et al.*, 2015)). This verifies that the observations in this study can be extended to other impacts as well.

## **Discussion and Conclusion**

The goal of this chapter was to establish a link between two of the most frequently used FE method software platforms, Abaqus and LS-DYNA. We started from anisotropic WHIM V2 along with Enhanced Integrated Hexahedral Elements (C3D8I). Initially, we implemented RELAX STIFFNESS HG control with high SF, after parametrically proving that the results from such HG configuration match closely with the C3D8I in Abaqus. We revalidated the resulting model using experimental cadaver data. Then, we conducted a material optimization to match the results obtained from the strain map from the previous step. In the final step with Abaqus, we conduct a material optimization to model the anisotropic material with an isotropic material, while maintaining the heterogeneity between WM and GM. Finally, we convert the best model to LS-DYNA format with different configurations and identify the one that matches the Abaqus results the best, which establishes a link between the two software packages (Error! Reference source not found.).

Within the LS-DYNA software package, S/R did not yield comparable results, suggesting that the integration in the two software packages is performed differently. The final results from LS-DYNA suggested that reduced integration with HG types 1, 2, and 3 coupled with the default QM of 0.1 produced the most similar results relative to the baseline C3D8I elements in Abaqus.

However, the similarity of the results from these HG types decreased as the QM decreased. The results further indicate that when using HG types 4, 5, a QM lower than the default value results in a higher Pearson correlation coefficient, and hence should be used for more reliable results. This was while HG type 6 appeared to become less stable as QM decreased and finally became unstable at QM = 0.001. However, all of the simulations with this HG type were unrealistic although they were terminated normally. In addition, the results from HG type 10 was always unstable.

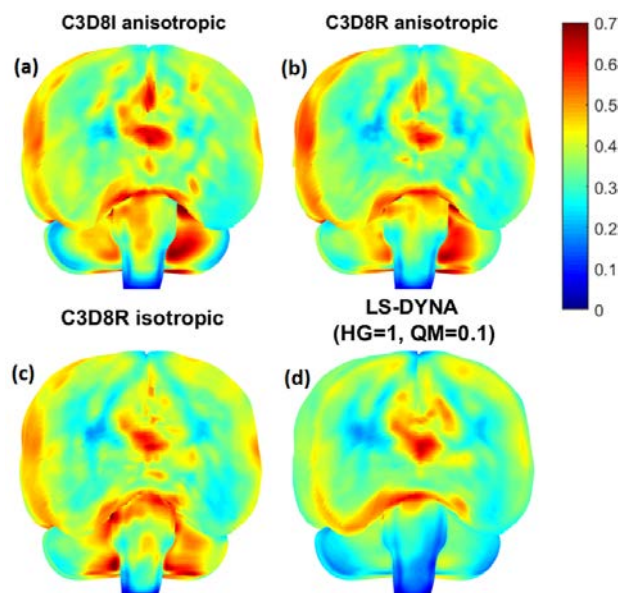


**Figure 6:** Cumulative maximum principal strain from C3D8I with an anisotropic material model (a), C3D8R with anisotropic material and high SFs (b), optimized isotropic material with GM/WM heterogeneity using C3D8R and high SFs (c), and same isotropic materials converted into LS-DYNA (d).

In conclusion, based on these results we can confirm that using different software packages can indeed cause discrepancies in model simulations. Based on the results from this section, these differences could be minimized by using the properties described above. However, many models, to maximize validation performance, do not conform to these settings, which can introduce a divorce between models simulated in different packages and preclude

cumulative knowledge. Addressing this problem could be a worthwhile contribution to the modeling-based research and resolve some of the inconsistencies as a result of using different software packages. However, this exploration is beyond the scope of this thesis.

## **ACKNOWLEDGEMENT**

Funding is provided by the NIH grant R01 NS092853.

## **Chapter 4: Aim 1: Assessment of a CNN based approach to obtain real-time element-wise strain prediction for the entire brain directly from impact profile**

Published in the Journal of Neurotrauma as:

Kianoosh Ghazi, Shaoju Wu, Wei Zhao, and Songbai Ji. 2020. “Instantaneous Whole-Brain Strain Estimation in Dynamic Head Impact.” *Journal of Neurotrauma*, in press.

<https://doi.org/10.1089/neu.2020.7281>.

### **Introduction**

TBI is a major health concern across the world (Faul *et al.*, 2004) and is caused by the strain generated in the brain tissue as a response to the exposure of the head to extreme dynamic movement. These movements are then translated to the brain and generate large tissue strains that can result in injury. Several methods were developed in the span of several years to reliably assess the risk of concussion. A majority of these are based on translating the six degree-of-freedom impact temporal profile into a scalar value. These values are then translated into injury risk using various techniques such as a logistic regression technique. Some of these methods are the head injury criterion (HIC; (Versace, 1971)) and Brain Injury Criterion (BrIC; (E. G. Takhounts *et al.*, 2013)) which consider the acceleration profile. However, as mentioned previously, these metrics are scalar and neglect the temporal profile shape of the impact, which has a significant effect on the generated strains in the brain tissue. Further, as they are scalar, a majority of them neglect the impact directionality. Hence, these metrics oversimplify the impact and are insufficient to provide insight into the brain tissue level strains to an impact.

To that end FE models play an increasingly important role to provide insight into the tissue level response. With the advancements in the computational power, the sophistication of these models have proportionally increased to better model a brain impact scenario (Yang et al., 2011; Madhukar and Ostoja-Starzewski, 2019). To increase the biofidelity, recent models have increased the mesh resolutions (Miller, Urban and Stitzel, 2016; Ghajari, Hellyer and Sharp, 2017; Zhao and Ji, 2019a; Zhou, Li and Kleiven, 2019a), incorporated more realistic brain anatomy (Atsumi *et al.*, 2018; Zhou, Li and Kleiven, 2019b; Zhao and Ji, 2020c), and more accurate brain-skull boundary conditions (Scott, Margulies and Coats, 2016; Zhou, Li and Kleiven, 2018). Further these efforts have expanded to the model validation in different ranges of impacts from high-rate (Hardy *et al.*, 2001, 2007) to mid-rate (Alshareef *et al.*, 2018a; Guettler *et al.*, 2018) and in vivo loading conditions (Knutsen *et al.*, 2014; Chan *et al.*, 2018; Lu *et al.*, 2019).

Yet, these advances in FE modeling of the brain increase the resources needed to model even a single simulation substantially. This is a known drawback with FE modeling. For instance, simulating a single head impact will on average take from several hours to upwards of days (Mao et al. 2013; Miller et al. 2016; Zhao and Ji 2019b; (Lu *et al.*, 2019; Zhou, Li and Kleiven, 2019b). This significant computational cost renders this method unfeasible on a football field where neither the time nor the resources are available.

The need to increase the efficiency of brain FE models is a well-known issue (Franklyn *et al.*, 2005; Takhounts *et al.*, 2008), and several strategies were introduced to mitigate the computational cost from FE modeling. One of these methods is to develop injury metrics that are based on a more simplistic model, the response of which can be obtained instantaneously. In other words, these models map the complex FE simulation onto a more simplistic problem that can be readily solved. The embedded parameters of these simple models are determined

offline using regression against the peak MPS from the FE simulation (Gabler *et al.*, 2018; Laksari *et al.*, 2020a). Once the parameters are determined, the simple model can be used to provide an accurate estimation of the peak MPS instantaneously. However, similar to the other scalar metrics discussed hitherto, these methods result in an over-simplification of the information obtained from the FE model into a single value. Additionally, simply using the peak resultant acceleration from the impact can outperform the use of MPS which renders such methods potentially less effective (Beckwith *et al.*, 2018; Wu, Zhao, Rowson, *et al.*, 2019; Anderson *et al.*, 2020).

To address this shortcoming of the scalar models, Ji and Zhao proposed using pre-computation (Ji and Zhao, 2015) (as discussed in the background section). This methodology is a real-time technique to obtain the whole brain strain pattern to an impact using a set of pre-defined impacts. These impacts are spread in across different directions and severities. Given a new impact, this method uses interpolation or extrapolation to predict the brain strain pattern based on the available data. This method can accurately estimate the strains for an impact with one major rotational velocity peak. However, for more complex impacts, this method significantly under-estimates the brain strains. This is expected as a result of the simplicity of the pre-defined impacts.

Recently pre-computation has been extended to deep learning approaches (Wu, Zhao, Ghazi, *et al.*, 2019). These approaches pre-process the impact profiles into discrete data points which are then inputted into the network for training. These models can then output an FE model output, such as peak MPS. Wu *et al.* uses this approach to train a CNN. They first translate the impacts in the entire database into a two-dimensional (2D) image format with the same size in their pre-processing step. Then using this data and the available peak MPS from the simulation, the CNN is able to implicitly (as opposed to explicitly (Ji and Zhao, 2015)) learn

the non-linear relationship between the impact profile and the peak MPS. This method proved successful with multiple real-world impacts measured in sports-fields. However, this success was limited to the peak MPS of the entire brain and specific regions of the brain.

Hence, the next step is to extend this methodology to predict the entire brain strain pattern. This is important since the strain pattern that can be uniquely obtained from FE simulations contains important information about the condition of the brain tissue. Yet, it mitigates the long and costly process of simulation which could render this approach feasible for a sideline setting. Further, the strain pattern generated by an impact allows for machine learning classification approaches (such as network-based injury assessment methods (Wu, Zhao, Rowson, *et al.*, 2019)) to assess the risk of injury.

In the following sections of this aim, we first systematically optimize the network architecture and hyper parameters, using the CNN from (Wu, Zhao, Ghazi, *et al.*, 2019) as a starting point. This process is done using a 10-fold cross validation for our entire database. Then, to test the CNN with an independent testing dataset, we retain the CNN architecture from the previous step and predict the MPS distribution for a set of injury labeled data from the National Football League (NFL; N=53, 20 concussions and 33 non-injury cases). This step helps characterize any performance degradation as a result of using the CNN compared to direct FE simulation. If successful, testing the CNN with the independent database could illustrate the capability of this method as a far more efficient substitute for direct FE simulation, while sacrificing very little accuracy.

## Methods

### CNN Training Data

The original data used for this study is a combination of a dataset from the Stanford University (SF) with a size of 110 (Hernandez *et al.*, 2015), a dataset from the National Football League (NFL) with a size of 53 (Sanchez *et al.*, 2018), and a dataset of 314 impacts recorded in American high-school football (HF) (Montenigro *et al.*, 2017). However, this data size is small compared to the databases often used to train CNNs (which is in the order of thousands or even millions (Günther *et al.*, 2014)). Hence, we used data augmentation based on the SF and NFL databases to increase the number of training data.

In the process of augmentation, we first used permutation with the 3 components of the rotational velocity (i.e., xyz, xzy, yxz, yzx, zxy, and zyx). Then we rotated the rotation axis in each time step using a randomly generated rotation axis. The azimuth and elevation angles ( $\theta$  and  $\alpha$ , respectively) of the rotational axis,  $\Omega(\theta, \alpha)$ , were then determined based on peak magnitude of rotational velocity. Due to head symmetry about the mid-sagittal plane, only half of the  $\Omega$  sampling space was necessary (Zhao, Kuo, *et al.*, 2017b). Therefore, for  $\Omega$  with  $\theta > 90^\circ$ , its corresponding “conjugate rotational axis”,  $\Omega'(180^\circ - \theta, -\alpha)$ , was used to maximize the use of  $v_{\text{rot}}$  profiles for generating unique brain responses. If axes were conjugated the strain pattern of the brain was mirrored to match the velocity profile. In the same fashion, several batches of data were constructed. The SF data was used to create a dataset of ( $n = 1320, 110 \times 6 \times 2$ ) and the NFL dataset was used to create four batches of augmented data ( $n = 1272, 53 \times 6 \times 4$ ). These augmentations were focused on the more severe range of impacts (21.9-40 rad/sec (Rowson *et al.*, 2012)). The same process was used to create less severe impacts in the sub-concussive range (2-21.9 rad/sec) using the SF and NFL data sets. This led to 2592 ( $110 \times 6 \times 2 + 53 \times 6 \times 4$ ) additional training samples. **Fig. 6** illustrates the distribution of the database.

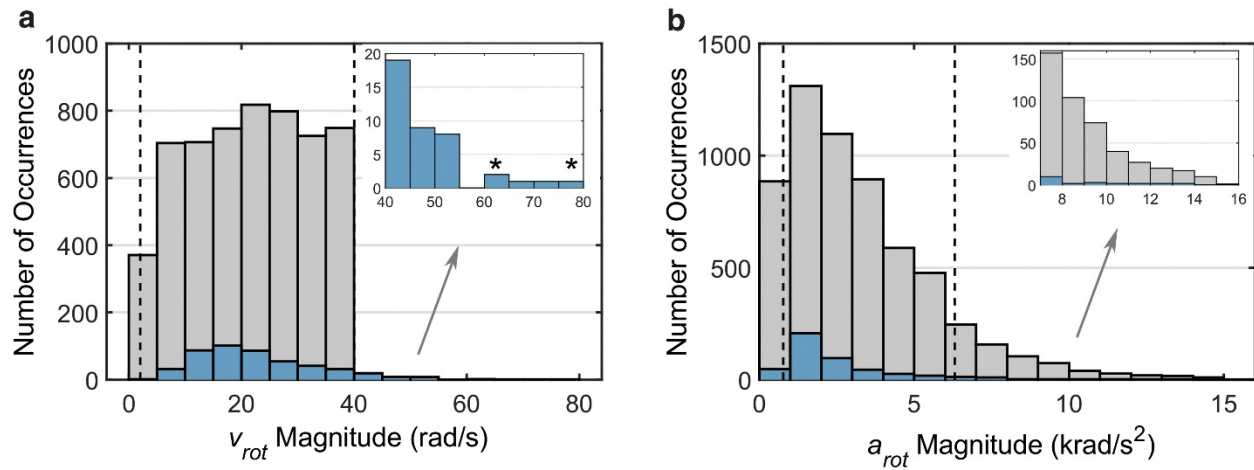


**Figure 7:** Histograms of peak resultant rotational velocity (a;  $v_{rot}$ ) and acceleration (b;  $a_{rot}$ ) for the entire training sample ( $n = 5661$ ). The real-world impacts are overlaid. Regions between the two vertical lines are considered “in range.” The starred cases are explained in more detail in **Fig. 10**. The blue bars are a subset of the database we used as independent validation data (scaled by 10 for visibility). This process is detailed in the following sections.

## CNN Architecture

The previous CNN architecture (Wu, Zhao, Ghazi, *et al.*, 2019) was further empirically optimized to estimate element-wise peak MPS (regardless of the time of occurrence), by minimizing a weighted loss function (described subsequently) in a 10-fold cross validation using the entire training data set ( $n = 3069$ ). Compared with the previous architecture, the updated network consists of three convolutional layers, with 64, 64, and 32 filters, each with sizes of  $3 \times 30$ ,  $1 \times 3$ ,  $1 \times 3$ , and stride sizes of  $1 \times 2$ ,  $1 \times 2$ ,  $1 \times 1$ , respectively (**Fig. 7**). They are followed by a pooling layer of a size of  $1 \times 2$  with a stride size of  $1 \times 2$ , a flattening layer (with a dropout rate of 0.2), and three fully connected layers with sizes of 200, 100, and 55 k (the last of which corresponds to the number of brain elements to predict responses). The pooling layer and the first fully connected layer (of a size of 200) adopted a rectified linear unit (ReLU) activation function, while all other layers used a linear activation function. A batch size of 256 was chosen with the number of epochs set to 400. An early stopping criterion was used to avoid overfitting.

The CNN architecture was implemented using Keras library (Version 2.2.4) with Tensorflow (Version 1.11.0) backend.

To further increase the performance of the CNN, we designed our loss function in a way that would impose more penalty to FE model elements that frequently result in a larger variance across all impacts. To that end, we calculated the variance of each element across all impacts in the dataset, and used them as a weighting coefficient in the loss function.

$$loss = \frac{1}{p} \sum_{i=1}^p \left( \frac{1}{q} \sum_{j=1}^q \sigma_i \times (x_{ij} - y_{ij})^2 \right) \times 100$$

where  $x_{ij}$  and  $y_{ij}$  are the estimated and directly simulated MPS values for the  $i^{\text{th}}$  brain element in the  $j^{\text{th}}$  training sample impact, respectively;  $p$  is the number of the brain elements in the anisotropic WHIM V1.0,  $q$  is the number of the training samples (e.g., 90% of the 3069), and  $\sigma_i$  is the standard deviation of the  $i^{\text{th}}$  brain element among the  $q$  training samples. An additional scaling factor of 100 was used to mitigate the loss of data precision resulting from round-off errors during the iterative training process, as values of  $x_{ij}$ ,  $y_{ij}$ , and  $\sigma_i$  were typically small. This was important as the internal CNN architecture uses 32-bit single-precision floating numbers

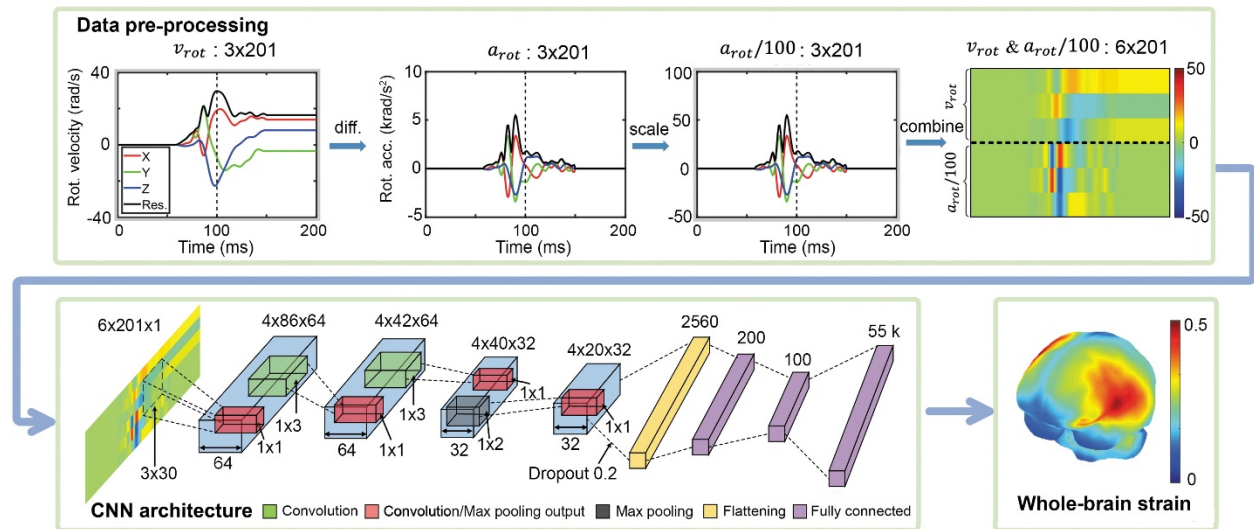


**Figure 8:** Flow chart showing preprocessing of a head impact kinematic profile (top) and an empirically optimized convolutional neural network (CNN) architecture (bottom) to predict the distribution of peak maximum principal strain (MPS) of the entire brain. The preprocessed vrot profile (after transforming to its “conjugate rotational axis,” and if needed, shifting, and padding (Wu, Zhao, Ghazi, *et al.*, 2019)) is combined with the corresponding pre-processed and scaled arot profile (effectively, with a unit of 100 rad/sec<sup>2</sup> after scaling). The resulting two-dimensional [2D] image representation serves as the CNN input.

## CNN Estimation Performance

The CNN performance was characterized by a 10-fold cross validation across the entire dataset ( $n = 5661$ ). In this process, a linear regression model is fit to each predicted strain pattern from the CNN and the directly simulated counterpart. Further, for cases that required rotational axis conjugation, the strain pattern was mirrored with respect to the mid-sagittal plane to reflect the conjugated rotational axis. In an ideal case where the CNN pattern prediction is identical to the direct simulation, the linear regression slope ( $k$ ) and the Pearson correlation coefficient ( $r$ ) between these strain patterns are both equal to 1. We empirically determined that the prediction is sufficiently accurate when the  $k$  and  $r$  error are less than 10% ( $0.9 < k < 1.1$  and  $r > 0.9$ ). The ratio of cases that satisfy this criteria to the entire database is referred to as the “success rate”.

As the augmented dataset was controlled in terms of peak rotational velocity (2-40 rad/sec; **Fig 6a**), a majority of the peak velocity ranges were in this range. However, such concentration did not exist in the acceleration since it was not controlled in the augmentation procedure. Further, a number of impacts had a large initial rotational velocity. This is because the SF dataset was given in terms of rotational velocity (as opposed to rotational acceleration) and contained non-zero values at the starting point  $s$  (the ratio to the peak  $v_{rot}$  magnitude of 18.1 – 22.2% for the given data set, range 0–100%). This issue could be further exacerbated by the scaling, perturbation, and the rotations in the augmentation procedure. This is important since

the large initial velocity will effectively decrease the change in rotational velocity magnitude and result in outliers.

In order to evaluate the performance of the CNN independent of the non-zero initial velocity characteristic of some impacts in the database and “out of range” velocity or acceleration, we removed them and reassessed the CNN performance. Impacts with peak rotational velocity outside the targeted range (1.5% of the cases), with peak rotational acceleration below the 10th or above the 90th percentile (20.0% of the cases), or with the ratio between the initial and rotational velocity peak values  $>10\%$  (11.0% of the cases), were empirically removed, which resulted in a new database with 4298 impacts (75.9% of the initial database; some of these category ratios have overlap). The new obtained database was also used in a 10-fold cross validation and compared against the directly simulated counter parts.

## **Injury Prediction**

The final goal of FE analysis of the brain is to assess the risk of injury. Consequently, it is crucial to ensure using the CNN does not degrade the injury prediction performance based on the strain pattern. To that end, we use the injury labeled original NFL database ( $N = 53$ ). To ensure that the NFL data is used as an independent dataset, we remove the original NFL dataset as well as all the augmented data that were generated based on the NFL data and retrain the CNN model. Removing these cases resulted in a database with 3064 impacts (5661-53 x 6 x 8 - 53) to retrain the CNN architecture with. The resulting distribution of the peak rotational velocity and acceleration are shown in **Fig. 8a** and **4b** respectively. The assessment of the CNN performance for strain pattern prediction is done similarly to the previous parts in terms of  $k$  and  $r$ .

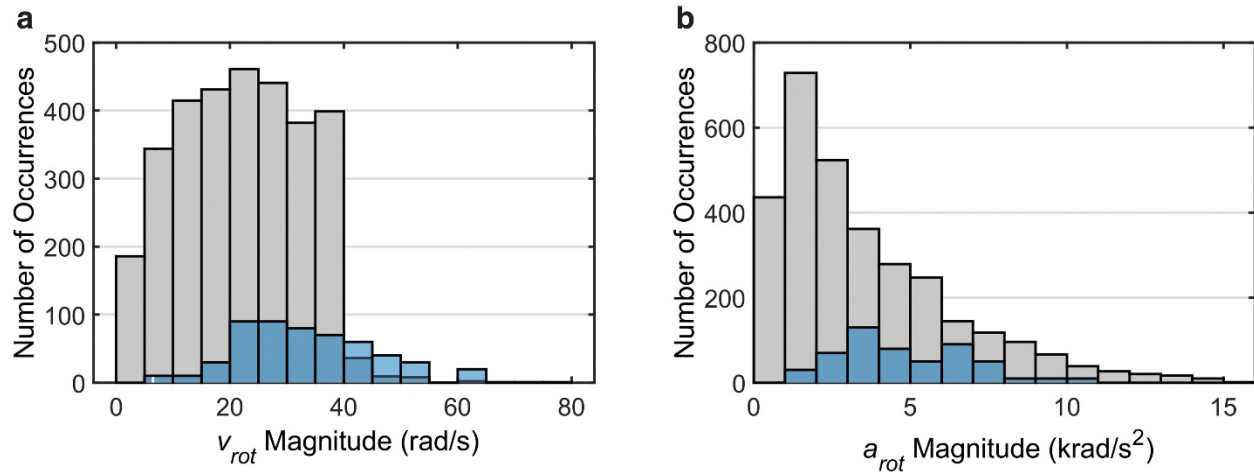


**Figure 9:** Histograms of peak resultant rotational velocity (a;  $v_{rot}$ ) and acceleration (b;  $a_{rot}$ ) for a subset of data ( $n = 3064$ ) used to train and test on an independent National Football League (NFL) data set ( $n = 53$ ), which is overlaid (number of occurrences multiplied by 10 to improve visualization).

MPS distribution can be regarded as a set of features (50k, one for each element strain value) to classify an impact into the injury or non-injury group. To that end, we used machine learning algorithms—namely Support Vector Machine (SVM) and Random Forest (RF)—for the classification. The classification was repeated in the exact same way for the CNN estimated and the directly simulated MPS pattern. Further, as these methods both require some kind of feature selection, we implemented two feature selection methods using either F-score or RF “gini” importance ranking separately. To characterize the performance of the classification in each case, we reported the accuracy, sensitivity, specificity, and area under the receiver operator’s curve (AUC). All injury performances were carried out using a leave-one-out cross-validation. This approach was following a similar publication that was previously published (Cai *et al.*, 2018).

The hyper parameters of the SVM and RF method were empirically determined. In case of using feature selection, following the findings of (Cai *et al.*, 2018), we used the top 4% of

features using F-score. The SVM used a linear kernel and the depth of the RF was determined separately for feature selection and classification (Table 2).

**Table 6:** The number and the depth of trees, (N, D), used in RF depended on whether RF was used for feature selection (FS) or classification (CL), as shown below.

	<b>SVM (CL)</b>	<b>RF (CL)</b>
<b>RF (“gini” importance ranking), FS</b>	(10, 2): FS	(100, 2): FS (1000, 2): CL
<b>F-score, FS</b>	N/A	(50, 2): CL

## Data Analysis

All head impacts were simulated using the anisotropic WHIM V1.0, which took ~30 min for one impact of ~100 ms duration (double precision with 15 central processing units [CPUs] and graphics processing unit [GPU] acceleration; Intel Xeon E5-2698 with 256 GB memory, and 4 NVidia Tesla K80 GPUs with 12 GB memory). Another 30 min was necessary to extract peak MPS distribution across the impact duration. In total, this study required ~8 months of nonstop computations to generate the data, which was mitigated by concurrent running of 5–10 jobs. Each CNN training took ~9 min per fold for the entire data set on an NVIDIA Titan X Pascal GPU with 12 GB memory. Predicting the response distribution for a testing profile was instant (<0.05 seconds)

## Results

In a 10-fold cross validation, the linear regression slope and the Pearson correlation coefficients ( $k$  and  $r$ , respectively) were found to have an average value of  $0.99 \pm 0.06$  and  $0.96$

$\pm 0.04$  respectively. This resulted in a 92.1% “success rate” across all impacts in the database (Fig. 9a).

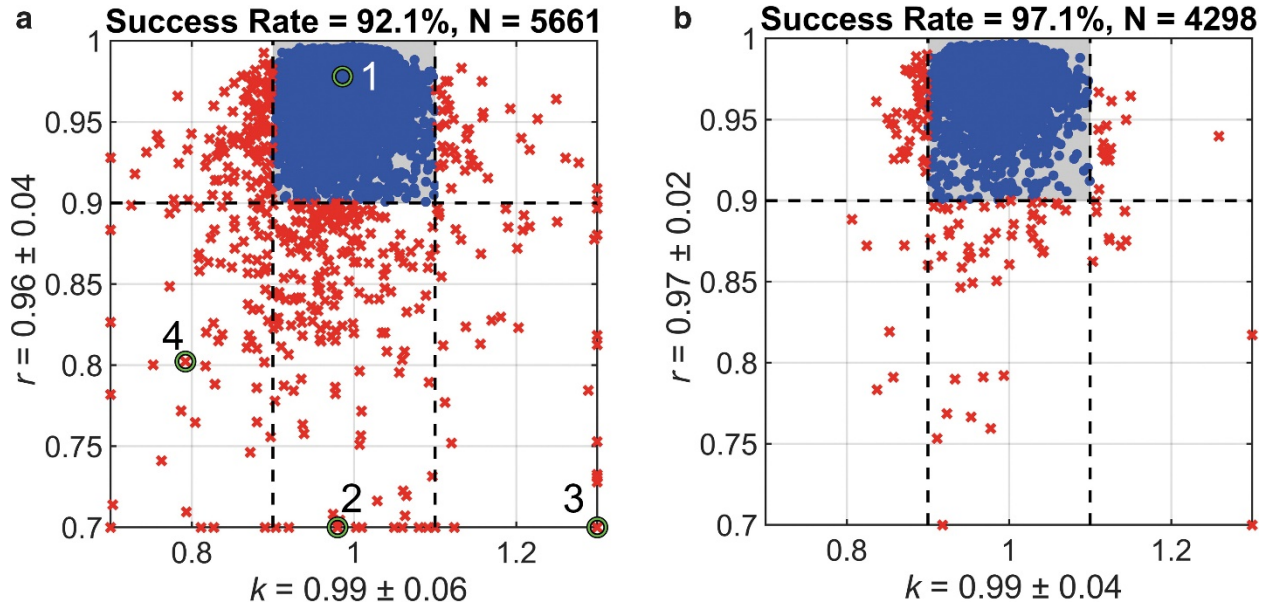


**Figure 10:** Summary of  $k$  and  $r$  when comparing convolutional neural network (CNN)-estimated and directly simulated maximum principal strain (MPS) distributions using a 10-fold cross-validation, using either the entire (a) or a subset of (b) the impact data set focusing on “in-range” impacts (after removing “outliers”). The shaded area represents impact cases of sufficient accuracy (i.e.,  $0.9 < k < 1.1$  and  $r > 0.9$ ). The  $k$  and  $r$  axes are capped to improve visualization. The identified four cases in (a) are further illustrated in Fig. 10.

A majority of the failed cases were observed to have similar traits: (1) out-of-range velocity (Fig. 8b) peak, (2) out-of-range acceleration (Fig. 8c), and (3) a high initial velocity (Fig. 8d). Removing these outliers resulted in an increase in the success rate (Success Rate = 97.1%; Fig. 7b) using a 10-fold cross validation.

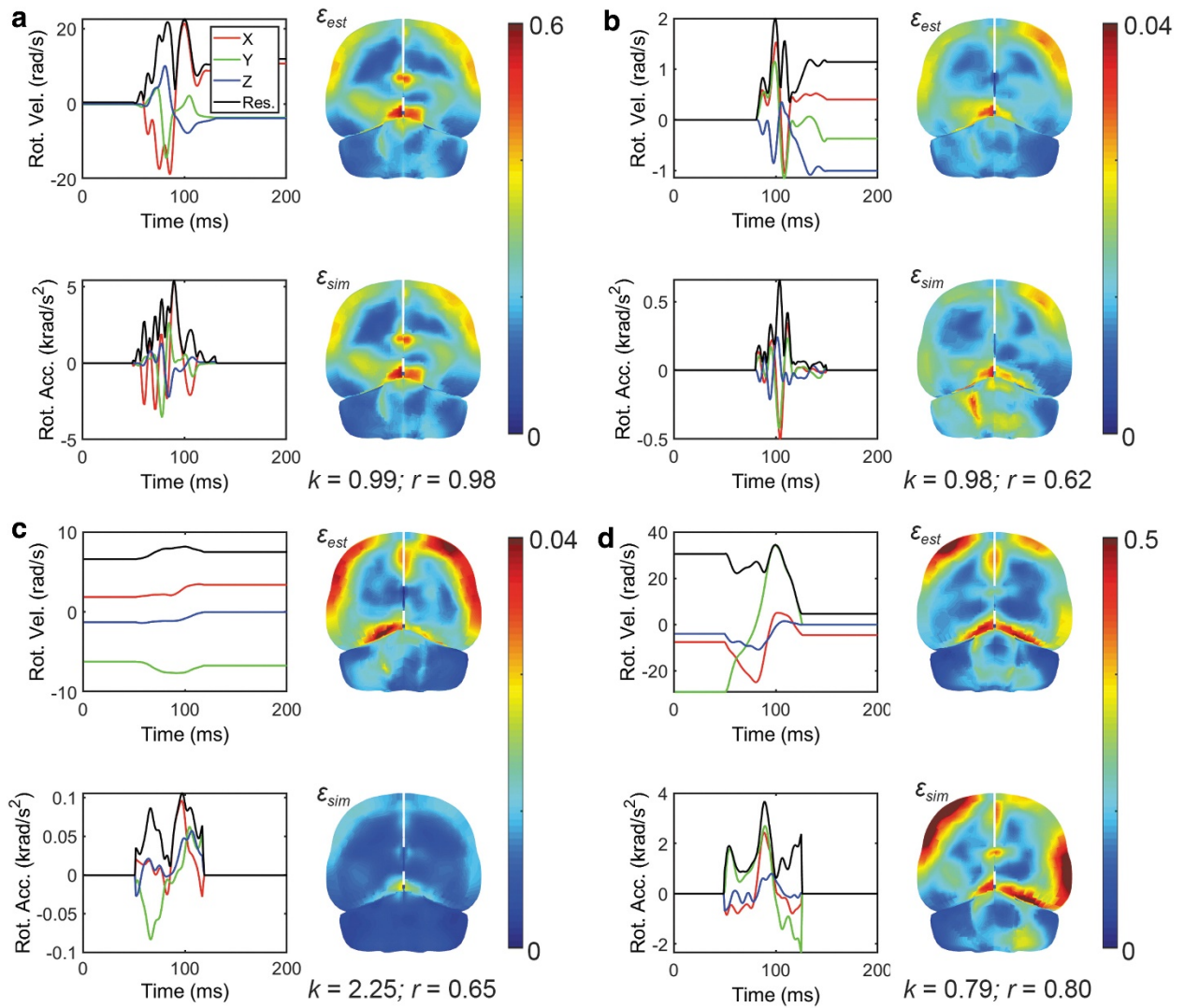


**Figure 11:** Representative impact cases showing impact vrot and arot profiles with the convolutional neural network (CNN)-estimated ( $\epsilon_{est}$ ) and directly simulated ( $\epsilon_{sim}$ ) maximum principal strain (MPS) distributions for a successful prediction (a) or “failed” cases resulting from (1) out-of-range vrot peak magnitude (b); (2) out-of-range arot peak magnitude together with a large initial vrot value (c); and (3) a large initial vrot value (d). The four cases correspond to cases 1–4 identified in **Fig. 6**.

**Fig. 11 a** illustrates the performance of the CNN when using the NFL dataset as an independent testing data.  $k$  and  $r$  were found to have average values of  $0.99 \pm 0.05$  and  $0.96 \pm 0.02$  respectively. 96.6% (51 out of 53) of the impact strains were predicted with sufficient accuracy. Yet, even the impacts that did not pass the “hard” success threshold were reasonably accurate (**Fig. 11b-d**).

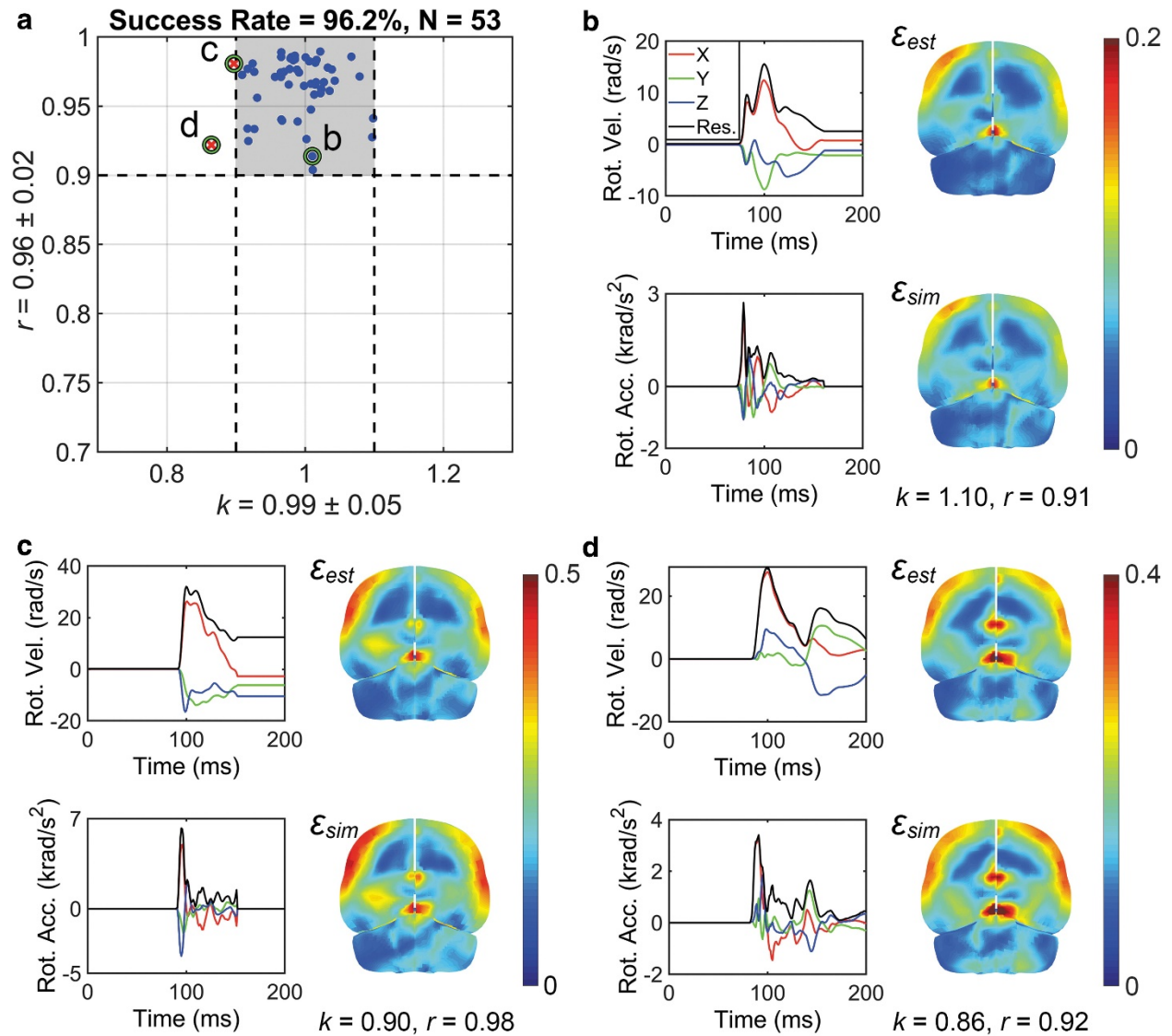


**Figure 12:** Summary of  $k$  and  $r$  for convolutional neural network (CNN)-estimated ( $\epsilon_{est}$ ) and directly simulated ( $\epsilon_{sim}$ ) maximum principal strain (MPS) distribution for an independent National Football League (NFL) impact data set (a; shaded area represents impacts of sufficient estimation accuracy, i.e.,  $0.9 < k < 1.1$  and  $r > 0.9$ ). Three representative impacts are selected to show a successful estimation (b; purposefully chosen to represent an  $r$  toward the threshold value for success) and two “failed” cases (c and d). The latter two cases only failed “marginally”; that is, their corresponding  $k$  and  $r$  were rather close to their success threshold values.

**Table 7:** Summary of injury prediction performances in terms of accuracy, sensitivity, specificity and AUC using CNN-estimated (“CNN”) or directly simulated (“WHIM”) MPS distributions. Injuries are predicted using either SVM or RF with feature selection (specified in parenthesis) based on either F-score or RF “gini” importance ranking (Cai *et al.*, 2018). For comparison, baseline performances using peak MPS of the whole brain and logistic regression are also reported. All performances are evaluated *via* leave-one-out cross-validation for objective comparison. Using

RF either for injury prediction or feature selection, 50 trials are used to account for the random initialization. Performances that are higher than the baseline are in bold ( $p < 0.05$ ; where appropriate).

Performance category		Accuracy	Sensitivity	Specificity	AUC
SVM (F-Score)	CNN	<b>0.79</b>	0.65	<b>0.88</b>	0.84
	WHIM	<b>0.79</b>	0.65	<b>0.88</b>	0.82
SVM (“gini”)	CNN	<b>0.83±0.02</b>	0.62±0.06	<b>0.96±0.03</b>	<b>0.88±0.01</b>
	WHIM	<b>0.83±0.02</b>	0.63±0.04	<b>0.94±0.03</b>	<b>0.87±0.01</b>
RF (F-Score)	CNN	<b>0.81±0.01</b>	<b>0.74± 0.02</b>	0.85± 0.01	0.79±0.01
	WHIM	<b>0.78±0.01</b>	<b>0.66±0.02</b>	0.85±0.004	0.80±0.01
RF (“gini”)	CNN	<b>0.83±0.02</b>	<b>0.71±0.03</b>	<b>0.90±0.03</b>	<b>0.87±0.01</b>
	WHIM	<b>0.83±0.02</b>	<b>0.71±0.03</b>	<b>0.90±0.03</b>	<b>0.87±0.01</b>
Peak MPS	WHIM	0.77	0.65	0.85	0.86

## Discussion

Brain strain distributions are of high importance to understand the mechanics of concussion and classify injury. The main method to obtain the brain strain distribution is through FE modeling, which requires significant computational power and a substantial amount of time. Hence, they are unfeasible in a sideline setting. The outcome of this aim reduces the significant amount of time required to complete a single simulation (hours or even days depending on the duration of the impact and the FE model), to less than one second on a low-end laptop. This achieves a ~36k fold speedup, which would be even more with some other models that require more time to simulate than WHIM. This work is a significant improvement over the previous work, which used a simpler CNN architecture to predict only the peak MPS of the entire brain or specific regions of the brain (a single value), and extends that to predict the spatially detailed

brain strain pattern in the entire brain (50k values, one for each brain element in WHIM). This work can be readily used in a sideline setting without any additional equipment.

Further, the CNN-estimated brain strains can be reliably used for feature-based injury classification as its performance is comparable to that of the direct simulation. The fact that feature-based injury metrics often outperform scalar metrics along with logistic regression lends more strength to the CNN approach used in this study. The random forest (RF) classification technique using the “gini” importance ranking for feature selection consistently had the best performance across almost all categories. Collectively, these findings support the use of CNN to instantly estimate spatially detailed brain strains for real-world applications in the future.

## **Potential Applications**

This approach has the potential to revolutionize the field of TBI research and head gear standards and testing as it makes the brain strain distribution readily available. This would have a broad application in the field of brain biomechanics in general. For instance, despite the consensus that the brain strain-based approximations are more closely related to injury than kinematic metrics (King *et al.*, 2003), kinematic-based approximations (e.g. acceleration-based approximations) are still widely used for headgear design and clinical applications. This is perhaps due to the lack of availability and the demanded resources for FE models. Our model fills the gap of readily translating the available impact data into cumulative brain strains. This method adds a level of sophistication to the currently available methods that are solely based on impact kinematics (e.g., Risk Weighted cumulative Exposure [RWE]. (Urban *et al.*, 2013; Davenport *et al.*, 2014) Cumulative Head Impact Index [CHII], (Montenigro *et al.*, 2017) and impact density (Broglia *et al.*, 2017)).

The transition to using cumulative injury metrics using FE model strains is already underway (Karton, Hoshizaki and Gilchrist, 2020). Yet, the current approaches are limited to the peak

strain value of the entire brain from a subset of impacts. The advantage of the CNN approach compared to peak MPS based approaches is the ability to provide a detailed, region-specific strain distribution. This enables obtaining correlation between region-specific, cumulative strain exposure with the corresponding localized brain injury findings, either on an individual level or a groupwise basis. This is a significant improvement in neural health monitoring over the “hybrid” injury metrics that provide instant peak MPS in the entire brain but not its anatomical location or distribution (Lee F Gabler, Crandall and Panzer, 2018; Laksari *et al.*, 2020a). Injury metrics that provide regional MPS exist but do not account for cumulative effects from repeated head impacts (Chiara Giordano, 2014; Zhao, Cai, *et al.*, 2017b).

Another potential application of the pre-trained CNN model is in protective head gear design. In practice, the CNN could be used to provide insight into the distribution of the strains sustained by the brain as a feedback to help assess the effectivity of the design. It can pinpoint specific regions of the brain that are experiencing the largest strains for a given test scenario using the head gear. a targeted multi-scale modeling could also be launched. This approach could serve as a vessel to answer questions about how the impact external energy is transmitted to the brain and leads to axonal undulation, swelling, and microtubule breakage (Ahmadzadeh, Smith and Shenoy, 2014; Zhu, Gatti and Yang, 2016; Montanino and Kleiven, 2018) that are characteristic of diffuse axonal injury (Smith, Meaney and Shull, 2003). These applications could pave the way for swift advancements in TBI biomechanics.

## **Limitations and further developments**

A less recognized limitation with not only this aim but the current stage of TBI biomechanics is that it focuses solely on the peak positive strains. This, in effect, neglects the negative strain values—tissue compression—that are also important and can cause injury (Bar-Kochba *et al.*, 2016). Further, while the current understanding focuses on a “static picture” of the

strain pattern (cumulative strains), the temporal history of tissue strain/strain rate during the head impact could also play a role in the risk of brain damage. This is similar to the temporal profile of dynamic head impact kinematics, on which, numerous injury metrics are shaped and is also the driver for any impact simulation. Rapidly reproducing the spatiotemporal details of brain strain (vs. spatial distribution alone) is another potential path that hold value for exploration in the future.

Second, while this method achieves comparable injury prediction results compared to direct simulation, the peak angular acceleration outperforms the FE based metrics for this particular dataset (e.g., sensitivity of 0.80 for peak  $a_{rot}$  vs. 0.71 using RF for both classification and feature selection based on MPS distribution, or 0.65 based on peak MPS via logistical regression). The same observation was made using the Global Human Body Models Consortium (GHBMC) model when compared with peak MPS (Anderson *et al.*, 2020). However, the NFL injury dataset is known to suffer from reconstruction errors (Pellman *et al.*, 2003; Sanchez *et al.*, 2018) and the under-sampled non-injury cases may have significant implications in injury prediction as well (Chiara Giordano, 2014). Further, this database does not indicate the effects of repeated sub-concussive impacts, which are now thought to be important. Hence, further investigation is needed into injury prediction capability, perhaps with a more realistic database.

Yet, there are methodologies that outperform all kinematic metrics. For instance, a recent network-based injury metric outperformed peak  $a_{rot}$  across all five performance categories evaluated (e.g., sensitivity of 0.85 vs. 0.80 for peak  $a_{rot}$  (Wu, Zhao, Rowson, *et al.*, 2019)). The network-based “response feature matrix” encodes the peak MPS of the regions of interest in the gray matter as well as their white matter interconnections. This suggests a way to expand the CNN model and increase the injury prediction performance even more could be to include white

matter fiber strains. The earlier success in predicting peak fiber strain in the corpus callosum (Wu, Zhao, Ghazi, *et al.*, 2019) provides some initial confidence along this line for further development.

### **CNN architecture and estimation performance**

The architecture used in this aim is based on a previous architecture from (Wu, Zhao, Ghazi, *et al.*, 2019). However, the same architecture did not work well for predicting the strain pattern directly (Success rate = 67.2%). A contributor to the poor performance is that the penultimate layer size (10 in the original architecture) is small to project the strain values for 50k elements. To mitigate that in the current study, we replace this layer with two fully connected layers with sizes 200 and 100 respectively. Alternatively, it was possible to use a single layer with a large size (e.g. 500), but the convergence rate dropped. We characterized the improvements in the network with each tweak by empirically observing the progression of the loss function, the convergence rate, overfitting (Figure 13 c), as well as the success rate as discussed before (Figure 13 a and b). The final network had a faster convergence, a lower overall loss function, and a higher success rate.

However, further tweaking the fully connected layers did not further improve performance. Additionally, we found that including the  $a_{rot}$  profile as an additional input signals/features can further significantly increase the success rate (from 83.2% to 92.1%; **Fig. 9a**). This led us to the final architecture design and use the  $v_{rot}$  and  $a_{rot}$  configuration profiles as the input for CNN training (**Fig. 7**). The CNN estimates appear to have sufficient accuracy, especially for the "in-range" test impact, even the "unsuccessful" cases only fail slightly (i.e.,  $k$  and  $r$  are not much different from their respective success thresholds; **Fig. 9b**). Compared with the previous study (Wu, Zhao, Ghazi, *et al.*, 2019), the updated CNN architecture and input structure also achieved almost the same performance in estimating the peak MPS of the entire brain. For real-world impacts where the magnitudes of the  $v_{rot}$  peaks were outside the target

range ( $> 40 \text{ rad / s}$ ; **Fig. 6a**), 65 of 73 cases or 89% were successful, with two impacts illustrated in **Fig. 13** (correspond to those identified in **Fig. 6a**). These results highlight the robustness of the technique and suggest the feasibility of applying our pre-trained CNN to the vast majority of head hits in contact sports.

Physically, the  $v_{\text{rot}}$  and  $a_{\text{rot}}$  contain the same information about describing the head impact with three degrees of freedom—that is with the exception that  $a_{\text{rot}}$  does not include the initial velocity. Yet, it was necessary to combine them as a CNN entry. This shows that in the current CNN structure, some high-order information from  $a_{\text{rot}}$  features is not derived or well represented by the  $v_{\text{rot}}$  profile. Understanding of the underlying mathematics of this problem improves the performance of CNN. It should also be noted that there already exists techniques such as “attention mechanisms” for identifying the “important features” behind the observed response. However, this knowledge-based “inverse” approach probably far exceeds the ability of the conventional “forward approach with the limited data available (Zhao and Ji, 2017), however this method is worth pursuing in the future.

Little success-rate improvement was achieved when MPS variance was incorporated as a weighting factor into the loss function (Eqn. 1;  $\sim 1\%$ ). As the linear regression slope and Pearson correlation we adopted for accuracy assessment do not discriminate the absolute response magnitude in their calculations, the MPS magnitude was not included as an additional weighting factor. Nevertheless, if needed, applying the weighting factor to focus more on higher strain regions that are likely more injury-relevant is straightforward. Another difference from the previous architecture is the use of linear activation functions as opposed to exclusively ReLU in the original architecture. This resulted in a  $\sim 1.3\%$  improvement in the success rate in the 10-fold cross-validation, and also increased the convergence rate.

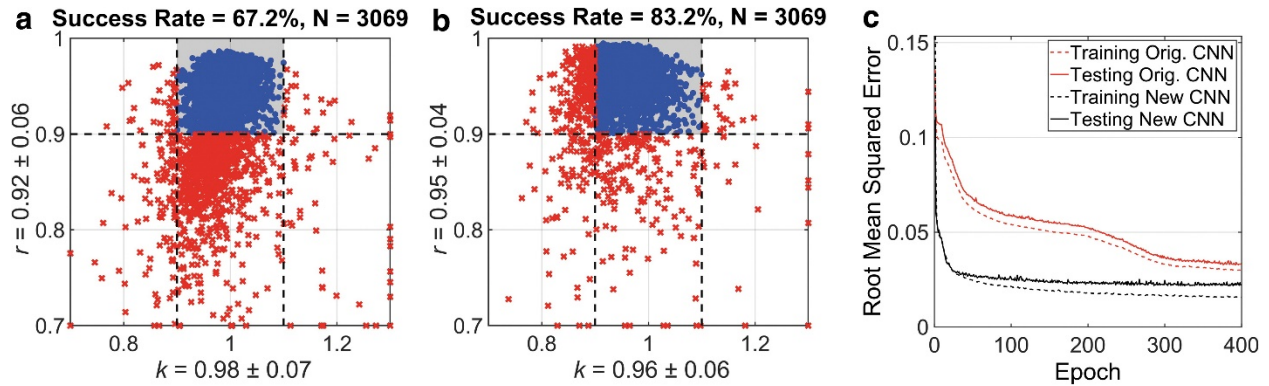


**Figure 13:** Comparison of estimation performance using the previous convolutional neural network (CNN) architecture (a; with the size of the last output layer changed to 55 k to match the number of brain elements for response prediction<sup>39</sup>) and the one updated in this study (b). Their convergence behaviors in terms of root mean squared error (RMSE) between the two distributions versus epochs are also compared (c). All performance measures reported here are based on the previous impact data set ( $n = 3069$ ) using  $v_{rot}$  profiles alone as CNN input, without the addition of  $a_{rot}$  profiles.

Finally, we observed a significant effect caused by the non-zero initial velocities in the impacts compared to the impacts with a zero initial velocity. Physically, one can force the initial velocity to zero with little difference in the brain strains generated (verified but not shown). Hence, applying a step to force the initial velocity to zero is a potential way to improve the performance which will minimize “confusion” by the CNN. The very existence of a large non-zero velocity is an indicator that the impact event was incompletely captured. This is beyond the scope of modeling efforts.

Nevertheless, our outlier criteria used to outline impacts that are not compatible to our network provides a way to estimate how much the CNN results can be trusted. More precisely, the outliers in terms of peak rotational acceleration and velocity are less concerning. This is because the impacts with a magnitude below the outlined acceleration and velocity levels are unlikely to cause injury. This is while impact events with magnitudes above the outlined bounds are likely to cause injury, even without the CNN strain predictions. Yet, in a real-world scenario,

non-zero velocities should be “flagged” and forced to have a zero initial velocity (as discussed above).

These empirical observations enrich the knowledge base of CNN behavior in the context of TBI biomechanics, which may promote future continuous development to further improve performance.

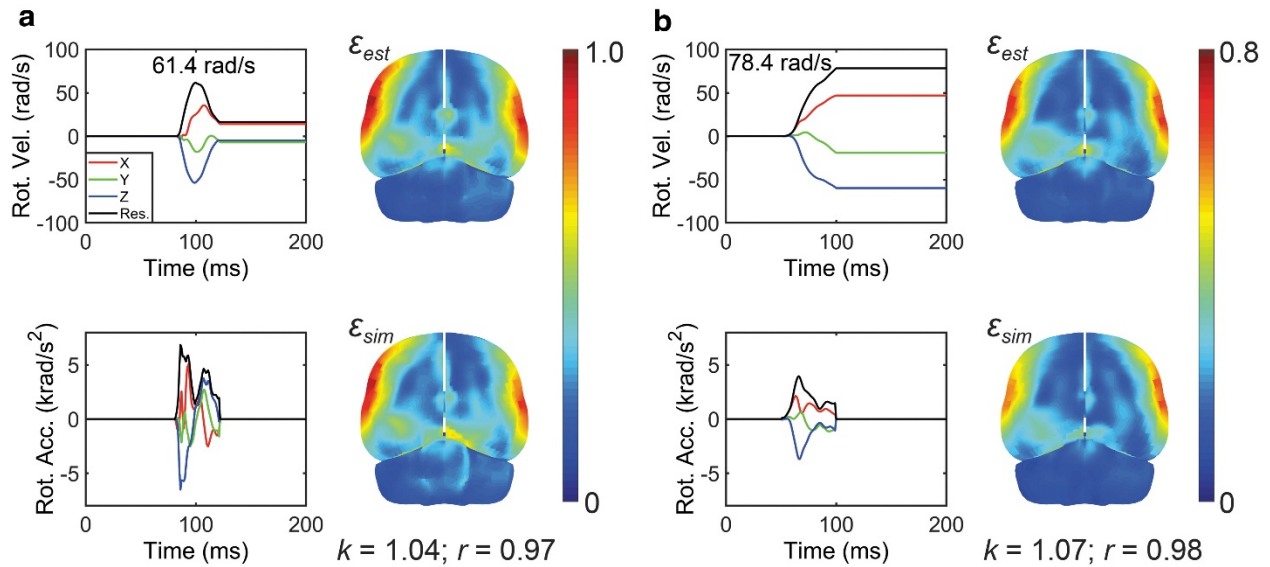


**Figure 14:** Illustration of a National Football League (NFL) concussive head impact (a; Case125HD0243) and another head impact from the HF data set (b; no injury diagnosis available). Even though their vrot peak magnitudes are significantly larger than the targeted range (61.4 rad/sec and 78.4 rad/sec, respectively, vs. 40 rad/sec as the upper bound of the targeted range; corresponding to the two cases identified in **Fig. 6a**), the convolutional neural network (CNN)-estimated strains were sufficiently accurate. Note, strain in (a) is higher than that in (b), even though its vrot peak magnitude is lower, because of its significant deceleration, which is lacking in the recorded profile in (b).

## Conclusion

So far, the work of developing head injury models has focused on improving the complexity and biological fidelity of the models and little attention was paid to how to maximize the practicality of the model in practical applications. This research further developed a Convolutional Neural Network (CNN) for offline training, enabling real-time online applications.

The pre-trained CNN can immediately estimate the whole-brain strain distribution on the low-end computing platform, so it has sufficient accuracy when most head impact contact motions. This ability may have broad significance for the study of the final findings, mitigation and prevention mechanisms of TBI.

## **Acknowledgments**

We thank the NFL Committee on Mild Traumatic Brain Injury (MTBI) and Biokinetics and Associates Ltd. for providing the reconstructed head impact data. We also thank Dr. David Camarillo at Stanford University and Dr. Adam Bartsch at Prevent Biometrics for sharing head impact data. The Titan X Pascal GPU used in this work was donated by the NVIDIA Corporation.

## **Funding Information**

Funding was provided by the National Institutes of Health (NIH) Grant R01 NS092853 and the Ford University Research Program.

## **Chapter 5: Aim 2: Feasibility assessment of the functionality of simplified “effective kinematics” to map complex profiles to equivalent simple profiles while maintaining brain strain map.**

Submitted to ABME as:

Kianoosh Ghazi, Shaoju Wu, Wei Zhao, and Songbai Ji. 2021. “Effective head impact kinematics to preserve brain strain.” *Annals of Biomedical Engineering*, submitted.

### **Introduction**

One of the major health concerns in the world is Traumatic brain Injury (TBI) (CDC, 2015; Dewan *et al.*, 2019). On average one out of every four TBIs is considered severe (~3%) or moderate (~23%) injuries, both of which can cause long lasting and devastating neurological problems (Faul, Xu and Coronado, 2010). The remaining injuries are considered “mild” TBI’s, with a rate of occurrence of 40 million cases world-wide according to the World Health Organization (Cassidy *et al.*, 2004). The number of mTBI cases in the United States is between 1.6 to 3.8 million cases annually and is particularly prevalent in contact sports (Graham *et al.*, 2014; Dompier *et al.*, 2015).

The primary mechanism of injury is believed to be caused by rapid head movement, resulting in sudden brain tissue deformation (King *et al.*, 2003; Meaney, Morrison and Bass, 2014). However, as the brain is not easily accessible *in vivo*, the tissue deformation in the brain cannot be measured directly. Hence, the sole way to gain insight into the brain tissue deformation and the resulting strains is Finite Element Simulations (Yang *et al.*, 2006; Madhukar

and Ostoja-Starzewski, 2019). Yet, a significant barrier on the way of readily utilizing FE models for obtaining the brain strains is their significant computational cost, resulting in hours (Mao, Zhang, *et al.*, 2013; Miller, Urban and Stitzel, 2016; Zhao and Ji, 2020c) to even days (Lu *et al.*, 2019; Li, Zhou and Kleiven, 2020) of simulation run time.

Although recently a deep learning convolutional neural network (CNN) based approach (Wu, Zhao, Ghazi, *et al.*, 2019; Ghazi *et al.*, 2020) successfully provided a sufficiently accurate estimation of brain strain distribution from FE simulation, impact kinematics such as acceleration and velocity remain widely used in TBI biomechanics research field. This could shift in the coming years as the mentioned CNN based method has the potential to shift acceleration-based injury biomechanics to focus more on tissue strain. Yet, the current preference of the kinematics based metrics extends to different applications within the field of TBI. For instance, They have long been adopted as the basis for head protection standards in the automotive and sport safety industries (Gadd, 1966; Lemmon and Huston, 1994; National Operating Committee on Standards for Athletic Equipment, 2019). This preference could be partially explained since kinematic variables are readily measurable and have specific physical interpretations easily accessible to the general public.

The most basic kinematic parameters used for injury risk estimation are the peak linear and rotational acceleration and peak rotational velocity. They are often used to characterize the impact severity in terms of rotational and translational head motion. Yet, several studies have shown that the brain strains are generated mainly by the rotational component of the impact as a result of the brain incompressibility (Bradshaw and Morfey, 2001; Kleiven, 2007; Ji, Zhao, *et al.*, 2014; Bian and Mao, 2020). As a result, the focus of injury metrics has shifted towards the impact rotation. Because of the contribution of kinematic features such as temporal profile shape in terms of acceleration and deceleration phases (Zhao and Ji, 2017) as well as direction and impulse

duration (Bian and Mao, 2020) to brain strain variation, peak rotational acceleration/velocity magnitudes do not typically correlate well with brain strain (Lee F. Gabler, Crandall and Panzer, 2018). This has resulted in an increase in the sophistication of the kinematic metrics that were developed recently to account for the variation in impact kinematic profile shapes and anatomical components. Some of these metrics are empirically derived metrics such as Rotational Injury Criterion (RIC) (Kimpara and Iwamoto, 2012), Brain Injury Criterion (BrIC) (E. G. G. Takhounts *et al.*, 2013), and Rotational Velocity Change Index (RVCI) (Yanaoka, Dokko and Takahashi, 2015). Others metrics, such as the universal brain injury criterion (UBrIC) (Lee F Gabler, Crandall and Panzer, 2018), diffuse axonal multi-axis general evaluation (DAMAGE) (Lee F. Gabler, Crandall and Panzer, 2018), and brain angle metric (BAM) (Laksari *et al.*, 2020b) are based on the physics of brain rotational mechanics.

With an increase in the level of sophistication, these injury metrics usually outperform peak rotational velocity and acceleration when comparing with model simulated brain strain. Two strain measures are often used benchmark the performance of these metrics (Lee F. Gabler, Crandall and Panzer, 2018; Bian and Mao, 2020): (1) peak MPS of the whole brain and (2) cumulative strain damage measure (CSDM) (Takhounts *et al.*, 2008). The latter equals the percentage of brain volume, whose strains exceed a given threshold value. The DAMAGE model, which is a physics-based reduced order model, has achieved a high correlation with peak MPS (~0.96) across a variety of impact conditions (Lee F. Gabler, Crandall and Panzer, 2018). This method effectively maps the brain strains into an analytically solvable simplified second-order system of equations of the brain mass displacement at every time point. Then the peak displacement is correlated with peak MPS, while the system critical parameters are determined by fitting simulated responses from a set of simplified multi-directional head rotations.

Despite these advances, the all kinematics based injury metrics to date are scalar values (a single numerical number to infer brain strain response on the global level). This results in two major oversimplifications that can affect the reliability of the injury assessment from these metrics. Firstly, using such metrics prohibits representation of the brain strain distribution as well as the region of the brain where the high strain occurs. This is important due to the diffuse nature of strain (Koerte *et al.*, 2015). Further, easily accessible physical interpretations (such as in peak rotational velocity) may be lost in sophisticated injury metrics. Thus, promoting complex kinematics-based injury metrics for routine real-world use in the general public, such as in head protection safety industries could be challenging.

This aim addresses these shortcomings by developing the concept of “effective impact kinematics” to translate an arbitrary head impact rotational profile into a set of basic impact scalar kinematic variables. These values are determined by the best approximation within a pre-computed brain response atlas (pcBRA) (Ji and Zhao, 2015; Zhao, Kuo, *et al.*, 2017a). This atlas serves as a common strain “dictionary” to represent all impacts. First, we determine effective peak rotational velocity ( $v_{rot}^p$ ) to maintain the same peak MPS. Here the MPS is regarded as a scalar value to describe the global level of brain strain. This is a similar approach to the conventional scalar injury metrics to simplify a complex head impact into a single numeric value. Next, we take a similar best approximation approach to identify the “effective kinematic triplets” to preserve elementwise MPS. Effective kinematic triplets are the effective  $v_{rot}^p$  and the associated rotational axis (delineated by the azimuth and elevation angles ( $\theta$  and  $\alpha$ , respectively)). Unlike other conventional scalar injury metrics to date, the effective kinematic triplets approach can preserve spatially detailed brain strain, which is consistent with the direction-specific peak rotational velocity for predicting brain strain (Bian and Mao, 2020).

Finally, we develop a CNN structure to automatically simplify a given real-world impact and avoid the computational cost of the simulation for obtaining brain strain distribution. A given impact can be readily simplified into a common reference in terms of easily understandable peak rotational velocity and the associated rotational axis using the trained and validated CNN. This approach may allow for more effective comparisons of head impacts by simplifying real-world impacts into an idealized “impact mode”, be it in terms of global peak MPS or spatially detailed strain. However, the implications of this study could be extended to a wide variety of applications in other injury scenarios such as fall and automotive impacts in the future.

## Methods

### Workflow Overview

For an arbitrary head impact recorded from a measuring instrument (e.g. instrumented helmet or mouthguard), a simulation was constructed and ran using the Worcester Head Injury Model (WHIM) V1.0 (Zhao and Ji, 2019c). Then the strain distribution resulted from the simulation is compared to those in the pcBRA (Zhao, Kuo, *et al.*, 2017a) to identify the corresponding effective kinematic variables, depending on how the strain is to be preserved (peak or elementwise MPS). Finally, a CNN is trained to instantly predict the corresponding effective kinematic variables. The details of this process are outlined in the following sections.

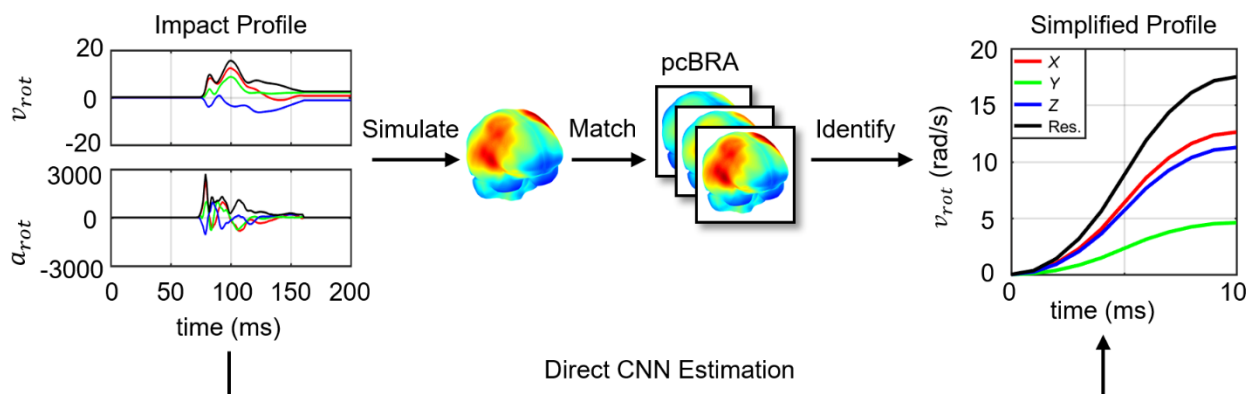


**Figure 15:** Flowchart of the study to translate an arbitrary head impact into effective impact

kinematics to preserve either peak MPS or spatially detailed MPS. Elementwise MPS of the brain for an arbitrary head impact is first obtained and compared with the pcBRA library to identify an idealized impact. With a CNN, this process is automated without the need for actual costly impact simulation. pcBRA: pre-computed brain response atlas.

## **Impact dataset**

A previously simulated set of impacts obtained from contact sports (N = 3069) we used for this study. This dataset includes on-field recorded impacts (Hernandez *et al.*, 2015; Zhao *et al.*, 2019), reconstructed impacts from the National Football League (Sanchez *et al.*, 2018), as well as their augmented impacts *via* data augmentation as explained in the previous aim (Wu, Zhao, Ghazi, *et al.*, 2019). The target range of the augmented data in this dataset were designed to increase the number of “more severe” head impacts (i.e., peak rotational velocity magnitude range of 21.9–40 rad/s, which corresponds to 50<sup>th</sup> concussive and above the 95<sup>th</sup> concussive impact, respectively (Rowson *et al.*, 2012)). Impact simulations were conducted using the WHIM V1.0 (Wu, Zhao, Ghazi, *et al.*, 2019). The database in the previous aim was not feasible in this aim as a result of the incompatibility of the anisotropic WHIM (used for the simulations in the previous aim) and the pcBRA (which was developed on the isotropic WHIM).

## **Strain responses from idealized impacts in a pcBRA**

A set of idealized rotational acceleration pulses of a triangular shape were used to pre-define and simulate brain impacts that construct the pcBRA library (Ji and Zhao, 2015; Zhao, Kuo, *et al.*, 2017a). This technique has recently been adopted to develop strain-based cumulative impact exposure (Miller *et al.*, 2020). The impact duration of the impulses used in pcBRA is fixed to 10 ms as it was found that maintaining the same peak rotational velocity with varying acceleration impulse durations did not significantly alter strain for impacts in contact sports (Zhao, Kuo, *et al.*, 2017a; Bian and Mao, 2020). This reduced the number of defining parameters which

resulted in a significant reduction of the total number of idealized impacts necessary for costly impact simulation.

Hence each pcBRA impact can be identified by triplets consisting of peak resultant rotational velocity ( $v_{rot}^p$ ) and the azimuth and elevation angles ( $\theta$  and  $\alpha$ , respectively) of the rotational axis. **Table 3** in the background provides a summary of the ranges and step sizes of the three discretizing variables. **Fig. 15** provides a visual illustration of an idealized impact profile (**Fig. 15a**) as represented by a 3D vector emanating from the WHIM head center of gravity (**Fig. 15b**). As a result of the head symmetry about the mid-sagittal plane, the range of directionalities in the pcBRA only cover half of the space (**Fig. 15c**). The impacts outside this region can be mapped into this region using conjugation (explained in the previous sections) (Ji and Zhao, 2015).

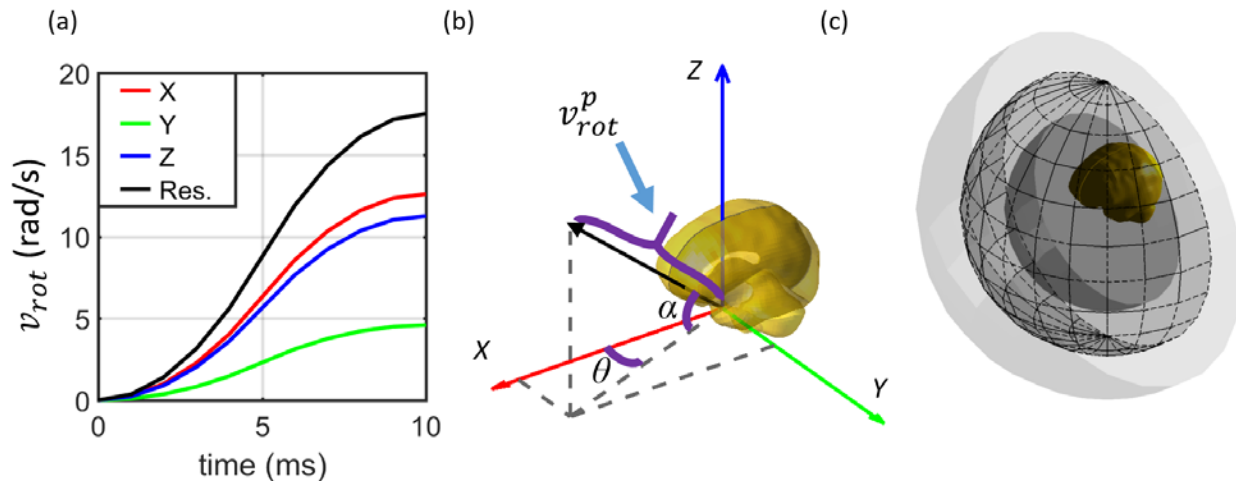


**Figure 16:** (a) Example of an idealized three-degree-of-freedom (3DOF) impact rotational velocity profile; (b) the corresponding kinematics triplets ( $v_{rot}^p, \theta, \alpha$ ) represented by a vector emanating from the head center of gravity to characterize the peak velocity magnitude and directionality in the WHIM coordinate system. For a given  $v_{rot}^p$ , traversing the vector end point in space would generate a hemisphere shown in (c). In the middle hemisphere, the discretized  $(\theta, \alpha)$  pairs are also shown as grid on the hemisphere.

## Effective peak rotational velocity magnitude to preserve peak MPS

One  $v_{rot}^p$  value about an arbitrary head rotational axis is sufficient to preserve peak MPS of the whole brain (assessed at the 95<sup>th</sup>-percentile level). However, this  $v_{rot}^p$  value is dependent on the direction and does not consider the strain distribution in the brain. Therefore, we chose to separately identify a  $v_{rot}^p$  value along each of the three anatomical directions (X, Y, and Z).

Impacts around the same rotational axis were grouped together (i.e.,  $v_{rot}^p$  range of 7.5–37.5 rad/s along each anatomical direction; **Table 3**). Then we fit a constrained third order polynomial function against  $v_{rot}^p$  (i.e., peak MPS of zero when  $v_{rot}^p$  is zero) to their respective peak MPS. Thereby, we inversely identified  $v_{rot}^p$  to generate the same peak MPS from the fitted function for for an arbitrary head impact. This process led to three corresponding effective  $v_{rot}^p$  values along the three anatomical axes  $v_{rot}^x$ ,  $v_{rot}^y$ ,  $v_{rot}^z$ , respectively (**Fig. 16**). Here we treat  $v_{rot}^x$ ,  $v_{rot}^y$ ,  $v_{rot}^z$  as the effective values because we are mapping peak MPS onto rotational velocities. In other words, as we choose to only into the pcBRA impacts along anatomical directions, where  $\theta$  and  $\alpha$  are constant along each direction.

Some impacts can have peak MPS values that are outside of the pcBRA sampling range, which leads to extrapolation (**Fig. 16**). To identify a reasonable range of extrapolation to avoid large errors we iteratively removed MPS- $v_{rot}^p$  sampling points (**Fig. 16b**) along the axial rotation at the higher end and refitted the remaining sampling points with a constrained third order polynomial. In each step we extrapolated the MPS to find the highest  $v_{rot}^p$  available in the baseline pcBRA (37.5 rad/s; **Table 3**). The peak MPS was then compared against the directly simulated counterpart.

This experiment outlined that up to three sampling points could be removed to yield an extrapolation error in strain <0.01, which was considered sufficiently accurate. Based on this

finding, we assumed the extrapolation within 3  $v_{rot}^p$  step-sizes to be reasonably accurate when using all of the 9 MPS- $v_{rot}^p$  sampling points for fitting (that is  $v_{rot}^p < 48.75$  rad/s or  $a_{rot}^p < 9750$  rad/s<sup>2</sup>equivalently)). This extrapolation range was applied to the impacts along all rotational axes. This allowed for re-using existing impact simulations without the need to re-simulate new impacts. 90.7% of impacts were successfully simplified using this approach ( $v_{rot}^p$  within the extrapolation range; **Fig. 16**).

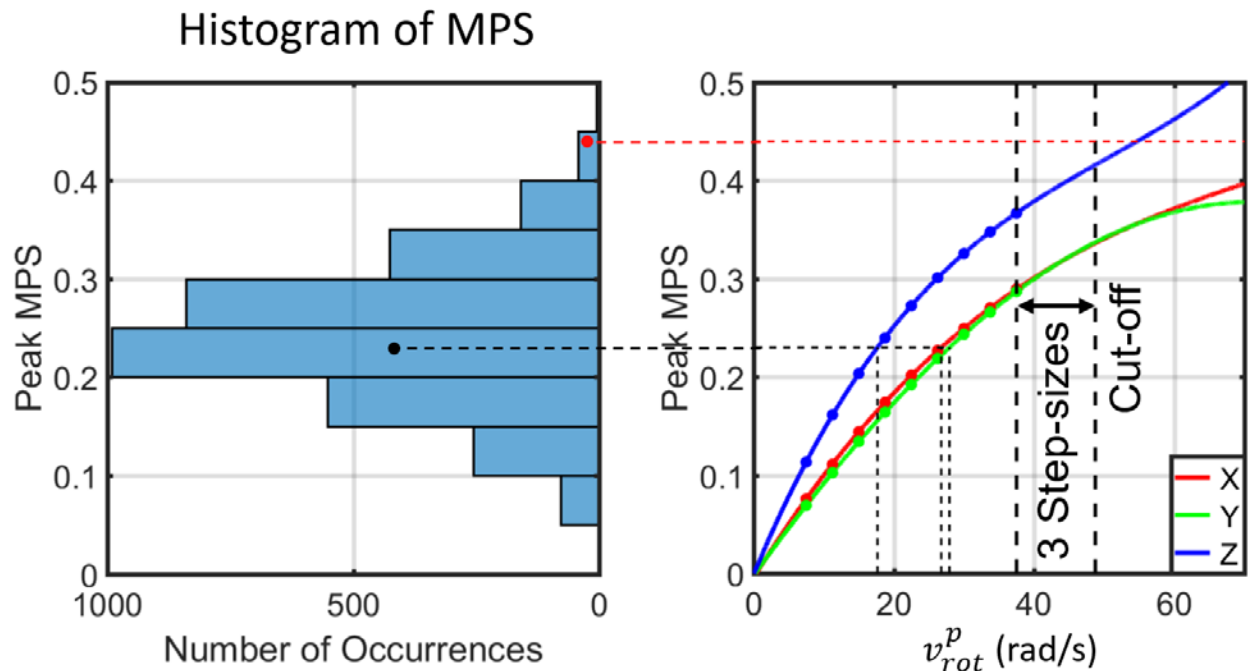


**Figure 17:** (a) Histogram distribution of peak MPS for the N=3069 impacts. (b) Peak MPS values corresponding to the same anatomical axis from the pcBRA are grouped to fit a constrained third order polynomial. The MPS of each impact is used to identify the corresponding  $v_{rot}^x$ ,  $v_{rot}^y$ ,  $v_{rot}^z$  along the three anatomical axes. The two dashed lines on the far right show the extent of  $v_{rot}^p$  extrapolation range deemed of sufficient accuracy. For the same  $v_{rot}^p$ , an axial rotation produces a considerably higher MPS than a coronal or a sagittal rotation. The red line shows an unsuccessful case that did not coincide with the X and Y polynomials within the allowed margin for extrapolation.

### Effective kinematic triplets to preserve elementwise MPS

Based on the construction of the pcBRA impacts, three independent parameters were necessary to preserve elementwise MPS accounting for spatial distribution:  $v_{rot}^p$  and the

associated rotational axis,  $\theta$  and  $\alpha$  angles. These variables were determined by comparing with the pcBRA impacts. This comparison was done according to linear regression slope,  $k$ , and Pearson correlation coefficient,  $r$  between elementwise MPS. In an ideal scenario where the two MPS distributions are identical, both  $k$  and  $r$  would be 1.0. Hence, we used an empirical error threshold of 0.1 both  $k$  and  $r$ . In other words, an impact was considered to be sufficiently similar to an idealized impact when both  $k$  and  $r$  did not deviate from 1.0 by more than an empirical threshold of 0.1 (Ghazi *et al.*, 2020).

To match the real-world impacts to the pcBRA impacts, we used a two-step approach. First, we identified a subset of pcBRA impacts that best matched the simulated MPS.

The following objective function was used for minimization to account for the differences in peak MPS magnitude and spatial distribution simultaneously:

$$loss_{strain} = |1 - k| + |1 - r| .$$

A brute-force approach was used to identify 10 idealized impacts that produced the lowest  $loss_{strain}$  values. The resulting kinematic triplets formed a neighborhood of idealized impact within the pcBRA parametric space (**Fig. 17a**). As the second step, they were weight-averaged to approximate  $\theta$  and  $\alpha$  based on their corresponding  $r$  values (Eqns. 2 and 3), as higher  $r$  values indicate closer similarity in MPS distribution. This led to 59.7% of the impacts remaining to continue with subsequent analysis (N=1900; **Fig. 19**).

$$\theta = \frac{\sum_{i=1}^{10} \theta_i \times r_i}{\sum_{i=1}^{10} r_i}$$

$$\alpha = \frac{\sum_{i=1}^{10} \alpha_i \times r_i}{\sum_{i=1}^{10} r_i}$$

Using the obtained directionality from the weight-averaged  $\theta$  and  $\alpha$ , discrete  $v_{rot}^p$  values were grouped following the same range and step size (**Table 1**) and Interpolation was used to

obtained their corresponding elementwise MPS distributions. Their elementwise MPS values were regressed against those from the arbitrary impact. The resulting  $k$  values were then obtained to fit a constrained third order polynomial function. Then, using the obtained polynomial relating the  $v_{rot}^p$  to the  $k$  value about the given rotational axis,  $(\theta, \alpha)$ , the  $v_{rot}^p$  resulting in a  $k$  of 1.0 was identified (**Fig. 17b**).

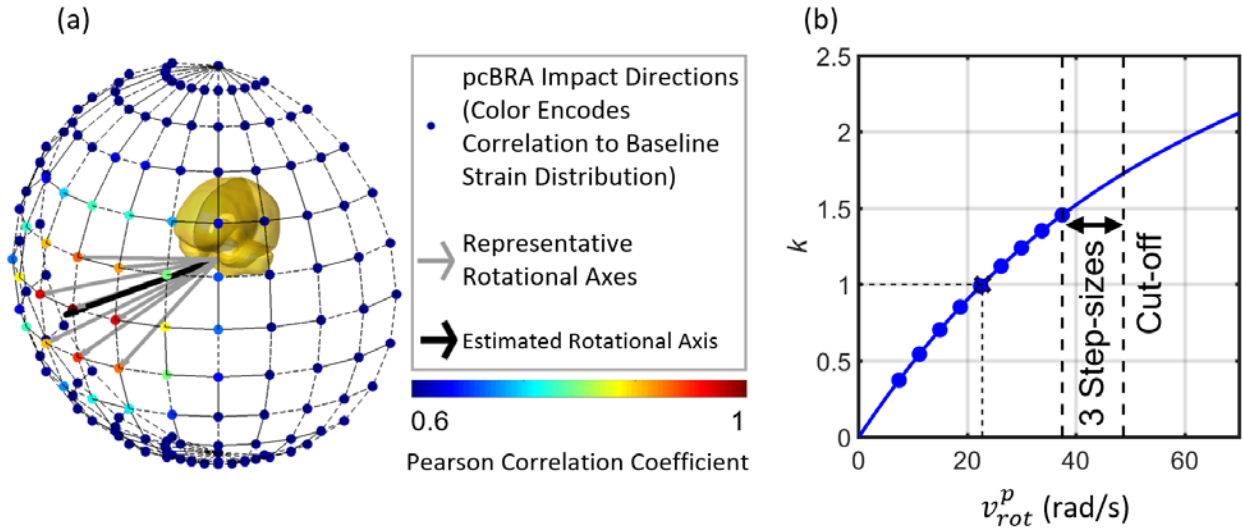


**Figure 18:** (a) Illustration to identify nearest neighbors in the pcBRA parametric space for an arbitrary head impact based on brain strain. The rotational axis is weight averaged and then fixed to interpolate a number of brain strains for a range of  $v_{rot}^p$  values based on the pcBRA. Their corresponding  $k$  values as regressed against simulated elementwise MPS for a given impact are used to generate a constrained third order polynomial fitting (b). The effective  $v_{rot}^p$  is finally determined by intersecting a horizontal line with  $k$  of 1.0.

### CNN model to derive effective impact kinematics directly

The Head impact profiles and their identified effective kinematics were used to train a CNN model to automate the process. The same earlier CNN architecture was adopted, with input concatenated from both rotational velocity and acceleration profiles as a 2D image. This was found to improve accuracy in estimating elementwise MPS (Ghazi *et al.*, 2020).

The CNN architecture consists of 3 convolutional layers, with 64, 64, and 32 filters, each with sizes of  $3 \times 60$ ,  $1 \times 3$ ,  $1 \times 1$ , and stride sizes of  $1 \times 2$ ,  $1 \times 2$ ,  $1 \times 1$ , respectively (**Fig. 18**).

They are followed by a pooling layer of a size of  $1 \times 2$  with a stride size of  $1 \times 2$ , a flattening layer (with a dropout rate of 0.2), and three fully connected layers with sizes of 200, 100, and 3 (the last of which corresponds to the number of values to predict in the effective kinematics triplets). The pooling layer and the first fully connected layer (of a size of 200) adopted a ReLU activation function, while all other layers used a linear activation function. A batch size of 16 was chosen with the number of epochs set to 500. An early stopping criterion was used to avoid overfitting. The CNN architecture was implemented using Keras library (Version 2.2.4) with Tensorflow (Version 1.11.0) backend.

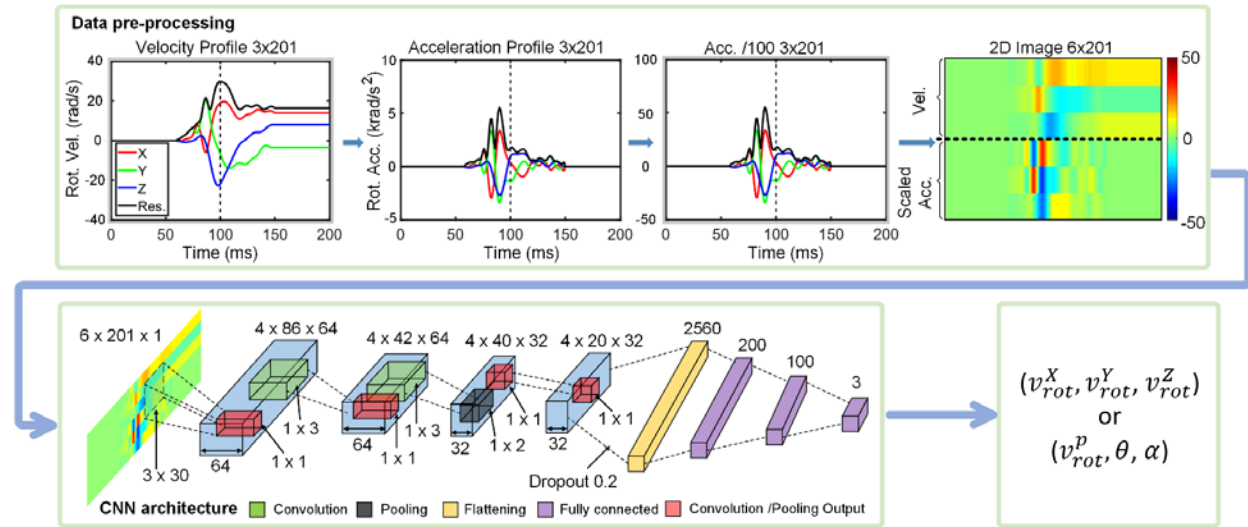


**Figure 19:** The CNN architecture used in this study, which shares the architecture with the one in aim 1 with the exception of the final layer.

We used the mean squared error as the loss function to train and predict the three effective  $v_{rot}^p$  values to preserve peak MPS along the three anatomical directions. However, both  $v_{rot}^p$  and rotational axis ( $\theta$  and  $\alpha$ ) were important to preserve elementwise MPS. Hence, we designed a composite loss function to penalize the magnitude error and angular error in a weighted manner:

$$loss_{dir.} = \frac{1}{N} \sum_{i=1}^N (|\vec{v}_i^{CNN}| - |\vec{v}_i^{label}|)^2 + \gamma \frac{1}{N} \sum_{i=1}^N \cos^{-1} \left( \frac{\vec{v}_i^{CNN} \cdot \vec{v}_i^{label}}{|\vec{v}_i^{CNN}| \times |\vec{v}_i^{label}|} \right),$$

where  $\vec{v}_i^{CNN}$  and  $\vec{v}_i^{label}$  are the predicted and baseline rotational axis of the  $i^{\text{th}}$  impact, respectively,  $N$  is the number of the training samples, and  $\gamma$  is a Lagrange multiplier (empirically chosen to be 0.1) to balance the different scales of the two error terms (angular and  $v_{rot}^p$  error, **Fig. 19**).

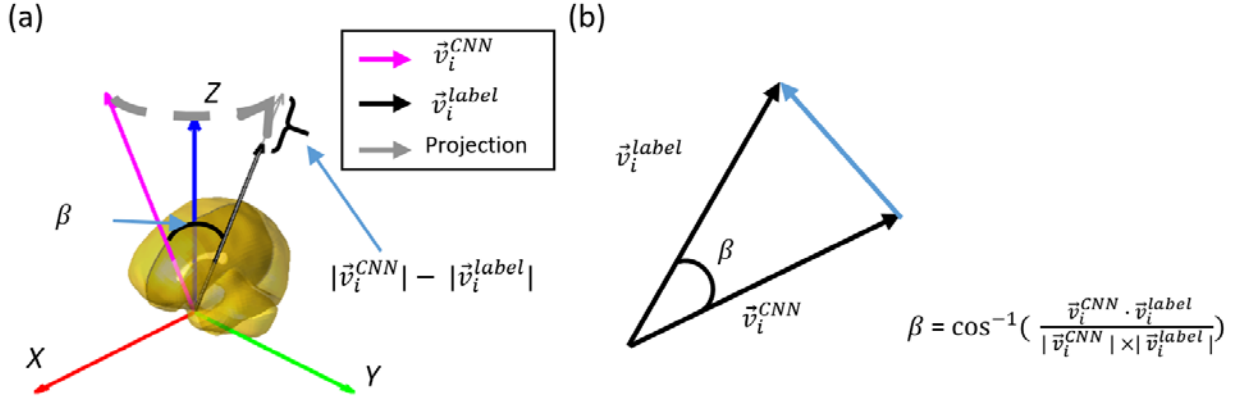


**Figure 20:** (a) shows the definition of angular and magnitude errors. Angular error is represented by  $\beta$ .

## Data Analysis:

### Effective peak kinematics to preserve peak MPS

We compared the peak effective rotational velocity ( $v_{rot}^x$ ,  $v_{rot}^y$ , and  $v_{rot}^z$ ) magnitudes with their corresponding “nominal peaks” from the resultant profiles for impacts that were successfully identified with peak rotational velocity along the three anatomical axes to preserve peak MPS. We then evaluated the CNN performance using a 10-fold cross-validation. Here, we compared the predicted  $v_{rot}^p$  values against those inversely identified *via* the coefficient of determination ( $R^2$ ) and root mean squared error (RMSE). Then, we converted the two sets of simplified kinematics converted into peak MPS *via* the pcBRA, and further evaluated the performance of the CNN in terms of the corresponding peak MPS.

### Effective kinematic triplets to preserve elementwise MPS

We identified the impacts that could be accurately represented with effective kinematic triplets  $(v_{rot}^p, \theta, \alpha)$ . For these impacts the  $k$  and  $r$  values of their elementwise MPS as compared to those from actual model simulation did not deviate from the value of 1.0 (when they were identical) by more than 0.1 (Ghazi *et al.*, 2020). For these impacts,  $v_{rot}^p$  from the simplified impacts were compared with the corresponding nominal  $v_{rot}^p$  derived from the arbitrary resultant profiles.

Further, we evaluated the performance of the CNN model *via* 10-fold cross-validation, where we compared each variable in the predicted triplets with the corresponding value reported from the inverse mapping. Additionally, In addition, we generated elementwise MPS based on the pcBRA using the triplets for further comparison in terms of  $k$  and  $r$ . Similarly, success criteria for the CNN prediction of elementwise MPS was when neither  $k$  nor  $r$  deviated from the value of 1.0 by more than 0.1. Success rate for the CNN model was finally reported. All data analyses were conducted using MATLAB (R2020b; MathWorks, Natick, MA).

## Results

### Effective peak rotational velocity magnitudes about the three anatomical axes

Out of the 3069 impacts, 90.7% could be successfully mapped to effective  $v_{rot}^p$  along all three anatomical axes. Other impacts resulted in one or more of the corresponding  $v_{rot}^p$  exceeding the maximum extrapolation range and hence “failed”. For the remaining “successful” impacts the effective  $v_{rot}^p$  and  $a_{rot}^p$  were compared against their corresponding nominal peaks (**Fig. 20**). Because this dataset had augmented impacts focusing on between ~22–40 rad/s in terms of nominal peak velocity magnitude (Wu, Zhao, Ghazi, *et al.*, 2019) a large portion of the data points clustered this data range. Although each pair corresponded to the same peak MPS,

the effective  $v_{rot}^p$  from the simplified head impacts had a relatively low correlation with the nominated counterparts along all anatomical directions ( $R^2$  ranged 0.337 – 0.344).

Generally, the effective  $v_{rot}^p$  along the x and y (i.e., coronal and sagittal head rotation, respectively) directions had a comparable trend with the nominal peaks (as their regression slopes were close to 1.0), yet, with a large deviation (RMSE = ~7–12 rad/s). However, their effective rotational acceleration peaks,  $a_{rot}^p$ , were significantly higher than the nominal counterparts along the two directions ( $k=1.23 – 1.26$ ; **Fig. 21**). However, for  $v_{rot}^p$  and  $a_{rot}^p$  along the z axis (axial rotation), the effective peaks were both lower than the nominal counterparts ( $k=0.6\sim0.8$ ).

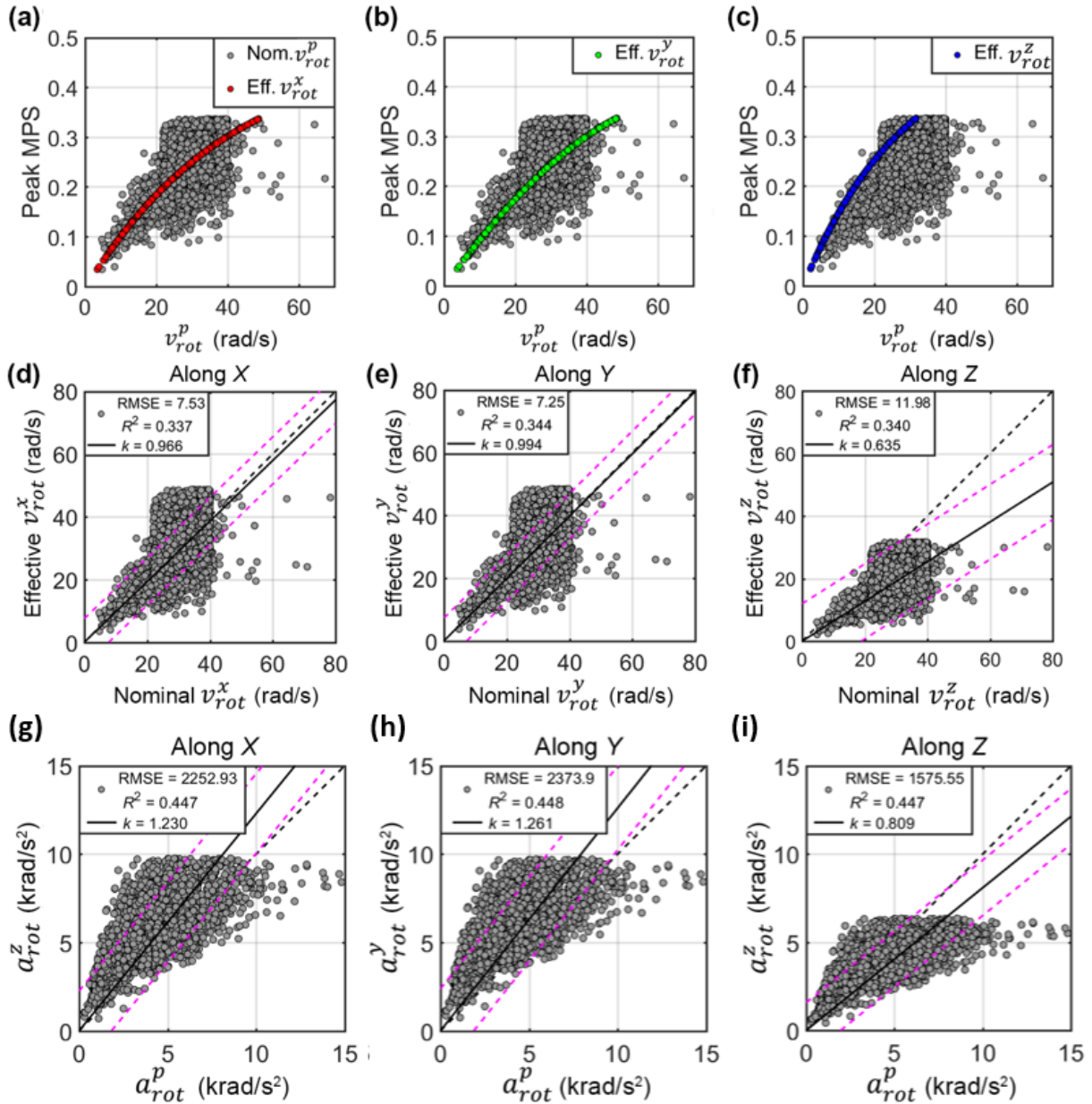


**Figure 21:** A scatterplot between the peak MPS and peak effective rotational velocity and the nominal counterparts are shown along X, Y, and Z ((a) through (c)). Comparison between effective and nominal peak rotational velocity and acceleration along the x, y, and z axis (coronal, sagittal, and axial directions, respectively, as defined in Fig. 15) in ((d) through (f) and ((g) through (i)).

An  $R^2$  of 0.954–0.955 with RMSE of ~1.2–1.9 rad/s was achieved using the CNN predictions of  $v_{rot}^p$  along all anatomical axes (Fig. 22 top). The MPS obtained by translating these

effective  $v_{rot}^p$  values using the pcBRA, they had an  $R^2$  of 0.955-0.960 with RMSE of 0.011-0.012 (Fig. 21 bottom).

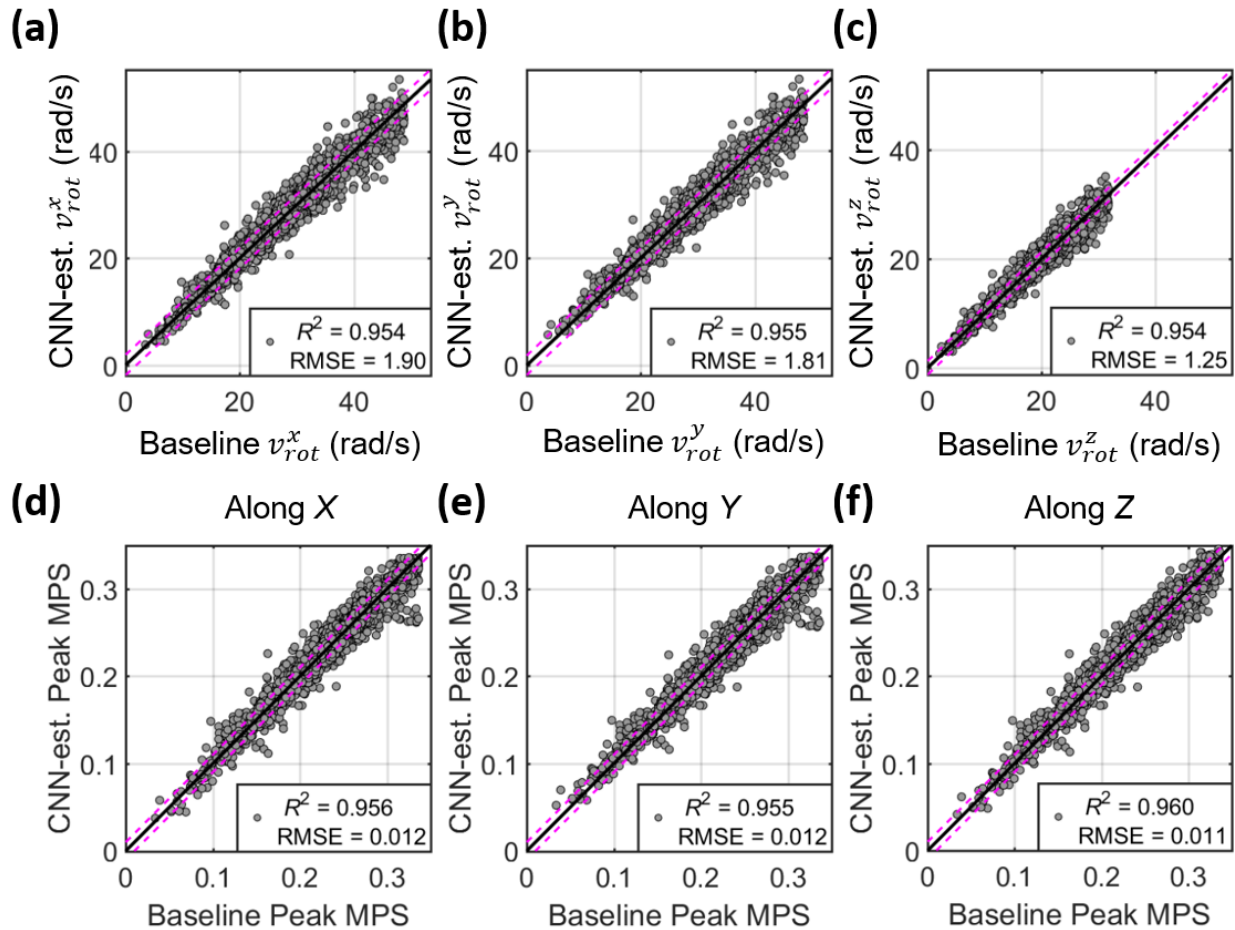


**Figure 22:** (Left) shows the scatterplot of CNN prediction of effective peak rotational velocity magnitude against the label counterpart for all three axes. (Right) shows the scatterplot of CNN predictions translated to MPS compared against the ground-truth MPS.

### Effective kinematic triplets to preserve elementwise MPS

The elementwise MPS of the impacts that successfully matched with idealized impact modes all had a  $k$  value of 1.0 relative to the pcBRA counterparts because of the way the effective  $v_{rot}^p$  values were determined. Their Pearson correlation coefficients,  $r$ , are reported as a histogram in Fig. 22a. The effective  $v_{rot}^p$  and their nominal counterparts for those “successfully matched” are also compared (Fig. 22b). Some representative cases are shown (Fig. 22c and d).

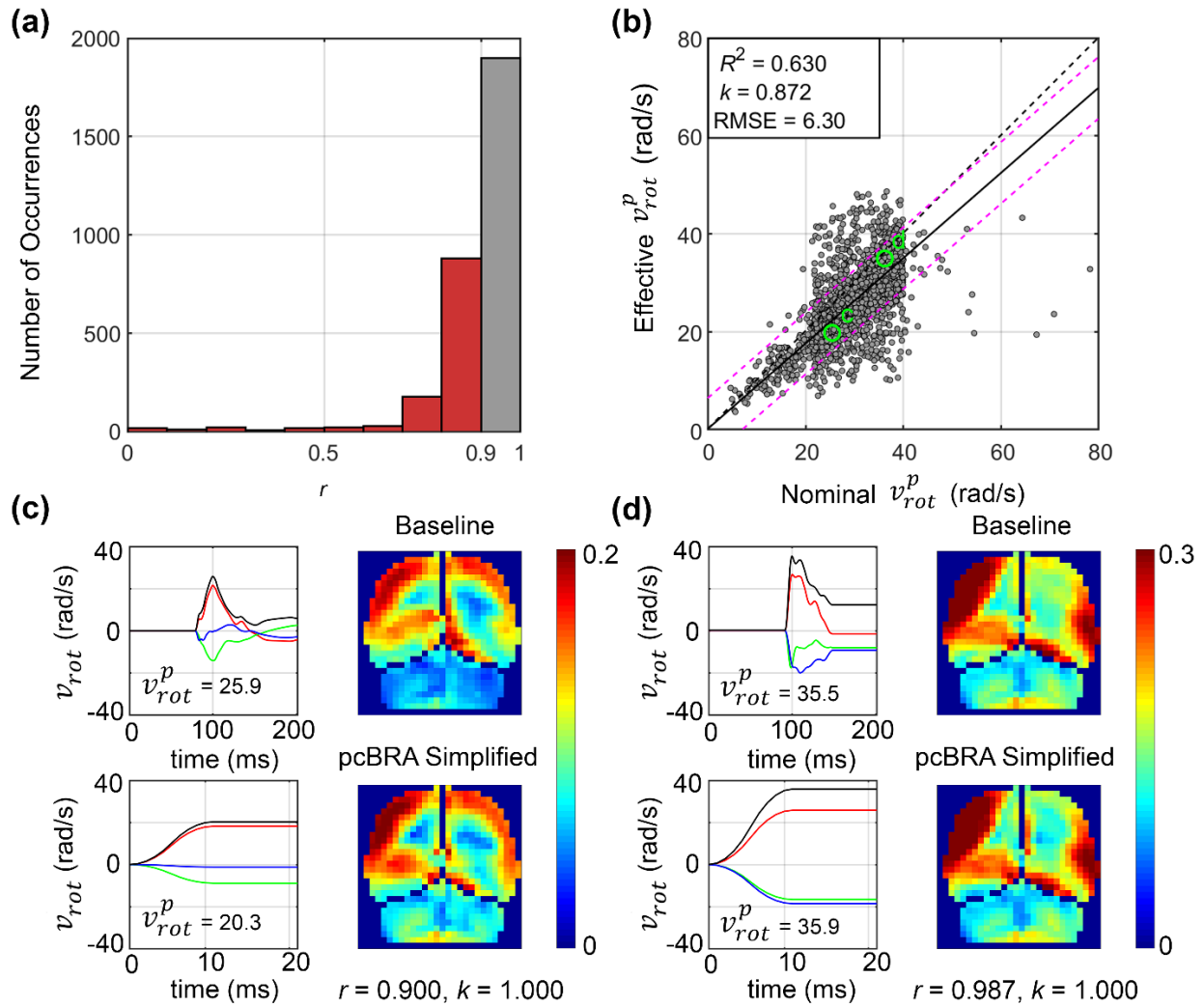


**Figure 23:** (a) Summary of element-wise Pearson correlation coefficient ( $r$ ) with the most similar idealized impact in the pcBRA database when the linear regression slope ( $k$ ) was forced to be 1.0 by adjusting the effective  $v_{rot}^p$  (those with  $r > 0.9$  were considered “successfully matched”). (b) a comparison of effective  $v_{rot}^p$  and the nominal counterparts for the successfully matched impacts; (c) and (d) illustration of example cases showing their actual and idealized impact profiles, together with the corresponding elementwise MPS.

The angular differences between predicted and baseline rotational axes as well as the errors in  $v_{rot}^p$  values were used to evaluate the estimation performance of the CNN (Fig. 23a and b) based on the N=1900 impacts successfully idealized. A success rate of 73.5% was obtained from the elementwise MPS based on the CNN estimated kinematic triplets compared against the

baseline responses in terms of  $k$  and  $r$  (**Fig. 23c**). All evaluations were based on a 10-fold cross-validation.

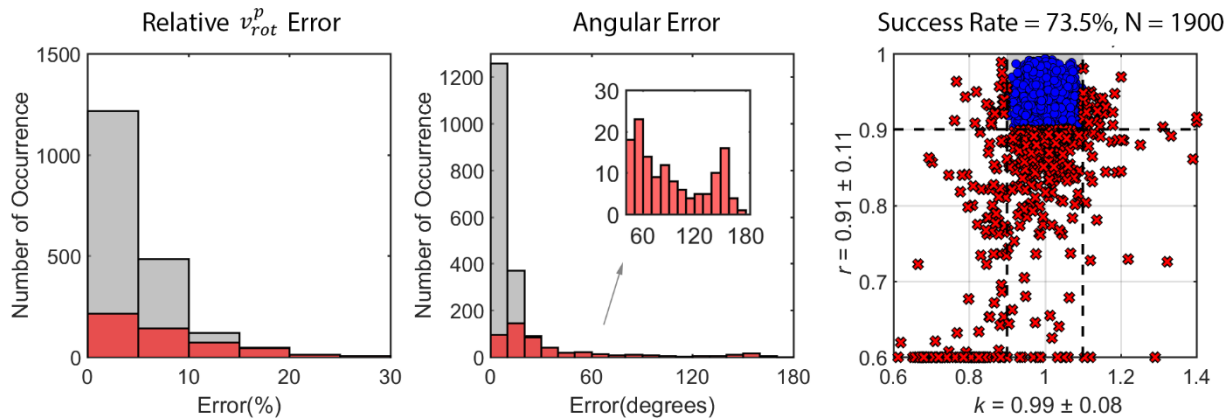


**Figure 24:** The histograms of error in terms of “angular” and “ $V_{rot}$  percentage magnitude” errors respectively using a 10-fold cross validation. The relative error in (a) is the percentage of the absolute magnitude error. The unsuccessful impacts are shown in red. For clarity, data points outside the shown range on the subfigure on the left were shown on the border.

## Discussion

In the TBI biomechanics field, impact kinematics such as peak rotational acceleration and velocity are used ubiquitously. This can be partially explained by their physical interpretations, which allow them to be easily accessible to the general public. However, there is often a discordance between the peak kinematic values and injury-causing brain strains due to their complex relationship resulting from the nonlinear and viscoelastic properties of the brain parenchyma and its complicated anatomical geometry. In this aim, we develop the concept of “effective impact kinematics” which translates a real-world, complex, time-varying head rotational kinematic profile into an idealized impact characterized by the peak rotational velocity and the associated rotational axis, with a fixed time span. This aim is supporting the development of direction-specific peak rotational velocity for predicting brain strain (Bian and Mao, 2020). It also establishes a common ground using an earlier study by using a pre-computed brain response

atlas (pcBRA) (Zhao, Kuo, *et al.*, 2017a) with idealized head impact modes to facilitate real-world impact simplification.

The concept of our work is similar to conventional injury metrics that map the complicated head impact kinematic profiles into a common scalar reference for comparison. Yet the innovation of our approach lies within using effective kinematics which may have two notable advantages. First, it retains the physical meaning of the peak rotational velocity, which may help promote this method in the general public. Second, it maps a potentially complicated head impact into an idealized but actual impact allowing for preservation of brain strain distribution, which is infeasible with conventional injury metrics. The time-consuming impact simulation is avoided in this methodology by developing and training a deep learning convolutional neural network (CNN) to automate the process to identify the effective kinematics for strain preservation, which mitigates the alternative of using model-simulated brain strains.

Nonetheless, compared to most other injury metrics which are explicit and typically rely on a mathematical formula to derive the injury metric value, this process is implicit hence the burden of fitting a mathematical model is not on the shoulder of the users.

### **Effective peak rotational velocity magnitude to preserve peak MPS**

Three effective  $v_{rot}^p$  values were obtained along the three anatomical axes when matching peak MPS. The process of matching the MPS is the practical standard for current kinematics-based injury metrics. For these values, a relatively low correlation coefficient and a large scatter was observed along with a statistical correlation with the nominal counterparts (**Fig. 20**). This is reaffirmed by other reports of relatively low correlation between peak MPS and nominal peak velocity (Lee F. Gabler, Crandall and Panzer, 2018; Bian and Mao, 2020). The CNN was able to successfully predict the effective  $v_{rot}^p$  values directly. It consistently achieved an  $R^2$  of 0.955–

0.960 in terms of both  $v_{rot}^p$  and peak MPS (with RMSE of 0.011–0.012; **Fig. 20**) based on a 10-fold cross-validation. These results were comparable to the use of CNN to predict peak MPS directly ( $R^2$  of 0.966 with RMSE of 0.013; (Wu, Zhao, Ghazi, *et al.*, 2019)) and another best-performing kinematics-based injury metric ( $\sim 0.96$  for DAMAGE; (Lee F. Gabler, Crandall and Panzer, 2018)). However, this method outperforms other empirical injury metrics (e.g.,  $R^2$  of 0.638, 0.326, 0.602, 0.853 for HIP, PRHIC, RIC, and BrIC, respectively, based on real-world impacts (Lee F. Gabler, Crandall and Panzer, 2018)). We observed a variation in the effective  $v_{rot}^p$  values for the same impact across the anatomical axes, with the lowest value occurring about the z-axis or axial rotation (**Fig. 16**). This finding was consistent with the “critical maximum angular velocity” values developed for BrIC (E. G. G. Takhounts *et al.*, 2013) using the SIMom head injury model (Takhounts *et al.*, 2008), where the critical value (corresponding to a 50% risk of Abbreviated Injury Scale (AIS) 4+ injury) in the axial direction was  $\sim 30$ – $50\%$  lower than in the other two directions. Hence head rotation about the axial direction would be more vulnerable to induce higher peak MPS than rotation about the coronal or sagittal axes given that the effective  $v_{rot}^p$  value is the same (Bian and Mao, 2020).

### **Effective peak rotational velocity magnitude to preserve elementwise MPS**

Perhaps most importantly, this aim allows for real-world impact simplification into an actual idealized impact characterized by triplets consisting of the effective  $v_{rot}^p$  and the associated rotational axis (azimuth and elevation angles,  $\theta$  and  $\alpha$ , respectively). Simplifying an impact in this fashion enables preserving elementwise MPS relative to a common reference, which is not feasible with other scalar injury metrics. The earlier effective  $v_{rot}^p$  aimed at preserving peak MPS can be considered as a degenerated case when the head rotational axis is aligned with one of the anatomical directions.

As a result of the limited sampling of the pcBRA (the idealized head impacts only consider head rotational acceleration but not deceleration (Ji and Zhao, 2015; Zhao, Kuo, *et al.*, 2017a)), only ~60% of the impacts were successfully matched with an idealized impact from the pcBRA.

In reality, head deceleration always occurs in impact events, the alternative of which is not physically feasible. The rationale behind adopting acceleration-only head rotation with the pcBRA was because, historically, head impact kinematics were often characterized by linear and rotational or angular acceleration (Rowson *et al.*, 2009; Camarillo *et al.*, 2013). Some recorded impact profiles also focused on peak acceleration and may not capture the complete deceleration phase (Liu *et al.*, 2020). Yet, if deceleration is introduced to an impact with an identical peak rotational velocity generated from acceleration, the resulting strain magnitude would increase (Zhao, Kuo, *et al.*, 2017a) (or CSDM value as found for the GHBM model (Bian and Mao, 2020)).

A straightforward way to overcome this limitation is using half-sine biphasic rotational velocity profiles as adopted previously (Zhao, Kuo, *et al.*, 2017a; Lee F. Gabler, Crandall and Panzer, 2018) by including an additional deceleration phase into the idealized head rotational modes. This strategy was previously proven to be effective – for impacts failed to match with the monophasic impacts, their match significantly improved when using the biphasic idealized impacts (Zhao, Kuo, *et al.*, 2017a). To mitigate the time required for the simulation of biphasic rotational profiles, the latest CNN-based model (Ghazi *et al.*, 2020) can be conveniently and efficiently used to estimate the MPS distribution without the time-consuming direct simulation. This is illustrated in **Fig. 24**.

A real-world impact, on the other hand, could include vastly more features. These features include constant change in impact rotational axis, complex acceleration and deceleration profiles, velocity reversals, and some “impacts” are also a combination of two or more impacts. Each of these features introduces additional complexity to the cumulative strain pattern, which explains

why the pcBRA could only simplify 60% of the impacts. Further, these features could introduce questions over the importance of strain rate as well, which are beyond the scope of this study, but worth investigating in the future.

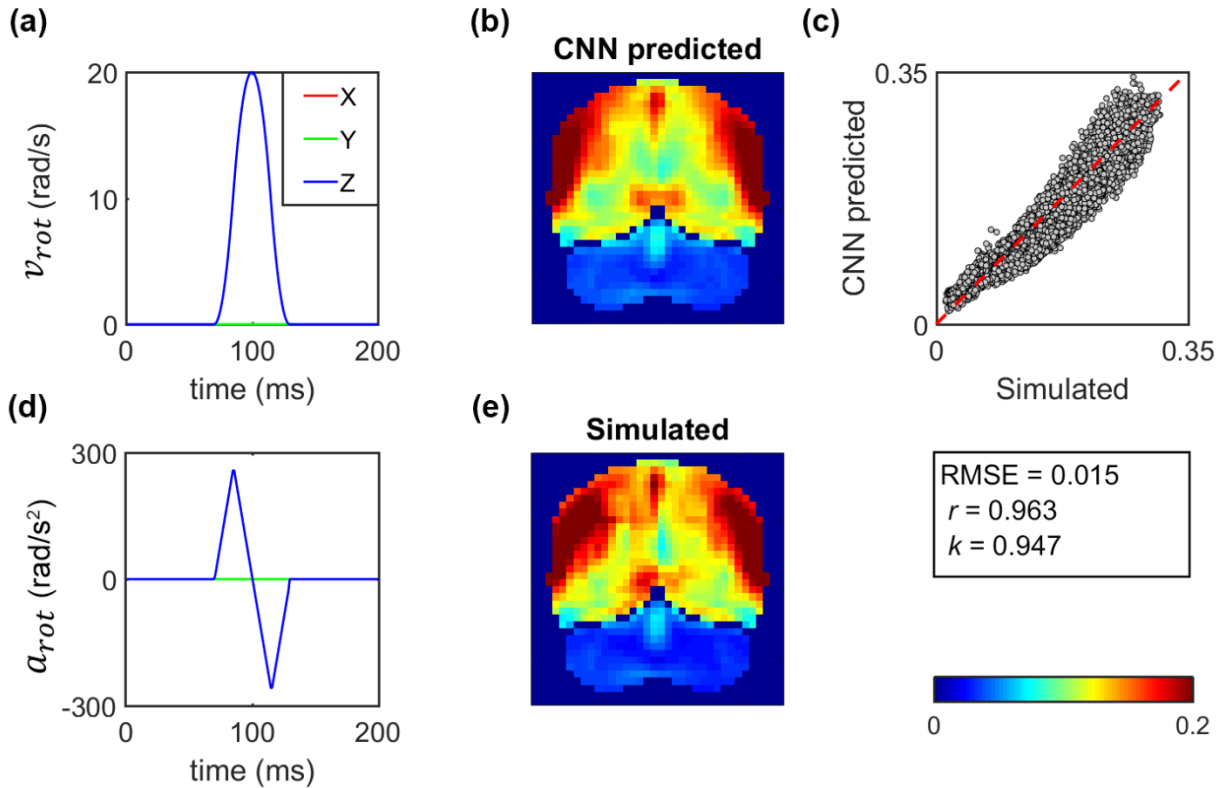


**Figure 25:** An example of a biphasic impact in pcBRA format. The CNN from aim 1 is fully capable of predicting the strain distribution for this impact.

~75% of the impacts that were predicted by the CNN were successful after being translated into elementwise MPS. Compared to estimating the strain directly (aim 1; success rate of 92–97% was achieved (Ghazi *et al.*, 2020)), the achieved performance was considerably lower. Which, was the result of at least two factors.

First, the smaller size of impact database was notably compared to the earlier aim (~1.9 k vs. 5.6 k). Second, the element-wise MPS obtained from the pcBRA was sensitive to the angular error in the rotational axis. To verify this, we introduced random angular perturbations to the rotational axis for  $N=100$  impacts in the pcBRA. Then the obtained elementwise MPS responses

were compared to the baseline counterparts. The  $r$  value was rapidly reduced when the angular perturbation exceeded 10 degrees compared to the baseline (e.g.,  $r$  degraded to a value of  $95.23 \pm 0.0266$  when perturbed by 10 deg, or  $0.8422 \pm 0.0668$  by 20 deg). Furthermore, the rate of failure rapidly increases after the 10 degree error mark, with all cases failing with an error of more than 30 degrees, in **Fig. 24**. This error could be minimized by increasing the data size to increase the accuracy of the CNN in terms of angular error.

### **Idealized head impact mode**

In essence, the goal of kinematics-based injury metrics is to transform head impact profiles into a common, numerical reference for comparison of impact severity. The comparison would then have the ability to infer the relative impact severity in terms of brain strain when using impact-induced brain strain as the benchmark to evaluate their performances. The technique proposed in this aim is an extension of the earlier efforts by establishing the concept of “idealized head impact mode”. This results in a simplification that can provide an intuitive comparison based on impact severity as well as directionality. One major advantage of this method is to include directionality which is not achievable in conventional injury metrics.

### **Limitations**

The limitations of this study are largely due to the limited modality of the pcBRA (as it has one acceleration phase with no deceleration). This results in a limited number of impacts which can be simplified using this impact library. This can be easily addressed by appropriately expanding the atlas. Further, another limitation was the dependence of the effective impact kinematics from this study on the given head injury model used to assess brain strain. This results in inherent limitations of the given head injury model transferring to the findings from this aim.

Despite these limitations, a new avenue to simplify head impacts into idealized but actual “impact modes” is proposed in this aim, which is an improvement over the conventional single scalar values. This method could facilitate a more intuitive and meaningful impact comparison in the future.

### **Acknowledgements:**

Funding is provided by the NIH Grant R01 NS092853. The Titan X Pascal GPU used in this work was donated by the NVIDIA Corporation.

## Chapter 6: Aim 3: Football helmet comparison based on strain-based and kinematics-based metrics

### Introduction

Sports and recreation related mild traumatic brain injury (mTBI), or concussion, is one of the major health concerns in the world United States (CDC, 2015). To minimize the risk of concussion, participants wear helmets in some sports and recreations, including American football (Rowson and Duma, 2011), ice-hockey (Allison et al., 2014; Rowson, Rowson and Duma, 2015), bicycle (Cripton et al., 2014; Bland et al., 2020; Fahlstedt et al., 2021), motorcycles (McIntosh and Lai, 2013), or snow sport (DiGiacomo, Tsai and Bottlang, 2021). The National Operating Committee on Standards for Athletic Equipment (NOCSAE) (National Operating Committee on Standards for Athletic Equipment, 2012), the Consumer Product Safety Commission (CPSC) in the US (CPSC, 1998), and the European safety standards (European Committee for Standardization, 1997) provide a set of test standards to rate helmet performance in terms of peak linear acceleration when striking a helmet on a rigid surface. These standards were developed to minimize the most acutely severe head trauma resulting from high linear accelerations (Levy *et al.*, 2004), and helmets have proven to be highly effective in reducing severe head injury and TBI (e.g., by 60% and 53%, respectively, for bicycle helmets (Høye, 2018)).

For instance, the initial standards by the NOCSAE, developed in the 1970s, were focused on regulating the amount of linear head acceleration exposure, which can result in severe TBI (e.g. catastrophic events such as skull fracture). These standards were based on drop tests, which are consistent of predominantly linear motion (Hodgson VR, 1974). However, with the growing concern about concussion and the associated long-term neurological consequences,

NOCSAE recently adopted a modified version of their methodology to limit both head linear and angular acceleration by adding standardized pendulum tests (National Operating Committee on Standards for Athletic Equipment, 2019). This is due to the fact that linear acceleration induces little strain in the brain (King *et al.*, 2003; Meaney, Morrison and Bass, 2014) due to the near incompressibility property of the brain (Ji, Zhao, *et al.*, 2014; Bian and Mao, 2020). As a result, helmet designs are also shifting towards reducing peak rotational kinematics (Bottlang *et al.*, 2020; DiGiacomo, Tsai and Bottlang, 2021).

Despite this improvement, however, the NOCSAE standard is still a binary requirement, which does not provide the means to compare helmets that do satisfy the standard. Consequently, there is need for a meaningful way to quantitatively compare the helmets' injury mitigation capabilities of the available helmets that satisfy NOCSAE standard.

To quantify the overall helmet safety performance in mitigating the risk of concussion, a rating system called the Summation of Tests for the Analysis of Risk (STAR) was developed to condense helmet performance from a range of tests into a single value (Rowson and Duma, 2011). Initially, a helmet was subjected to a NOCSAE-style drop tests at representative locations from representative drop heights. The resulting peak accelerations were used to calculate the probability of injury based on real-world concussion rates. A composite injury risk was then obtained by a weighted summation of impact condition-specific injury risks according to the corresponding relative impact exposures. However, the STAR evaluation system has similarly evolved to combine linear acceleration with rotational acceleration (Rowson, Rowson and Duma, 2015) or, more recently, rotational velocity (Bland *et al.*, 2020), following pendulum impacts to formulate the injury risk function, following the recent updated NOCSAE standards. This effort was further extended by developing sport-specific variants to account for the difference in head

impact location and location-specific exposure (e.g., hockey (Rowson, Rowson and Duma, 2015) and bicycle (Bland *et al.*, 2020) helmets).

Nevertheless, the STAR evaluation system relies on peak accelerations to assess the risk of injury; thus, it suffers from the general limitations with kinematics-based injury metrics. Although extensively used, kinematics-based injury metrics such as peak accelerations lack specificity in estimating concussion risk (Broglia *et al.*, 2010; Guskiewicz and Mihalik, 2011; Beckwith *et al.*, 2013). They are particularly prone to generating a large number of false positives (Mihalik *et al.*, 2017). In contrast, brain strains estimated from a validated head injury model is generally believed to be a more realistic measure of injury risk. The metrics based on FE models have proven to outperform the kinematic metrics (Zhao, Kuo, *et al.*, 2017b). More precisely, as a result of down sampling the impact profile to the peak rotational and linear accelerations, the injury risk function loses the directionality of the impact which has a significant effect on the resultant brain strains resulting from the impact. Further, this down sampling neglects the important effects of the impact profile shape variation (Zhao and Ji, 2017). In addition, the STAR risk function is based on rotational and linear acceleration, however it is known that brain strain is primarily caused by impact rotation (King *et al.*, 2003) and is mostly correlated peak rotational velocity (Kleiven, 2006). This suggests that there is a need for a deeper understanding on the tissue level to accurately quantify the effectiveness of sports helmets.

Consequently, there has been a shift of efforts to rate helmet performance using a head injury model in recent years. For instance, Clark *et al.* sought to highlight the discrepancies of peak MPS of the whole brain obtained from head models and the kinematics metrics to compare the performance of three ice hockey goaltender helmets (Clark *et al.*, 2018). Further, as even “validated” head models produce significantly different intracranial responses even

under identical impact conditions (Ji, Ghadyani, *et al.*, 2014), a study by Fahlstedt *et al.* used eight major head injury models to compare the performance ranking of 17 bicycle helmets (Fahlstedt *et al.*, 2021) using peak MPS and cumulative strain damage measure (CSDM) (Takhounts *et al.*, 2008). These studies provide some context for the need to develop a strain based helmet performance comparison system.

To this end, Finite Element (FE) head models provide detailed insight into brain tissue mechanical response. Studies have shown that tissue response-based injury metrics outperform those based on kinematics (Chiara Giordano, 2014; Hernandez *et al.*, 2015). As a result, numerous head injury models have been developed and validated over the years (Giudice *et al.*, 2019). Essentially an FE model is a non-linear function translating the impact kinematics to the brain mechanical responses. Perhaps as a result of this non-linearity, kinematic metrics underperform compared to FE based metrics in injury prediction. To infer the injury risk of a given impact based on FE models, injury metrics are driven from the FE simulation. The most predominantly used FE based injury metrics to translate an FE simulation into injury risk include the peak maximum principal strain (MPS) of the entire brain, and the cumulative strain damage measure (CSDM) (Zhao, Kuo, *et al.*, 2017b).

Yet, despite their appeal for providing detailed mechanical responses, FE models are complex mathematical models that have a substantial computational cost. Consequently, a number of studies have been dedicated to alleviating the long duration and the computational resources required to complete even a single simulation. One proposed method used to this end was the concept of pre-computation proposed by (Ji and Zhao, 2015; Zhao, Kuo, *et al.*, 2017b). In a previous study, we developed a method to leverage the efficiency of Convolutional Neural Networks (CNN) to directly obtain the whole brain peak MPS from the impact profile

(Wu, Zhao, Ghazi, et al., 2019). In aim 1, we expanded this method to predict the whole brain strain pattern instantly based on real-world data efficiently (Ghazi et al., 2020b).

The transition from kinematics-based approximation to strain-based design and injury risk analysis may be a potential outcome of the CNN technique. Nevertheless, in the context of helmet testing, this method has not been verified. Therefore, this aim has two objectives. First, to investigate the reliability of the CNN-based model for the assessment of helmet safety ranking within the STAR evaluation system. We conduct this by comparing the CNN-estimated brain strain measures (peak MPS and CSDM) against the direct simulation counterparts using a subset of helmet testing data. Second, using the trained CNN, the corresponding MPS distribution of 23 commercially available football helmet tests are obtained. These MPS distributions are used to compare the helmets in terms of injury risk mitigation capabilities using either peak MPS or CSDM. This study may provide important initial insights into the feasibility of using a brain strain-based helmet safety performance ranking system in the future.

## Methodology

### Roadmap

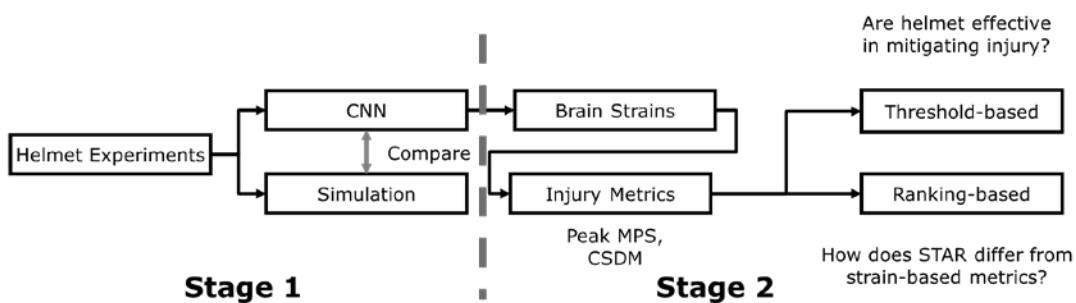


**Figure 26:** A flowchart of the current study. Firstly we obtain the brain strain patterns from the CNN in aim 1 (Ghazi *et al.*, 2020). Based on the strain pattern, we calculate the injury metrics (peak MPS and CSDM). Using the collected injury metrics we run two experiments to answer the questions of this study.

In this study we aim to examine the performance of helmets based on strains obtained from FE simulations. To achieve this goal, first revalidate our CNN from aim 1 with this database to ensure it can be used to obtain brain strains reliably. Then, we dive deep into the impact test database used for helmet performance analysis in the STAR method and compare the helmets based on the generated strains. The details of the helmets are given in table 8.

**Table 8:** The helmets used for this aim. The starred (\*) helmets were randomly selected for direct simulations.

ID	Helmet Model	Score	Weight (lbs)	Cost (\$)
A	Schutt_F7_LTD	0.75	5.1	975
B	Xenith_Shadow_XR	1.91	4.7	679
C	VICIS_Zero1	1.92	4.4	950
D	Schutt_F7_VTD	2.54	4.1	975
E	Xenith_X2E	2.92	4.1	289
F	Riddell_Precision_FIT	3.23	4.8	1700
G	Xenith_Shadow	3.35	4.3	479
H	Xenith_EPIC	3.79	4.2	349
I*	Riddell_SpeedFlex	4.49	4.4	410
J	LIGHT_LS1_CV	4.76	3.2	550
K	Schutt_Vengeance_Z10_LTD	4.97	3.4	499
L*	Schutt_Vengeance_Pro_LTD	5.24	3.8	299
M*	SG_DBS001	5.39	2.9	329
N	Schutt_Vengeance_Z10	6.28	3.7	210
O	Schutt_Vengeance_Pro	6.44	3.3	225
P	Schutt_F7	6.5	4.1	649
Q	Riddell_Speed	6.67	3.7	280
R	Schutt_Air_XP_Pro_VTD_II	6.98	4.5	220
S	Schutt_Vengeance_VTD_II	7.35	4.2	250
T	Schutt_Air_XP_Pro_Q10_VTD	8.42	4.1	336
U	Riddell_Speed_Icon	9.95	3.8	280
V	Schutt_Air_XP_Pro	18.22	3.7	200
W	Schutt_Air_XP_Pro_Q10	25.77	4	210

To assess the helmet performance based on the brain strains, FE models are used. However, one major drawback to FE modeling is the substantial computational cost and time consumption of simulations. For context, each impact in this study requires close to 30 minutes on a high-end computer cluster to simulate and an additional 30 minutes to extract brain strain patterns. This means to simulate the entire dataset in this study ( $N = 23 \times 48 = 1104$ ) we needed 46 days of constant simulation time. To mitigate that, we opted to use our previously established CNN (Ghazi *et al.*, 2020), which is capable of generating the whole brain strain pattern given the impact profile (aim 1). This CNN was validated against FE simulations from the Worcester Head Injury Model (WHIM) simulation results of a large database ( $N = 5661$ ) of real-world impacts using 10-fold cross validation. Hence, in this phase of the study we first we further validate our CNN from aim 1 to ensure it is sufficiently accurate with the impact data used in this aim. To do that we compare the CNN predictions to the direct simulation of all impacts corresponding to three randomly selected helmets. Once we ensure that our CNN performs sufficiently accurately, we generate the strain data for the entire helmet dataset. Finally, use the strain results to provide strain-based medical context for the difference in the performance of helmets.

### **STAR Methodology and Helmet Impact Database**

For the 12 standardized test conditions to obtain STAR values (3 pendulum angles: 40, 65, and 90 degrees, and 4 impact locations: Back, Front Boss, Front, Side), each experiment was repeated 4 times (2 trials  $\times$  2 specimens, and 48 total conditions). For this study, we averaged the resultant strains from the simulations for each scenario for each brain element (resulting in 12 mean MPS values, one for each scenario; **Fig. 25**) (Rowson, Rowson and Duma, 2015). The STAR risk assessment metric is based on the peak resultant rotational and

linear acceleration of impacts (**Fig. 25**). For the remainder of this study, the 4 trials for each of the 12 impact conditions were averaged to minimize the effects of testing variations.

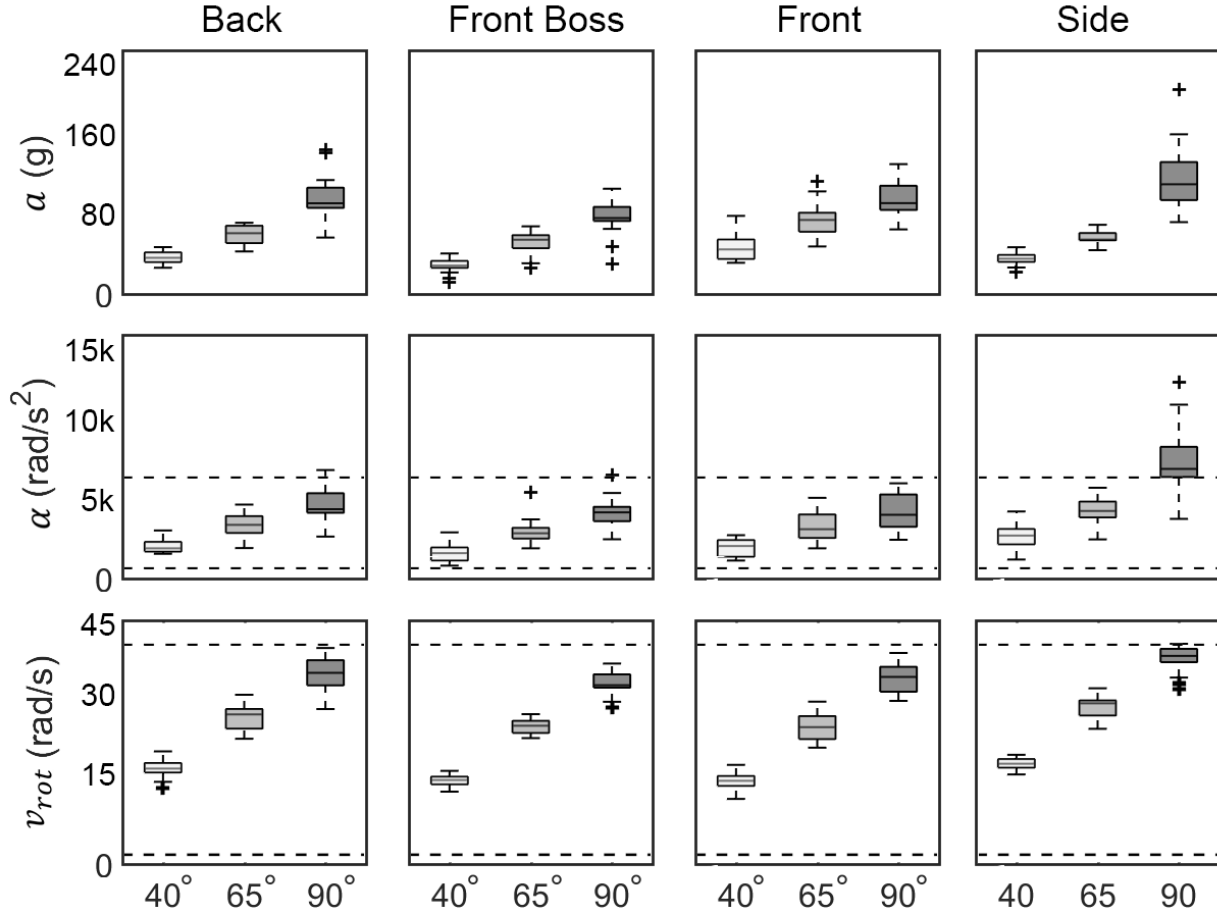


**Figure 27:** The distribution of the peak linear (first row) and rotational (second row) accelerations as well as the peak rotational velocity (third row) of the STAR test dataset used in this study. The dashed lines show the data range that the CNN in aim 1 was trained on (an acceleration range of 793 to 6313 rad/s<sup>2</sup> and a velocity range of 2 to 40 rad/s).

More precisely, the STAR score is defined as follows based on the impact kinematics:

$$STAR = \sum_{L=1}^4 \sum_{V=1}^3 E(L, V) \times R(a, \alpha)$$

Here, the terms  $L$  and  $V$  represent the impact location and velocity of each impact scenario respectively ( $V$  value of 1 through 3 corresponds to a pendulum angle of  $\theta = 40, 65,$

and 90).  $E$  is a statistically driven coefficient demonstrating the likelihood of each impact scenario (**table 9**).  $R$  is the concussion risk function, which is a function of linear acceleration ( $a$ ) and rotational acceleration ( $\alpha$ ). The risk function itself is a statistically driven property, which is defined as:

$$R(a, \alpha) = \frac{1}{1 + e^{-(-10.2 + 0.0433*a + 0.000873*\alpha - 0.000000920*a\alpha)}}.$$

Aside from the STAR values reported in **table 8**, we used an unweighted sum of the risk function as an additional injury metric in the next sections to facilitate better comparison.

**Table 9:** The exposures corresponding to each impact location and pendulum angle ( $\theta$ ) corresponding to the comparative likelihood of a representative impact being sustained (Virginia Tech Helmet Lab, 2020).

Location	$\theta = 40$	$\theta = 65$	$\theta = 90$
Back	42.3	9.2	2.0
Front	183.7	39.8	8.9
Front Boss	67.1	14.6	3.2
Side	39.0	8.5	1.9

For this study, we used an additional unweighted risk function, constituted from the unweighted summation of the risk functions in all 12 impact conditions to investigate the effects of the exposure factor.

$$STAR^* = \sum_{L=1}^4 \sum_{V=1}^3 R(a, \alpha)$$

## **Instantaneous brain strain estimation using a CNN-based brain injury model**

We use our previously developed CNN (Ghazi *et al.*, 2020) to predict the entire brain strain patterns to each impact in the database. To reaffirm the compatibility of the trained network with the experimental data, we randomly selected 3 helmets and simulated all the 48 corresponding experiments. Then we compared the CNN estimated brain strain patterns to the direct simulations via an element-wise regression model. Once we confirm that the brain strain distribution generated by the CNN are sufficiently accurate (Pearson correlation coefficient ( $r$ ) > 0.9 and  $0.9 < \text{linear regression slope } (k) < 1.1$ ), we use the CNN to estimate the brain strain pattern for the remainder of the data.

In addition, we compared the peak MPS and CSDM obtained from the CNN and the directly simulated counterparts to further reaffirm the accuracy of the CNN. The CSDM measure is the percentage of the brain volume that experiences MPS above a certain threshold (Takhounts *et al.*, 2008). In this study a strain threshold for CSDM was empirically chosen to be 0.15. We calculated the peak MPS values at the 95<sup>th</sup> percentile level for consistency. However, other percentile values (90<sup>th</sup>, 95<sup>th</sup>, or 100<sup>th</sup>) have also been used (Fahlstedt *et al.*, 2021). CSDM and peak MPS are global level strain-based metrics that are often used as the baseline for assessing the quality of kinematics-based injury metrics (Lee F. Gabler, Crandall and Panzer, 2018; Bian and Mao, 2020). The comparison of these two metrics was carried out based on coefficient of determination ( $R^2$ ) and root mean squared error (RMSE). If the comparison suggested sufficient accuracy in each scenario, the CNN-based model would then be applied to the rest of helmet impacts for strain estimation.

## **Range of helmet injury mitigation capabilities using brain strain**

The CNN MPS distribution estimation can allow for region-wise brain strains to assess the risk of injury, which can improve the injury assessment (Wu *et al.*, 2020). However, the global

scalar strain measures (e.g. CSDM and peak MPS) remain the most predominantly metrics today (Lee F. Gabler, Crandall and Panzer, 2018; Bian and Mao, 2020; Fahlstedt *et al.*, 2021). A logistic regression is usually used to derive an injury threshold value based on a real-world injury labeled database. An injury probability can be produced using this method for use for an arbitrary head impact according to the corresponding brain strain. Yet, an injury threshold based on strain is yet to be developed since a large on-field impact dataset and actual concussion cases is currently not available. A widely used reconstructed National Football League (NFL) dataset (Sanchez *et al.*, 2018) has been used for this application (Viano *et al.*, 2005; Kleiven, 2007; Anderson *et al.*, 2020; Wu *et al.*, 2020). Nevertheless, the reconstructed impacts substantially oversamples concussive impacts relative to non-injury cases (20 concussions vs. 33 non-injuries) and hence the resulting injury threshold is not applicable to real-world on-field impacts (Pellman *et al.*, 2003; Kleiven, 2007).

Therefore, here we utilized a range of sweeping injury thresholds over the entire range of peak MPS and CSDM, respectively, to characterize the helmet injury mitigation capabilities. Thereby an impact was said to be concussive if the corresponding peak MPS or CSDM exceeded the threshold value. To minimize the effects of the step-size, it was set at 0.1% of the corresponding value range. As the injury metrics were averaged across the two helmet test samples and the two impacts for each impact condition (location and pendulum height; N=12), the maximum number of likely concussions was 12 (which occurred when the injury threshold was at the lower end of the range). The minimum number of concussions was 0, which occurred when the threshold was set to the higher end of the range.

A range of strain-based concussion mitigation capabilities would be produced by the binarized numbers of possible concussions among the helmets at each injury threshold, which would provide insight into the uncertainty of concussion mitigation capabilities for helmets.

## Statistical Analysis

All head impacts from the randomly selected impacts were simulated using the anisotropic WHIM V1.0, which took ~30 min for one impact of ~100 ms duration (double precision with 15 central processing units [CPUs] and graphics processing unit [GPU] acceleration; Intel Xeon E5-2698 with 256 GB memory, and 4 NVidia Tesla K80 GPUs with 12 GB memory). Another 30 min was necessary to extract peak MPS distribution across the impact duration. In total, this study required ~46 days of nonstop computations to generate the data, which was mitigated by Using the trained CNN from the first aim. The CNN estimation took ~1 sec to predict the complete strain distribution of the brain for the entire data set on an NVIDIA Titan X Pascal GPU with 12 GB memory. The similar instant results were obtainable using a low-end laptop.

The Peak MPS was obtained using the 95<sup>th</sup> percentile of the voxel-wise (voxel size = 5mm) brain strain for each impact. The CSDM threshold in this study is 0.15 (commonly referred to as CSDM15), which was obtained by the number of voxels that exceeded the 0.15 cumulative strain threshold by the number of the entire voxels. Finally, the consistency in helmet performance ranking was compared by using either the STAR values or strain-based metrics among helmets, either aggregated from all impact conditions with exposure-based weighting, or under each impact condition separately.

All data analyses were conducted using MATLAB (R2019b; MathWorks, Natick, MA). Student's *t* tests were used to compare the injury prediction performances. Statistical significance was reached when the *p* value was <0.05.

## Results

### CNN Performance in Brain Strain Generation

The CNN was capable of accurately estimating the entire brain strain for almost all the impacts. The success rate for these impacts was 98.6%, which is consistent with the findings in the first aim. This was while the “unsuccessful” cases also fall within a reasonable estimation range (**Fig. 28**).

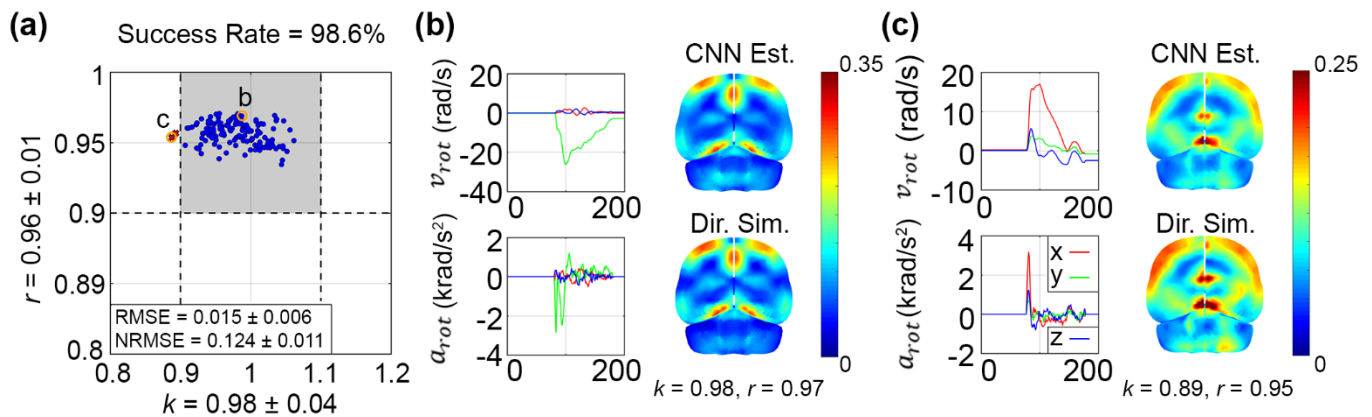


**Figure 28:** An illustration of the voxel-wise comparison between the strain distribution obtained from FE simulations and the CNN estimations. (a) illustrates the performance in terms of  $k$  and  $r$  between the CNN estimation and corresponding simulations. (b) and (c) illustrate two example cases of the CNN predictions.

### Comparison between CNN and simulation in injury metrics

Translating the generated strains from both the simulations and the CNN predictions revealed a high correlation between the two for both injury metrics (Figure). Hence, the CNN proved capable of injury metric estimation for the rest of the impacts.

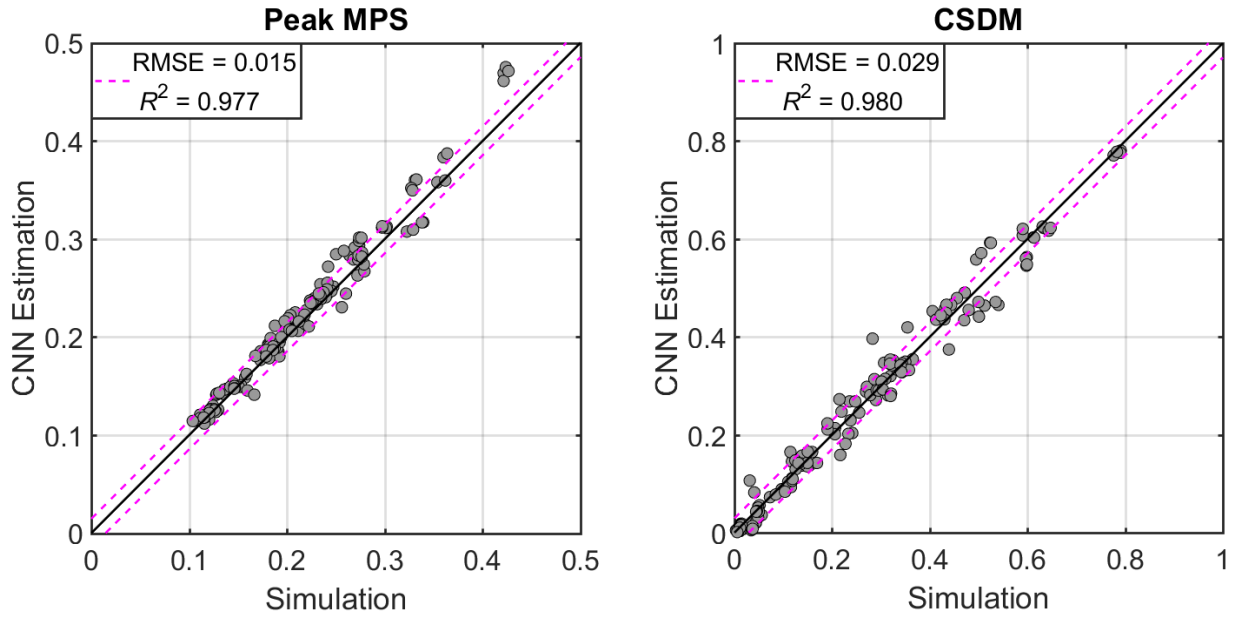


**Figure 29:** A scatter plot of the peak MPS (left) and CSDM (right) between each simulations and the corresponding CNN prediction.

### Strain-based uncertainty in helmet concussion mitigation capability

We observed a statistically significant difference between the concussion mitigation ability of the best and the worst helmets across all thresholds. This observation holds true for both peak MPS and CSDM comparison ( $p < 0.05$ ). The best helmet was on average able to mitigate 22.7% and 28.3% of the concussions across the threshold spectrum based on peak MPS and CSDM respectively (**Fig. 29**). For the peak MPS threshold of 0.3, the helmet ranked as the “worst” by the STAR function had no binarized concussion, while helmet “M” had 4.

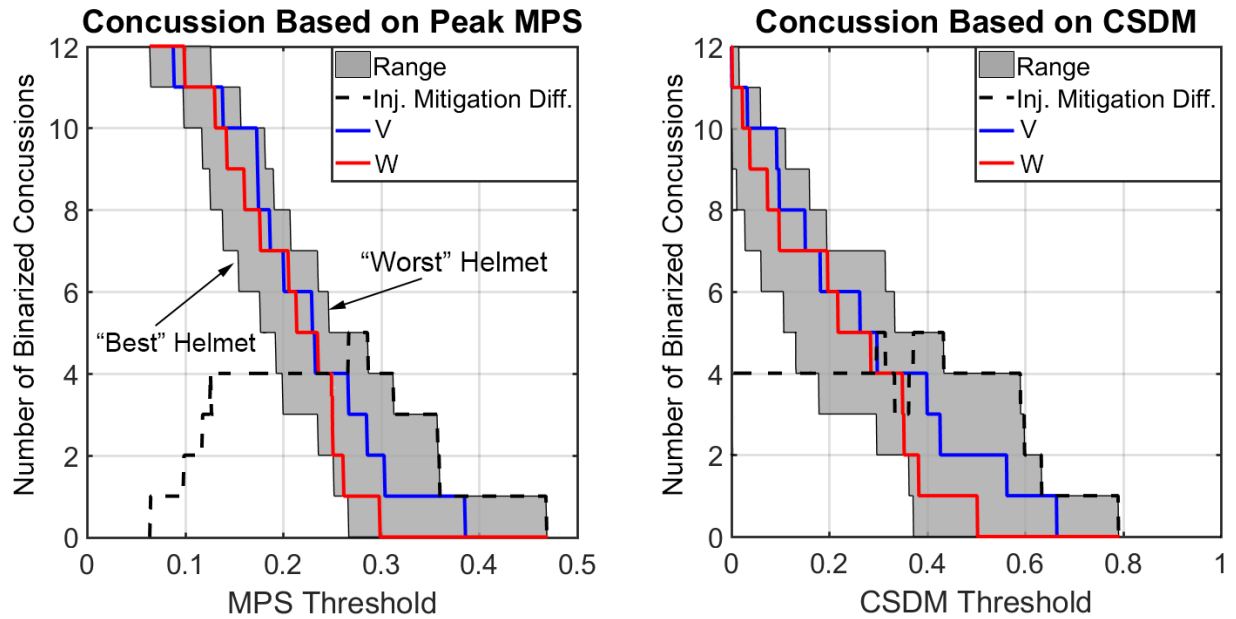


**Figure 30:** (a) shows the number of concussions between the best and the worst helmet based on each threshold value and regardless of helmet. The shaded area between the two curves shows the difference between the best and the worst helmet given each threshold. (b) Illustrates the same properties for CSDM. In both figures, the red and blue line illustrate the helmets ranked the poorest among all helmets. The dashed line in both sub-figures represents the injury mitigation difference between the best and the worst helmet in each threshold value.

## Investigation of Significance of Impact Directionality in Helmet Injury Mitigation

### Performance using an Impact location-based comparison

A close look at the distribution of the injury metrics (both peak MPS and CSDM) reveals a large difference between impact conditions (**Fig. 30**). In other words, comparative performance of the helmets differ significantly ( $p < 0.05$ ) in different impact conditions. This is consistent regardless of injury metric (CSDM or peak MPS).

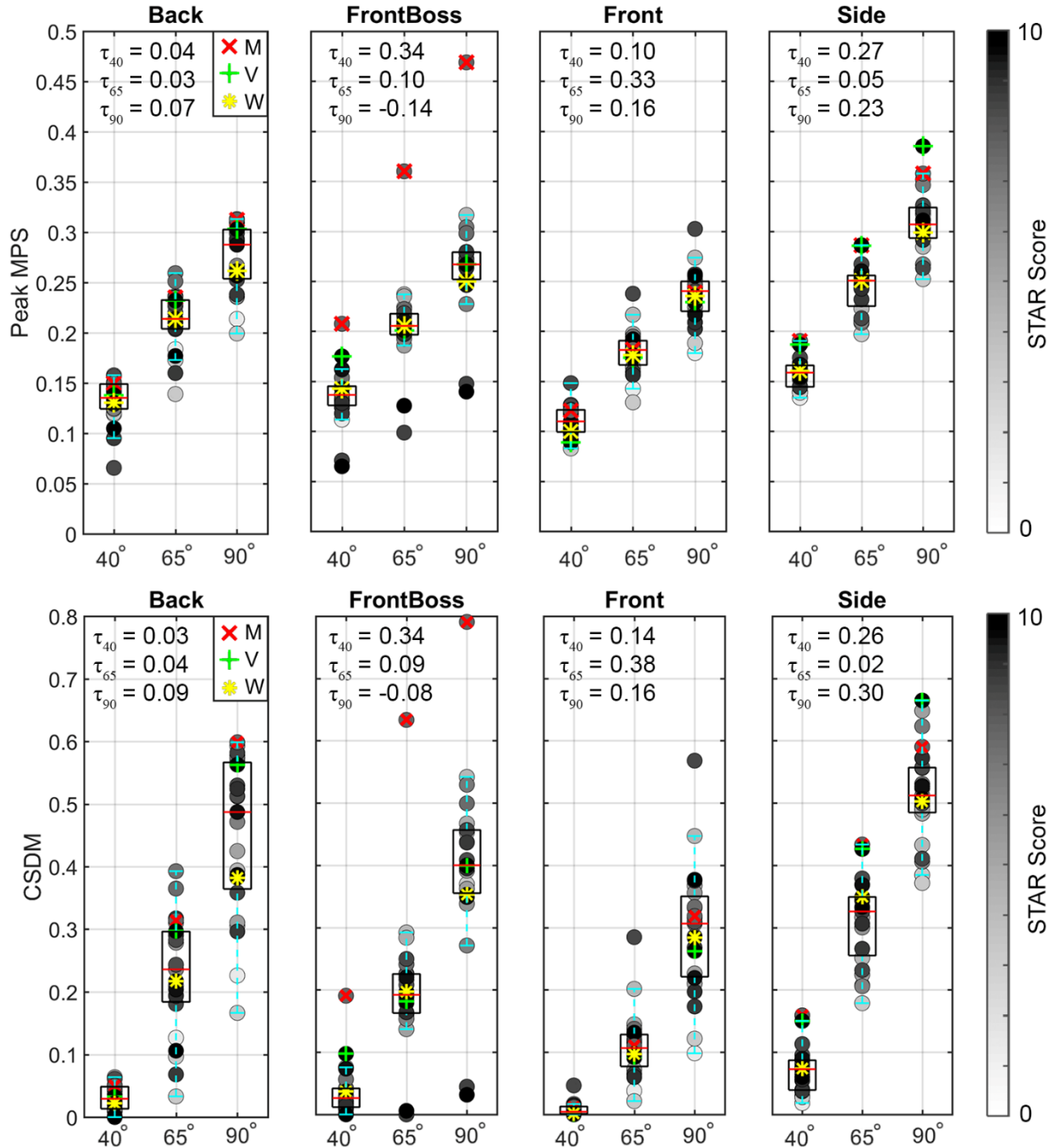


**Figure 31:** Box plot of the peak MPS (top) and CSDM (bottom) across helmets in each scenario. Helmets V and W (shown in green and yellow respectively) had the lowest STAR score yet performed average in terms of strain metrics. Helmet M (shown in red) generated large strains in the front boss direction, but perform close to the average in other directions.  $\tau$  denotes the kendall's tau value between the ranking in each scenario and the STAR ranking of the helmets.

## Discussion

Kinematic metrics are currently the most predominant method used in helmet safety performance rating and ranked. Recently, to mitigate the risk of concussion, helmet design criteria have shifted towards limiting head rotational motion in terms of peak rotational acceleration or velocity during helmet impact. This is a consequence of the mounting evidence that head rotation is the primary contributor to brain strain thought responsible for concussion. However, brain strains and peak rotational kinematics do not typically correlate well (Lee F. Gabler, Crandall and Panzer, 2018; Bian and Mao, 2020). Therefore, there is a potential that brain strain may potentially replace peak kinematics to improve the effectiveness of helmet safety performance evaluation, if it can be directly and efficiently obtained with sufficient accuracy.

In this study, we proved the capability of the developed CNN in the first aim is capable of instantly producing sufficiently accurate elementwise MPS of the entire brain. a success rate of 98.6% was achieved, based on 144 impact simulations from three randomly chosen helmets. Yet, the elementwise linear slope and the Pearson correlation coefficient only marginally deviated from the “success threshold” for the two “failed” cases ( $k$  no less than 0.8; **Fig. 27 a**). Further, the two “failed” cases poses some unique features in the corresponding head rotational velocity profile where the impact profiles go through a steep velocity increase, followed by a much less steep velocity climb before reaching to the peak. In other words, the peak velocity comes to a “flat” peak (as opposed to a sharp peak; **Fig. 27 b**) which can reduce the accuracy of the CNN.

The high accuracy was maintained when deriving the peak MPS and CSDM from the CNN elementwise estimation ( $R^2$  of 0.977 and 0.980, with RMSE of 0.015 and 0.029 respectively). This is similar to the performance of the CNN-based approach used to predict the peak MPS directly based on the impact profile (Wu, Zhao, Ghazi, *et al.*, 2019), and another state-of-the-art “best-

performing” kinematics-based injury metric, such as DAMGE (Lee F. Gabler, Crandall and Panzer, 2018).

The high estimation accuracy was not surprising, given that head rotational kinematic profiles in helmet testing were notably simpler than those directly measured on the field. Hence, they did not have impact “features” that are new to the trained CNN, which resulted in the good performance. Additionally, these impacts are well within the range, for which the CNN was trained and have a near zero initial velocity, which further contribute to the accurate MPS estimations.

Collectively, these results suggest the feasibility of applying the CNN-based brain injury model for routine use in helmet testing. In fact, in simpler impact settings such as those in the laboratory testing conditions, the CNN performs very reliably.

### **Disparities between strain-based helmet safety performances**

Firstly, substantial disparities were observed in helmet safety performance using strain-based measures. These disparities are particularly pronounced in different impact locations, even for the same helmet. For instance, the helmet “M” (SG DBS001) produced substantially higher strain values than all other helmets in the front boss direction and hence performed poorly based on our two strain metrics. This is due to the fact that as a result of the helmet design, it translates the impacts in the Front Boss direction into a large axial component, which is known to produce more strains in the brain compared to the sagittal and coronal counterparts (E. G. G. Takhounts *et al.*, 2013; Bian and Mao, 2020). This makes this helmet perform the “worst” in terms of strain driven metric ranking.

Second, even within each impact condition, a close peak MPS does not necessarily translate into the same injury risk. The reason is that the peak MPS samples the 95<sup>th</sup> percentile of strain in the entire brain regardless of the location, in which the high strain occurs. Hence the

strain could occur in a different area of the brain while maintaining the peak MPS value. **Fig. 33** illustrates an example of two helmets in the same impact condition that produce different strain distributions.

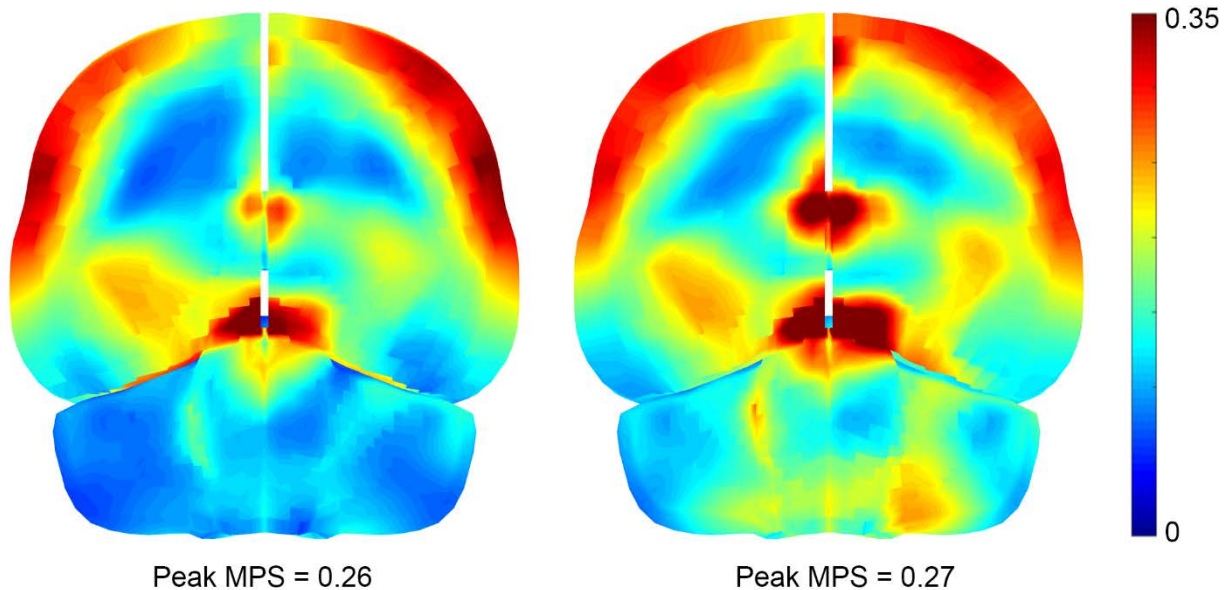


**Figure 32:** An illustration of the strain pattern difference between two impacts that have a low correlation. These two cases belong to the impact condition with  $\theta = 90^\circ$  and the Front Boss impact location, and the helmets O and P (“Schutt F7 LTD” and “Schutt F7” corresponding to the left and right figure respectively).

### Potential of CNN to facilitate helmet testing and iterative design

It is conceivable that the instantaneous CNN-based brain injury model could be adopted more widely in helmet testing and design, given the high accuracy in strain estimation (**Fig. 27**). This provides further evidence that this method would avoid inherent limitations with kinematics-based counterparts by providing a strain-based injury risk function reliably, which could improve the effectiveness in helmet performance evaluation. However, a complete six-degree-of-freedom (6-DOF) impact acceleration impact profile is required in this method to enable model simulation. This is yet not possible as such needed impact profiles for head rotation (Rowson and Duma, 2011) are not directly provided by earlier impacts based on the HITs system (Greenwald *et al.*, 2008). While mouthguards measure complete 6-DOF impact profiles (Liu *et al.*, 2020), a large

impact dataset consisting of both concussive and subconcussive impacts is yet to become available to allow deriving a strain-based injury risk function.

The STAR evaluation system relies on an injury risk function determined from actual on-field impact measurements and injury diagnoses. As a result, developing a tissue-level equivalent requires simulating all of head impacts used to develop the STAR system. Several challenges remain on the way of such approach. Firstly, to obtain the generated strains within the brain a large series of head impacts must be simulated using a FE head model. However, as discussed before, this is rather computationally expensive and can result in months of constant simulation time even on a high-end computing system. As shown in this aim, a potential way to address this problem is use of the efficiency that CNN readily offers, which addresses this challenge. Nevertheless, the CNN-based strain estimation is model-dependent and relies on the training dataset generated from the anisotropic WHIM.

While it is conceivable to use more sophisticated injury metrics that approximate brain strain with good accuracy (Lee F. Gabler, Crandall and Panzer, 2018) to develop a helmet ranking system, it would be ideal to use brain strain directly, if it is made feasible.

## **Limitations**

Firstly, this study is based on the current understanding of mTBI. Hence the findings in this study are based on the maximum principal strains only. While these metrics do generally outperform the kinematics based metrics (Zhao, Kuo, *et al.*, 2017b), there are other more sophisticated injury metrics that can provide a better injury prediction performance (e.g. a network-based injury prediction metric considering the gray matter regions of interest as well as the white matter interconnections between them (Wu, Zhao, Rowson, *et al.*, 2019)). This

suggests a more sophisticated understanding is needed for the mechanics of concussion. Yet, providing insight into the MPS distribution is a significant step forward from the *status quo*.

Second, although this study provides insight into the differences between helmets, it is still based on the standard tests used for obtaining the STAR score, which replicate certain peak linear and rotational accelerations. However, the strain generated in the brain tissue is significantly affected by the duration, directionality, and shape variations of the impact (Zhao and Ji, 2017). This illustrates that more investigation is needed to characterize and account for the impact shapes that result in injury relevant peak kinematics.

Third, to save time and computation, we used the trained CNN from the first aim to generate the strain patterns for the test data. Hence, another inherent limitation of this study is the limitations of the CNN. Although the CNN proved to work with this particular database, it needs to be stress tested before use for any impact database as it can be prone to error due to certain impact characteristics that were covered in aim 1.

Fourth, the strain-based performance comparison of helmet was limited to one head injury model. Yet, as discussed in the background section, different models are known to produce different strain responses even for the same impact (Ji, Ghadyani, *et al.*, 2014). Therefore, results from the strain-based evaluations may change when another model or the upgraded WHIM V2.0 (Zhao and Ji, 2020c) is used. Nevertheless, a recent study suggests that WHIM V1.0 is largely consistent with the majority of other head injury models when studying bicycle helmet safety ranking and rating in oblique impacts (Fahlstedt *et al.*, 2021).

Fifth, a more effective comparison with the STAR values would have been possible by a strain-based injury risk function, which is yet to be developed. An example of such risk function is a logistic injury risk function that would nonlinearly transform the peak MPS (range from 0 to ~0.5) or CSDM (range of 0–1) into an injury probability value in the range of 0–1. Yet, as a

result of the fact that such function would be monotonic (injury risk would increase with an increase in the injury metrics), we do not anticipate any significant change should the strain-based injury risk function become available in the future. For example, as similarly conducted before (Rowson and Duma, 2011) while accounting for concussion underreporting, the CNN-based brain injury model may be applied to a large on-field impact dataset to fit the strain measures against the recorded concussions. Such study is a valuable next step worth pursuing, which is beyond the scope of this study.

## **Conclusion**

The field of TBI is gradually shifting towards using FE based strain metrics to assess the risk of mTBI. This study is another milestone, providing a deep understanding of the substantial differences of helmets based on common FE based injury metrics as well as the brain strain distribution. Further, using the CNN tool, these analyses are readily available for the research community as well as the helmet manufacturing companies with insignificant computational cost, especial instrumentation, or any additional cost. This study provides a tissue based context for the necessity of investigating a strain-based approach to the helmet design cycle to improve the performance of helmets and minimize the devastating effects of mTBI in contact sports.

## Chapter 7: Conclusions and future directions

Mild Traumatic Brain Injury is a major health concern in the United States and around the world and is especially common in contact sports. These injuries are difficult to reliably diagnose as they are often diagnosed in a symptom-based fashion. Further, the competitive atmosphere of contact sports is a contributing factor that can cause the athletes to be less likely to recognize, appreciate the significance of, or disclose symptoms. Yet, undiagnosed mTBI can lead to serious health complications such as neurodegenerative diseases. As a result, there is a significant need to reliably predict the risk of concussion, and prevent concussion using preventative equipment. FE models are used to model such incidents, yet they are computationally expensive, making them infeasible in a side-line scenario. As a result there has been a recent shift to pre-computation based techniques to bypass the time consuming FE simulations. Nevertheless, as a result of the complex nature of impact profiles, referring to the pre-simulated database to exploit the full potential of such methods is a challenge. Here, we addressed this challenge by using deep learning based approaches, which are well-suited for modeling such complex scenarios with constant boundary conditions.

In this dissertation, we first identified a gap in the literature, which was addressed in chapter 3. The used software package for FE simulation is a potential point of discrepancy in FE based TBI research and has received little attention in the literature. Hence, we established a bridge between two of the most widely-used software platforms currently used in FE modeling: Abaqus and LS-DYNA. We designed a study in which we convert our Worcester Head Injury Model with material anisotropy, which was originally developed in Abaqus, into LS-DYNA format, and identified the differences between the two packages along the way. We used the most reliable element type in Abaqus (C3D8I) as a benchmark and converted the WHIM with C3D8I elements through a series of steps into an isotropic version with C3D8R elements that

could be directly translated into LS-DYNA format. Then, we translated the model into LS-DYNA without any alterations and compared the model with all the appropriate LS-DYNA element types and hourglass control techniques to the compatible Abaqus model. Then we identified the LS-DYNA configurations that perform the most similarly with Abaqus. This study shed light on a contributing factor to the disparity between different available FE models.

In the rest of the dissertation, we aimed to bridge the gap between FE based TBI research and utilization of such methods in real-world scenarios with limited time and computational power. As a result, we developed and assessed different machine learning based approaches with the goal of making different aspects of FE based injury assessment real-time. Firstly, we developed an approach to bypass FE based model simulations entirely and obtain the entire brain strain pattern directly from the impact profile using a pre-trained CNN. Second, we developed a new, strain-based injury metric using an inverse approach to map brain strains into a simple kinematic profile. The advantage of this approach is that unlike all other available kinematic based injury metrics, it accounts for impact directionality. Third, we put our developed methods to use in a real-world scenario by investigating the effectiveness of a number of helmets based on the generated strains in the brain.

The findings in aim 1 can effectively bypass FE simulations while providing reliable and reasonable brain strains. The novelty of this method is that it provides strains instantaneously and as it is constructed on real-world data, it is equipped to handle the level of complexity in a contact sports sideline setting. The CNN from the aim 1 was stress-tested a number of times with independent datasets (e.g. in aim 3) and has yielded consistent performance across all databases. This further increases our confidence in this methodology. There is a wide variety of potential applications for the CNN based method. For instance, this method can be reliably used in conjunction with state of art FE based injury metrics (e.g. simple logistic metrics such as peak

MPS or complex methods such as the injury matrix in (Wu, Zhao, Rowson, *et al.*, 2019)) in a sideline setting. This bridges the gap between the best currently available technologies for injury assessment (FE modeling) and the real-world application through overcoming the hurdle of computational cost. Further, as a result of the low computational cost and the fact that it is freely available, this methodology can be integrated into TBI research, preventative gear design cycles, and the process of designing the standards for such applications. Another advantage of such method is that it can improve by adding new impacts to the database to reliably predict strains for other applications, such as automotive applications, as well.

Yet, despite these advances in the FE based TBI research, the kinematics-based metrics are generally preferred in practice. One of these practical applications is the contact sports sideline scenarios, where even with the appropriate instrumented gear (e.g. instrumented mouthguards or helmets), the teams only use the peak values of the impact profile, which is not indicative of the injury relevant brain strains. Further, this under sampling neglects impact directionality as well as impact profile shape, both of which play a substantial role in the strains generated in the brain tissue. To bridge this gap, we developed a strain-based equivalent impact kinematics that can preserve peak MPS of the whole brain as well as elementwise MPS. This approach can accommodate the preference of the community for tangible impact kinematics and thereby revolutionize the *status quo*. This impact simplification also allows for an intuitive comparison across impacts based on commonly used kinematic metrics (e.g. peak acc), which is otherwise unfeasible with real-world impacts as a result of their complexity. This comparison is possible since the peaks in effective kinematics are strictly correlated to the FE based results (Aim 2).

Aim 3 illustrates a real-world scenario where the aim 1 could be used. It is a well-known fact that kinematics metrics cannot be directly translated into strains as a result of the non-linear

properties of the problem. However, kinematic metrics are the main means used for helmet standards as well as helmet performance comparison techniques today. This suggests the need for a deeper understanding of the tissue-level implications of using kinematics in helmet performance comparison. As a result, our aim 3 focuses on a strain based helmet performance comparison between a number of helmets that were similarly ranked with the current kinematics based methods (the widely accepted STAR method). We further took this opportunity to use our CNN from aim 1 to obtain strains for helmet tests. This served two purposes: first, to reaffirm our findings about the CNN performance from aim 1, and second, it saved days of simulation time which would be necessary have we used FE simulations. While comparing the helmets, we found even helmets that are similarly ranked sometimes substantially differ in terms of FE based injury metrics. Aside from the complex relationship between the impact profile and the brain strains, another contributing factor to this disagreement is the fact that the used STAR ranking system also considers linear acceleration, which plays a minimal role in strain generation. Our second finding was that helmets perform differently across different impact conditions. Hence, the ranking should be also based on the amount of exposure of the head to each impact location (as already implemented by the STAR method). Lastly, in the same impact condition, the regions of high strain were significantly different in some helmets. While this may have an effect on the probability or region of injury, this difference is not reflected in neither the kinematics based metrics of the impact nor the commonly used injury metrics (peak MPS and CSDM). This aim highlights the importance of incorporating a strain-based system into helmet comparison methodologies.

We developed two different data-driven approaches using deep learning to combat the computational cost of FE modeling. One of these two approaches (aim 1) have more implications for the research community while the other (aim 2) facilitates a more intuitive understanding of the injury mechanics and has more implications in the sports community. We

further used one of these aims to facilitate a deeper understanding about the medical implications of the current methods for helmet performance evaluation compared to a strain-based approach. However, as these findings are based on FE models, they inherit the limitations of FE modeling.

Firstly, a majority of head models are validated using the experimental relative brain-skull displacement from a number of available cadaver (Hardy, 2007; Hardy *et al.*, 2007; Sanchez *et al.*, 2018) and volunteer data (Alshareef *et al.*, 2018b). However, There are significant differences between the available head models, even after model validation (Zhao and Ji, 2020b). A number of studies have observed significant difference in terms of strains across various “validated” models in terms of strains and strain rate (Hardy *et al.*, 2007; Ji, Ghadyani, *et al.*, 2014). Further, the KTH head model (Giordano and Kleiven, 2016) showed up to a 45% whole brain strain reduction after incorporating white matter fiber reinforcements, with negligible change in the displacement-based validation score. Recent studies have shed light on this limitation and efforts are already being made to address this discrepancy (Zhao and Ji, 2020b).

Another limitation, which is not specific to this study but to FE based TBI research in general, is that the current literature focuses on the maximum principal strains only. Hence, the current studies are only focused only on brain tissue tension. However, this discards the negative brain tissue strain (compression) which can also result in injury (Bar-Kochba *et al.*, 2016). Further, the directions taken in this study and in the general direction of TBI research so far have been based on the cumulative strain distribution of the brain. This, however, the temporal exposure of the brain to high strains over time could be an avenue to pursue in the future.

As a result of the methodologies in this dissertation being data-driven, they are potentially prone to higher error when confronted with an unseen dataset. The functionality of

deep neural networks is based on learning the “features” of the input (in this case the impact profile). Hence, given a new dataset with new features in the impact profiles that were not included in the training data, the CNN might produce larger errors. This issue is especially important to consider since the different instruments, as well as different scenarios, may introduce additional features (e.g. variations in data sampling resolution, non-zero initial and final velocity, and impact duration). Further, some recorded impacts could be incomplete (e.g. only the acceleration or deceleration phase was captured), or irregular (high initial velocity as a result of a high impact recoding threshold) or occurrence of multiple serious impacts (multiple peak kinematics). To address this we included different real-world datasets (and augmented data based on the existing real-world impacts) and different sources (instrumented helmets, mouthguards, professional and high school football as well as other contact sports).

Another limitation to the current method is that it is bound to the WHIM V1 with the current characteristics and boundary conditions. Hence, with any change in the head injury model or the boundary conditions the CNN needs to be retrained, which is time-consuming. Nevertheless, this dissertation proves that the concept of a deep learning based method to accurately predict the strain pattern is possible.

In addition, a limited supply of impacts with a binary injury label was available to us for injury prediction. The injury labeled database used in this study is consistent of 53 reconstructed impacts from the NFL. However, it is well-known that concussive impacts are over-represented in this database. Hence, ML based method trained based on this data could potentially result in type 1 error in the injury classification.

Finally, we uncovered a large difference between strain-based metrics and a statistically-driven kinematics metric. Although the kinematic metric performs well in sports related concussion assessment, it is not based on injury mechanics. Hence, the performance could

improve if the same fitting methodology was developed on the tissue-level brain responses to increase the robustness of the method and potentially improve the performance. To our knowledge, an equally large dataset of real-world impacts with injury labels that has the complete impact profile (and can be simulated) is not available. But the same technique used for the development of STAR could be implemented for a tissue-level STAR, once such data becomes available.

In conclusion, we removed a significant hurdle on the way of using strain-based responses in real-world scenarios by introducing deep learning-based approaches to overcome the severe computational cost of FE modeling in TBI. This thesis addresses the logistical shortcomings of FE modeling as a result of their computational expense, which is otherwise a more accurate injury assessment method than the *status quo*. However, further investigation is needed to take advantage of whole-brain strain distribution to its full potential as well as to uncover other contributing factors to concussion. This can result in a more accurate assessment of brain injury in real-time and thereby prevent the devastating effects of multiple concussions such as CTE. We hope this work would contribute to timely diagnosis of concussion, improvement of protective gear design, and would benefit the general public as well as the TBI research community at large.

## Chapter 8: References

Van Der Aalst, W. M. P. *et al.* (2010) 'Process mining: A two-step approach to balance between underfitting and overfitting', *Software and Systems Modeling*, 9(1), pp. 87–111. doi: 10.1007/s10270-008-0106-z.

Abaqus (2016) 'Abaqus Online Documentation, Abaqus 2016'.

Ahmadzadeh, H., Smith, D. H. and Shenoy, V. B. (2014) 'Viscoelasticity of tau proteins leads to strain rate-dependent breaking of microtubules during axonal stretch injury: predictions from a mathematical model.', *Biophysical journal*. Biophysical Society, 106(5), pp. 1123–33. doi: 10.1016/j.bpj.2014.01.024.

Alshareef, A. *et al.* (2017) 'A Novel Method for Quantifying Human In Situ Whole Brain Deformation Under Rotational Loading Using Sonomicrometry', (434), pp. 1–31. doi: 10.1089/neu.2017.5362.

Alshareef, A. *et al.* (2018a) 'A Novel Method for Quantifying Human In Situ Whole Brain Deformation under Rotational Loading Using Sonomicrometry', *Journal of Neurotrauma*, 35(5), pp. 780–789. doi: <https://doi.org/10.1089/neu.2017.5362>.

Alshareef, A. *et al.* (2018b) 'A Novel Method for Quantifying Human In Situ Whole Brain Deformation Under Rotational Loading Using Sonomicrometry', *Journal of Neurotrauma*. Mary Ann Liebert, Inc. 140 Huguenot Street, 3rd Floor New Rochelle, NY 10801 USA, 35(5), pp. 780–789. doi: 10.1089/neu.2017.5362.

*American Academy of Neurology Report of the Quality Standards Subcommittee, Practice Parameter: The management of concussion in sports. Neurology (1997) Neurology*. Available at: <https://www.acr.org/-/media/ACR/Files/Practice-Parameters/arteriog.pdf>.

Anderson, E. D. *et al.* (2020) 'Predicting Concussion Outcome by Integrating Finite Element Modeling and Network Analysis', *Frontiers in Bioengineering and Biotechnology*. Frontiers, 8(April), p. 309. doi: 10.3389/fbioe.2020.00309.

Atsumi, N. *et al.* (2018) 'Human Brain Modeling with Its Anatomical Structure and Realistic Material Properties for Brain Injury Prediction', *Annals of Biomedical Engineering*, 46(5), pp. 736–748. doi: 10.1007/s10439-018-1988-8.

Bailey, A. M. *et al.* (2020) 'Comparison of Laboratory and On-Field Performance of American Football Helmets', *Annals of Biomedical Engineering*, 48(11), pp. 2531–2541. doi: 10.1007/s10439-020-02627-5.

Bar-Kochba, E. *et al.* (2016) 'Strain and rate-dependent neuronal injury in a 3D in vitro compression model of traumatic brain injury', *Scientific Reports*. Nature Publishing Group, 6(August), pp. 1–11. doi: 10.1038/srep30550.

Bazarian, J. J. *et al.* (2012) 'Subject-specific changes in brain white matter on diffusion tensor imaging after sports-related concussion', *Magnetic Resonance Imaging*. Elsevier Inc., 30(2), pp. 171–180. doi: 10.1016/j.mri.2011.10.001.

Beckwith, J. G. *et al.* (2013) 'Timing of Concussion Diagnosis Is Related to Head Impact Exposure Prior to Injury.', *Medicine and science in sports and exercise*, 45(4), pp. 747–754. doi: 10.1249/MSS.0b013e3182793067.

Beckwith, J. G. *et al.* (2018) 'Estimated Brain Tissue Response Following Impacts Associated With and Without Diagnosed Concussion', *Annals of Biomedical Engineering*. Springer US, 46(6), pp. 819–830. doi: 10.1007/s10439-018-1999-5.

Beckwith, J. G., Greenwald, R. M. and Chu, J. J. (2012) 'Measuring Head Kinematics in Football: Correlation Between the Head', *Bone*, 40(1), pp. 237–248. doi: 10.1007/s10439-011-

0422-2.

Belytschko, T. *et al.* (1984) 'Hourglass control in linear and nonlinear problems', *Computer Methods in Applied Mechanics and Engineering*, 43(3), pp. 251–276.

Belytschko, T. and Bindeman, L. P. (1993) 'Assumed strain stabilization of the eight node hexahedral element', *Computer Methods in Applied Mechanics and Engineering*, 105(2), pp. 225–260.

Belytschko, T. and Tsay, C. (1983) 'A stabilization procedure for the quadrilateral plate element with one-point quadrature', *International Journal of Numerical Methods in Engineering*, 19(3), pp. 405–419. doi: <https://doi.org/10.1002/nme.1620190308>.

Bian, K. and Mao, H. (2020) 'Mechanisms and variances of rotation-induced brain injury: a parametric investigation between head kinematics and brain strain', *Biomechanics and Modeling in Mechanobiology*. Springer, pp. 1–19. doi: 10.1007/s10237-020-01341-4.

Bland, M. L. *et al.* (2020) 'Development of the STAR Evaluation System for Assessing Bicycle Helmet Protective Performance', *Annals of Biomedical Engineering*. Springer, 48(1), pp. 47–57. doi: 10.1007/s10439-019-02330-0.

Bonet, J. and Burton, A. J. (1998) 'A simple average nodal pressure tetrahedral element for incompressible and nearly incompressible dynamic explicit applications', *Communications in Numerical Methods in Engineering*, 14(5), pp. 437–449. doi: 10.1002/(SICI)1099-0887(199805)14:5<437::AID-CNM162>3.0.CO;2-W.

Bottlang, M. *et al.* (2020) 'Impact Performance Comparison of Advanced Bicycle Helmets with Dedicated Rotation-Damping Systems', *Annals of Biomedical Engineering*. Springer, 48(1), pp. 68–78. doi: 10.1007/s10439-019-02328-8.

Boyd, S. K. and Müller, R. (2006) 'Smooth surface meshing for automated finite element model generation from 3D image data', *Journal of Biomechanics*, 39(7), pp. 1287–1295. doi: 10.1016/j.jbiomech.2005.03.006.

Bradshaw, D. and Morfey, C. (2001) 'Pressure and shear response in brain injury models', *Proceedings of the 17th International Technical Conference on the Enhanced Safety of Vehicles*, pp. 1–10.

Broglio, S. *et al.* (2017) 'Head Impact Density: A Model to Explain the Elusive Concussion Threshold', *J Neurotrauma*. doi: doi: 10.1089/neu.2016.4767.

Cai, Y. *et al.* (2018) 'Concussion classification via deep learning using whole-brain white matter fiber strains', *PLoS ONE*, 13(5), pp. 1–21. doi: 10.1371/journal.pone.0197992.

Camarillo, D. B. *et al.* (2013) 'An instrumented mouthguard for measuring linear and angular head impact kinematics in american football', *Annals of Biomedical Engineering*, 41(9), pp. 1939–1949. doi: 10.1007/s10439-013-0801-y.

Cassidy, J. D. *et al.* (2004) 'Incidence, risk factors and prevention of mild traumatic brain injury: results of the WHO Collaborating Centre Task Force on Mild Traumatic Brain Injury.', *J Rehabil Med* 43, 43, pp. 28–60.

CDC (2015) *Report to Congress on Traumatic Brain Injury in the United States: Epidemiology and Rehabilitation*. doi: 10.1161/HYPERTENSIONAHA.111.186106.

Chan, D. *et al.* (2018) 'Statistical characterization of human brain deformation during mild angular acceleration measured in vivo by tagged MRI', *Journal of biomechanical engineering*, 140(October), pp. 1–13. doi: doi:10.1115/1.4040230.

Chen, Y.-W. and Lin, C.-J. (2006) 'Combining SVMs with various feature selection strategies.',

in *Feature extraction*, pp. 315–324.

Chen, Y. and Ostoja-Starzewski, M. (2010) 'MRI-based finite element modeling of head trauma: Spherically focusing shear waves', *Acta Mechanica*, 213(1–2), pp. 155–167. doi: 10.1007/s00707-009-0274-0.

Chiara Giordano, S. K. (2014) 'Evaluation of Axonal Strain as a Predictor for Mild Traumatic Brain Injuries Using Finite Element Modeling', *Stapp Car Crash J.*, 58, p. 33.

Chong, S. L. *et al.* (2015) 'Predictive modeling in pediatric traumatic brain injury using machine learning Data analysis, statistics and modelling', *BMC Medical Research Methodology*, 15(1), pp. 1–9. doi: 10.1186/s12874-015-0015-0.

Clark, J. M. *et al.* (2018) 'Comparison of ice hockey goaltender helmets for concussion type impacts.', *Ann. Biomed. Eng.* Springer New York LLC, 46(7), pp. 986–1000. doi: 10.1007/s10439-018-2017-7.

Cortes, C. and Vapnik, V. (1995) 'Support-Vector Networks', *Machine Learning*, 20(3), pp. 273–297. doi: 10.1111/j.1747-0285.2009.00840.x.

Davenport, E. M. *et al.* (2014) 'Abnormal white matter integrity related to head impact exposure in a season of high school varsity football', *Journal of neurotrauma*.

Dewan, M. C. *et al.* (2019) 'Estimating the global incidence of traumatic brain injury', *Journal of Neurosurgery*. American Association of Neurological Surgeons, 130(4), pp. 1080–1097. doi: 10.3171/2017.10.JNS17352.

DiGiacomo, G., Tsai, S. and Bottlang, M. (2021) 'Impact Performance Comparison of Advanced Snow Sport Helmets with Dedicated Rotation-Damping Systems', *Annals of Biomedical Engineering*. Springer, pp. 1–9. doi: 10.1007/s10439-021-02723-0.

Van Dommelen, J. A. W., Hrapko, M. and Peters, G. W. M. (2010) *Neural Tissue Biomechanics, Studies in Mechanobiology, Tissue Engineering and Biomaterials*. doi: 10.1007/978-3-642-32563-2.

Dompier, T. P. *et al.* (2015) 'Incidence of concussion during practice and games in youth, high school, and collegiate American football players', *JAMA Pediatrics*, 169(7), pp. 659–665. doi: 10.1001/jamapediatrics.2015.0210.

Fahlstedt, M. *et al.* (2021) 'Ranking and Rating Bicycle Helmet Safety Performance in Oblique Impacts Using Eight Different Brain Injury Models', *Annals of Biomedical Engineering*. Springer, pp. 1–13. doi: 10.1007/s10439-020-02703-w.

Faul, M. *et al.* (2004) 'Traumatic Brain Injury in the United States: Emergency Department Visits, Hospitalizations, and Deaths.', *Atlanta, GA: Centers for Disease Control and Prevention, National Center for Injury Prevention and Control*.

Faul, M., Xu, L. and Coronado, V. G. (2010) *Traumatic Brain Injury in the United States: Emergency Department Visits, Hospitalizations, and Deaths*. Atlanta, GA.

Fernandes, F. A. O. *et al.* (2018) 'Development and validation of a new finite element human head model: Yet another head model (YEAHM)'. doi: <http://dx.doi.org/10.1108/MRR-09-2015-0216>.

Flanagan, D. P. and Belytschko, T. (1981) 'A uniform strain hexahedron and quadrilateral with orthogonal hourglass control'.

Franklyn, M. *et al.* (2005) 'Analysis of finite element models for head injury investigation: reconstruction of four real-world impacts.', *Stapp car crash journal*, 49(November), pp. 1–32.

Gabler, L. F. *et al.* (2018) 'Development of a Single-Degree-of-Freedom Mechanical Model for

Predicting Strain-Based Brain Injury Responses', *Journal of Biomechanical Engineering*.

American Society of Mechanical Engineers, 140(3), p. 031002. doi: 10.1115/1.4038357.

Gabler, Lee F, Crandall, J. R. and Panzer, M. B. (2018) 'Development of a Metric for Predicting Brain Strain Responses Using Head Kinematics', *Annals of Biomedical Engineering*. doi: 10.1007/s10439-018-2015-9.

Gabler, Lee F., Crandall, J. R. and Panzer, M. B. (2018) 'Development of a Second-Order System for Rapid Estimation of Maximum Brain Strain', *Annals of Biomedical Engineering*. doi: 10.1007/s10439-018-02179-9.

Gadd, C. (1966) 'Use of a weighted impulse criterion for estimating injury hazard', in *10th Stapp Car Crash Conference*. Minneapolis, NM, p. SAE paper 660793.

Ganpule, S. *et al.* (2017) 'A Three-Dimensional Computational Human Head Model That Captures Live Human Brain Dynamics', *Journal of Neurotrauma*, 34(13), pp. 2154–2166. doi: 10.1089/neu.2016.4744.

Gareth, J. *et al.* (2013) *An introduction to statistical learning*. New York: springer.

Garimella, H. T. and Kraft, R. H. (2017) 'Modeling the mechanics of axonal fiber tracts using the embedded finite element method', *International Journal for Numerical Methods in Biomedical Engineering*, 33(5), pp. 26–35. doi: 10.1002/cnm.2823.

Ghajari, M., Hellyer, P. J. and Sharp, D. J. (2017) 'Computational modelling of traumatic brain injury predicts the location of chronic traumatic encephalopathy pathology', *Brain*, 140(2), pp. 333–343. doi: 10.1093/brain/aww317.

Ghazi, K. *et al.* (2020) 'Instantaneous Whole-Brain Strain Estimation in Dynamic Head Impact', *Journal of Neurotrauma*, 13, p. in press. doi: 10.1089/neu.2020.7281.

Giordano, C. and Kleiven, S. (2016) 'Development of an Unbiased Validation Protocol to Assess the Biofidelity of Finite Element Head Models used in Prediction of Traumatic Brain Injury', *Stapp car crash journal*, 60, pp. 363–471.

Giudice, J. S. *et al.* (2019) 'An Analytical Review of the Numerical Methods used for Finite Element Modeling of Traumatic Brain Injury', *Annals of Biomedical Engineering*, pp. 1–18. doi: 10.1007/s10439-018-02161-5.

Graham, R. *et al.* (2014) *Sports-Related Concussions in Youth*, *Jama*. doi: 10.1001/jama.2013.282985.

Greenwald, R. M. *et al.* (2008) 'Head Impact Severity Measures for Evaluating Mild Traumatic Brain Injury Risk Exposure', *Neurosurgery*, 62(4), pp. 789–798. doi: 10.1227/01.neu.0000318162.67472.ad.Head.

Gu, J. *et al.* (2018) 'Recent advances in convolutional neural networks', *Pattern Recognition*. Elsevier Ltd, 77, pp. 354–377. doi: 10.1016/j.patcog.2017.10.013.

Guettler, A. J. (2017) *Quantifying the Response of Relative Brain/Skull Motion to Rotational Input in the PMHS Head*. Virginia Polytechnic Institute and State University. Available at: [https://vtechworks.lib.vt.edu/bitstream/handle/10919/82400/Guettler\\_AJ\\_T\\_2018.pdf?sequence=1](https://vtechworks.lib.vt.edu/bitstream/handle/10919/82400/Guettler_AJ_T_2018.pdf?sequence=1).

Guettler, A. J. *et al.* (2018) 'Kinematics Response of the PMHS Brain to Rotational Loading of the Head: Development of Experimental Methods and Analysis of Preliminary Data', in *SAE Technical Paper*, pp. 1–14. doi: <https://doi.org/10.4271/2018-01-0547>.

Guldberg, R. E., Hollister, S. J. and Charras, G. T. (1998) 'The Accuracy of Digital Image-Based Finite Element Models', *Journal of biomechanical engineering*, 120(2), p. 7. doi: 10.1115/1.2798314.

Günther, J. *et al.* (2014) 'First Steps Towards an Intelligent Laser Welding Architecture Using Deep Neural Networks and Reinforcement Learning', *Procedia Technology*. Elsevier B.V., 15, pp. 474–483. doi: 10.1016/j.protcy.2014.09.007.

Hallquist, J. O. (1986) *LS-DYNA theory manual*, *Studia Geographica (Brno)*. Livermore Softw. Technol. Corp. 3:25–31, 2006.

Hardy, W. N. *et al.* (2001) 'Investigation of Head Injury Mechanisms Using Neutral Density Technology and High-Speed Biplanar X-ray', *Stapp Car Crash Journal*, 45(November), pp. 337–368. doi: 2001-22-0016 [pii].

Hardy, W. N. *et al.* (2007) 'A Study of the Response of the Human Cadaver Head to Impact', *Stapp car crash journal*, 51(October), pp. 17–80. doi: 10.1016/j.bbi.2008.05.010.

Hardy, W. N. (2007) 'Response of the human cadaver head to impact', p. 281. Available at: [http://books.google.at/books?id=v9\\_K2fLIBCcC%5Cnhttp://books.google.at/books?id=v9\\_K2fLIBCcC&pg=PA56&lpg=PA56&dq=Entran+EPB-B02-500P+hermetically+sealed+pressure+transducers&source=bl&ots=Dk6mO1HQ53&sig=ufBarxDaWj88mQCCh6c0E\\_MqzDg&hl=de&sa=X&ei=35ZCT6uiEJ](http://books.google.at/books?id=v9_K2fLIBCcC%5Cnhttp://books.google.at/books?id=v9_K2fLIBCcC&pg=PA56&lpg=PA56&dq=Entran+EPB-B02-500P+hermetically+sealed+pressure+transducers&source=bl&ots=Dk6mO1HQ53&sig=ufBarxDaWj88mQCCh6c0E_MqzDg&hl=de&sa=X&ei=35ZCT6uiEJ).

Hastie, T., Tibshirani, R. and Friedman, J. (2017) *The Elements of Statistical Learning*. Available at: <https://web.stanford.edu/~hastie/Papers/ESLII.pdf>.

Hernandez, F. *et al.* (2015) 'Six Degree-of-Freedom Measurements of Human Mild Traumatic Brain Injury', *Annals of Biomedical Engineering*, 43(8), pp. 1918–1934. doi: 10.1007/s10439-014-1212-4.

Hideyuki, K. *et al.* (2006) 'Investigation of Anteroposterior Head-Neck Responses during Severe Frontal Impacts Using a Brain-Spinal Cord Complex FE Model', *Stapp Car Crash J.*, 50, p. 398.

Ho, J., Von Holst, H. and Kleiven, S. (2009) 'Automatic generation and validation of patient-specific finite element head models suitable for crashworthiness analysis', *International Journal of Crashworthiness*, 14(6), pp. 555–563. doi: 10.1080/13588260902895708.

Høye, A. (2018) 'Bicycle helmets – To wear or not to wear? A meta-analysis of the effects of bicycle helmets on injuries', *Accident Analysis and Prevention*. Elsevier Ltd, 117, pp. 85–97. doi: 10.1016/j.aap.2018.03.026.

Hubel, D. H. and Wiesel, T. N. (1968) 'Receptive fields and functional architecture of monkey striate cortex', *The Journal of Physiology*, 195(1), pp. 215–243. doi: 10.1113/jphysiol.1968.sp008455.

Hughes, T. J. R. (2012) *The finite element method: linear static and dynamic finite element analysis*. Courier Corporation.

J. O. Hallquist (2007) *LS-DYNA Keyword User's Manual*, Livermore Software Technology Corporation.

Ji, S., Zhao, W., et al. (2014) 'Head impact accelerations for brain strain-related responses in contact sports: a model-based investigation', *Biomechanics and Modeling in Mechanobiology*, 13(5), pp. 1121–1136. doi: 10.1007/s10237-014-0562-z.

Ji, S., Ghadyani, H., et al. (2014) 'Parametric comparisons of intracranial mechanical responses from three validated finite element models of the human head', *Annals of Biomedical Engineering*, 42(1), pp. 11–24. doi: 10.1007/s10439-013-0907-2.

Ji, S. et al. (2015a) 'Group-Wise Evaluation and Comparison of White Matter Fiber Strain and Maximum Principal Strain in Sports-Related Concussion', *Journal of Neurotrauma*, 32(7), pp. 441–454. doi: 10.1089/neu.2013.3268.

Ji, S. *et al.* (2015b) 'Group-Wise Evaluation and Comparison of White Matter Fiber Strain and Maximum Principal Strain in Sports-Related Concussion', *Journal of Neurotrauma*, 32(7), pp. 441–454. doi: 10.1089/neu.2013.3268.

Ji, S. and Zhao, W. (2015) 'A Pre-computed Brain Response Atlas for Instantaneous Strain Estimation in Contact Sports', *Annals of Biomedical Engineering*, 43(8), pp. 1877–1895. doi: 10.1007/s10439-014-1193-3.

Jin, X. *et al.* (2013) 'Development of a Finite Element Human Head Model Partially Validated With Thirty Five Experimental Cases', *Journal of Biomechanical Engineering*, 135(11), p. 111002. doi: 10.1115/1.4025101.

Karton, C., Hoshizaki, T. B. and Gilchrist, M. D. (2020) 'A novel repetitive head impact exposure measurement tool differentiates player position in national football League', *Scientific Reports*, pp. 1–14. doi: 10.1038/s41598-019-54874-9.

Kimpara, H. and Iwamoto, M. (2012) 'Mild traumatic brain injury predictors based on angular accelerations during impacts', *Annals of Biomedical Engineering*, 40(1), pp. 114–126. doi: 10.1007/s10439-011-0414-2.

King, A. I. *et al.* (2003) 'Is head injury caused by linear or angular acceleration?', *Proceedings of the International Research Conference on the Biomechanics of Impacts (IRCOBI)*, (September), pp. 1–12.

Kleiven, S. (2007) 'Predictors for traumatic brain injuries evaluated through accident reconstructions', *Stapp Car Crash Journal*, 51(November 2007), pp. 81–114. doi: 2007-22-0003 [pii].

Kleiven, S. and Von Holst, H. (2002) 'Consequences of head size following trauma to the human head', *Journal of Biomechanics*, 35(2), pp. 153–160. doi: 10.1016/S0021-

9290(01)00202-0.

Knutsen, A. K. *et al.* (2014) 'Improved measurement of brain deformation during mild head acceleration using a novel tagged MRI sequence', *Journal of Biomechanics*. Elsevier, 47(14), pp. 3475–3481. doi: 10.1016/j.jbiomech.2014.09.010.

Koerte, I. K. *et al.* (2015) 'A review of neuroimaging findings in repetitive brain trauma', *Brain Pathology*, 25(3), pp. 318–349. doi: 10.1111/bpa.12249.

Kutcher, J. S. and Giza, C. C. (2014) 'Sports concussion diagnosis and management', *CONTINUUM Lifelong Learning in Neurology*, 20(December), pp. 1552–1569. doi: 10.1212/01.CON.0000458974.78766.58.

Laksari, K. *et al.* (2020a) 'Multi-Directional Dynamic Model for Traumatic Brain Injury Detection', *Journal of Neurotrauma*. Mary Ann Liebert Inc, 37(7), pp. 982–993. doi: 10.1089/neu.2018.6340.

Laksari, K. *et al.* (2020b) 'Multi-Directional Dynamic Model for Traumatic Brain Injury Detection', *Journal of Neurotrauma*. Mary Ann Liebert Inc., 37(7), pp. 982–993. doi: 10.1089/neu.2018.6340.

Lemmon, D. R. and Huston, R. L. (1994) 'Automobile hood/fender design optimization for improved pedestrian head impact protection', *20th Design Automation Conference Proceedings*, 69(2), pp. 569–577.

Levy, M. L. *et al.* (2004) 'Birth and Evolution of the Football Helmet', *Neurosurgery*. Oxford Academic, 55(3), pp. 656–662. doi: 10.1227/01.NEU.0000134599.01917.AA.

Li, X., Zhou, Z. and Kleiven, S. (2020) 'An anatomically accurate and personalizable head injury model: Significance of brain and white matter tract morphological variability on strain',

*Biomechanics and Modeling in Mechanobiology*. Springer, pp. 1–29. doi:

10.1101/2020.05.20.105635.

Libertiaux, V., Pascon, F. and Cescotto, S. (2011) 'Experimental verification of brain tissue incompressibility using digital image correlation', *Journal of the Mechanical Behavior of Biomedical Materials*. Elsevier Ltd, 4(7), pp. 1177–1185. doi: 10.1016/j.jmbbm.2011.03.028.

Liu, Y. *et al.* (2020) 'Validation and Comparison of Instrumented Mouthguards for Measuring Head Kinematics and Assessing Brain Deformation in Football Impacts', *Annals of Biomedical Engineering*. Springer, 48(11), pp. 2580–2598. doi: 10.1007/s10439-020-02629-3.

Lu, Y. C. *et al.* (2019) 'A 3D Computational Head Model Under Dynamic Head Rotation and Head Extension Validated Using Live Human Brain Data, Including the Falx and the Tentorium', *Annals of Biomedical Engineering*. Springer New York LLC, 47(9), pp. 1923–1940. doi:

10.1007/s10439-019-02226-z.

Madhukar, A. and Ostoja-Starzewski, M. (2019) 'Finite Element Methods in Human Head Impact Simulations: A Review', *Annals of Biomedical Engineering*. Springer US, pp. 1–23. doi:

10.1007/s10439-019-02205-4.

Mao, H., Zhang, L., *et al.* (2013) 'Development of a finite element human head model partially validated with thirty five experimental cases.', *Journal of biomechanical engineering*, 135(11), pp. 111002–15. doi: 10.1115/1.4025101.

Mao, H., Gao, H., *et al.* (2013) 'Development of high-quality hexahedral human brain meshes using feature-based multi-block approach', *Computer Methods in Biomechanics and Biomedical Engineering*, 16(3), pp. 271–279. doi: 10.1080/10255842.2011.617005.

Marjoux, D. *et al.* (2008) 'Head injury prediction capability of the HIC, HIP, SIMon and ULP criteria', *Accident Analysis and Prevention*, 40(3), pp. 1135–1148. doi:

10.1016/j.aap.2007.12.006.

Marques, M. *et al.* (2017) 'A brain impact stress analysis using advanced discretization meshless techniques', *Journal of Engineering in Medicine*, 232(3), pp. 257–270. doi: <https://doi.org/10.1177/0954411917751559>.

Masoomi, A. *et al.* (2020) 'Instance-wise Feature Grouping', *Nips*, (NeurIPS), pp. 1–13.

McCrea, M. *et al.* (2004) 'Unreported Concussion in High School Football Players: Implications for Prevention', *Clinical Journal of Sport Medicine*, 14(1), pp. p13-17. Available at: [https://journals.lww.com/cjsportsmed/Abstract/2004/01000/Unreported\\_Concussion\\_in\\_High\\_School\\_Football.3.aspx](https://journals.lww.com/cjsportsmed/Abstract/2004/01000/Unreported_Concussion_in_High_School_Football.3.aspx).

Meaney, D. F., Morrison, B. and Bass, C. R. (2014) 'The Mechanics of Traumatic Brain Injury: A Review of What We Know and What We Need to Know for Reducing Its Societal Burden', *Journal of biomechanical engineering*, 136(February). doi: 10.1115/1.4026364.

Miller, L. E. *et al.* (2020) 'Brain Strain: Computational Model-Based Metrics for Head Impact Exposure and Injury Correlation', *Annals of Biomedical Engineering*. Springer, pp. 1–14. doi: 10.1007/s10439-020-02685-9.

Miller, L. E., Urban, J. E. and Stitzel, J. D. (2016) 'Development and validation of an atlas-based finite element brain model', *Biomechanics and Modeling in Mechanobiology*. Springer Berlin Heidelberg, 15(5), pp. 1201–1214. doi: 10.1007/s10237-015-0754-1.

Mitchell, T. (1997) *Machine Learning*.

Mitra, J. *et al.* (2016) 'Statistical machine learning to identify traumatic brain injury (TBI) from structural disconnections of white matter networks', *NeuroImage*. Elsevier Inc., 129, pp. 247–259. doi: 10.1016/j.neuroimage.2016.01.056.

Montanino, A. and Kleiven, S. (2018) 'Utilizing a Structural Mechanics Approach to Assess the Primary Effects of Injury Loads Onto the Axon and Its Components', *Frontiers in Neurology*. *Frontiers*, 9, p. 643. doi: 10.3389/fneur.2018.00643.

Montenigro, P. H. *et al.* (2017) 'Cumulative Head Impact Exposure Predicts Later-Life Depression, Apathy, Executive Dysfunction, and Cognitive Impairment in Former High School and College Football Players', *Journal of Neurotrauma*, 13(2), pp. 0–55. doi: 10.1089/neu.2016.4413.

Nahum, A. M., Randall, S. and Ward, C. C. (1977) 'Intracranial Pressure Dynamics During Head Impact', *SAE Technical Paper*.

National Operating Committee on Standards for Athletic Equipment (2019) 'STANDARD PERFORMANCE SPECIFICATION FOR NEWLY MANUFACTURED BASEBALL / SOFTBALL BATTER ' S HELMETS NOCSAE DOC ( ND ) 022- 10m12', (May), pp. 6–11.

Panzer, M. B. *et al.* (2012) 'Development of a finite element model for blast brain injury and the effects of CSF cavitation', *Annals of Biomedical Engineering*, 40(7), pp. 1530–1544. doi: 10.1007/s10439-012-0519-2.

Panzer, M. B., Myers, B. S. and Bass, C. R. (2013) 'Mesh considerations for finite element blast modelling in biomechanics', *Computer Methods in Biomechanics and Biomedical Engineering*, 16(6), pp. 612–621. doi: 10.1080/10255842.2011.629615.

*Part 571, Standard No. 202a–Head restraints.* (2014).

Pellman, E. J. *et al.* (2003) 'Concussion in professional football: reconstruction of game impacts and injuries.', *Neurosurgery*, 53(4), pp. 799–814. doi: 10.1227/01.NEU.0000083559.68424.3F.

Post, A. and Hoshizaki, T. B. (2012) 'Mechanisms of brain impact injuries and their prediction: A

review', *Trauma*, 14(4), pp. 327–349. doi: 10.1177/1460408612446573.

Roache, P. (1994) 'Perspective: A Method for Uniform Reporting of Grid Refinement Studies', *Journal of Fluids Engineering*, 116(3), pp. 405–413.

Rowson, B., Rowson, S. and Duma, S. M. (2015) 'Hockey STAR: A Methodology for Assessing the Biomechanical Performance of Hockey Helmets', *Annals of Biomedical Engineering*, 43(10), pp. 2429–2443. doi: 10.1007/s10439-015-1278-7.

Rowson, S. *et al.* (2009) 'Linear and angular head acceleration measurements in collegiate football.', *Journal of biomechanical engineering*, 131(6), p. 061016. doi: 10.1115/1.3130454.

Rowson, S. *et al.* (2012) 'Rotational head kinematics in football impacts: an injury risk function for concussion.', *Annals of biomedical engineering*, 40(1), pp. 1–13. doi: 10.1007/s10439-011-0392-4.

Rowson, S. and Duma, S. M. (2011) 'Development of the STAR evaluation system for football helmets: Integrating player head impact exposure and risk of concussion', *Annals of Biomedical Engineering*, 39(8), pp. 2130–2140. doi: 10.1007/s10439-011-0322-5.

Sabet, A. A. *et al.* (2008) 'Deformation of the human brain induced by mild angular head acceleration', *Journal of Biomechanics*, 41(2), pp. 307–315. doi: 10.1016/j.jbiomech.2007.09.016.

Sanchez, E. J. *et al.* (2018) 'A reanalysis of football impact reconstructions for head kinematics and finite element modeling', *Clinical Biomechanics*, (February). doi: 10.1016/j.clinbiomech.2018.02.019.

Scahill, R. I. *et al.* (2009) 'A Longitudinal Study of Brain Volume Changes in Normal Aging Using Serial Registered Magnetic Resonance Imaging', 60(July 2003).

Scott, G. G., Margulies, S. S. and Coats, B. (2016) 'Utilizing multiple scale models to improve predictions of extra-axial hemorrhage in the immature piglet', *Biomechanics and Modeling in Mechanobiology*. Springer Berlin Heidelberg, 15(5), pp. 1101–1119. doi: 10.1007/s10237-015-0747-0.

Smith, D. H., Meaney, D. F. and Shull, W. H. (2003) 'Diffuse axonal injury in head trauma', *Journal of Head Trauma Rehabilitation*, 18(4), pp. 307–16. doi: 00001199-200307000-00003 [pii].

Svein Kleiven (2002) 'Finite-element modeling of the human head'. Available at: <http://urn.kb.se/resolve?urn=urn:nbn:se:kth:diva-3347>.

Tadepalli, S. C., Erdemir, A. and Cavanagh, P. R. (2011) 'Comparison of hexahedral and tetrahedral elements in finite element analysis of the foot and footwear', *Journal of Biomechanics*. Elsevier, 44(12), pp. 2337–2343. doi: 10.1016/j.jbiomech.2011.05.006.

Takhounts, E. G. *et al.* (2004) 'On the Development of the SIMon Finite Element Head Model', *Stapp car crash journal*, 47, p. 385. doi: <https://doi.org/10.4271/2003-22-0007>.

Takhounts, E. G. *et al.* (2008) 'Investigation of Traumatic Brain Injuries Using the Next Generation of Simulated Injury Monitor (SIMon) Finite Element Head Model', *Stapp Car Crash J.*, 52, p. 403.

Takhounts, E. G. *et al.* (2013) 'Development of brain injury criteria (BrIC).', *Stapp car crash journal*, 57(November 2013), pp. 243–66. Available at: <http://www.ncbi.nlm.nih.gov/pubmed/24435734>.

Takhounts, E. G. G. *et al.* (2013) 'Development of Brain Injury Criteria (BrIC).', *Stapp car crash journal*, 57(November), pp. 243–66.

- Taubin, G. (2000) 'Geometric signal processing on polygonal meshes. In: Eurographics 2000-state-of-the-art report, Interlaken, Switzerland, 2000.', *Eurographics*, 33(2).
- Thomas R. Frieden, Debra Houry, G. B. (2015) 'Traumatic Brain Injury In the United States: Epidemiology and Rehabilitation', *Centers for Disease Control and Prevention (CDC)*, pp. 1–72. doi: 10.3171/2009.10.JNS091500.
- Trosseille, X. *et al.* (1992) 'Development of a F.E.M. of the Human Head According to a Specific Test Protocol', *SAE Technical Paper*.
- Tyson, A. M. and Rowson, S. (2018) *Varsity football helmet STAR protocol*.
- Urban, J. E. *et al.* (2013) 'Head impact exposure in youth football: High school ages 14 to 18 years and cumulative impact analysis', *Annals of Biomedical Engineering*, 41(12), pp. 2474–2487. doi: 10.1007/s10439-013-0861-z.
- Versace, J. (1971) 'A review of the severity index', in *15th Stapp Car Crash Conference*. Coronado, CA, USA, p. SAE paper 710881. doi: 10.4271/710881.
- Viano, D. C. *et al.* (2005) 'Concussion in professional football: Brain responses by finite element analysis: Part 9', *Neurosurgery*, 57(5), pp. 891–915. doi: 10.1227/01.NEU.0000186950.54075.3B.
- Virginia Tech Helmet Lab (2020) 'Varsity Football STAR Methodology'.
- Więckowski, Z. (2004) 'The material point method in large strain engineering problems', *Computer Methods in Applied Mechanics and Engineering*, 193(39-41 SPEC. ISS.), pp. 4417–4438. doi: 10.1016/j.cma.2004.01.035.
- Willinger, R. and Baumgartner, D. (2004) 'Numerical and physical modelling of the human head under impact - towards new injury criteria', *International Journal of Vehicle Design*, 32(1). doi:

<https://doi.org/10.1504/IJVD.2003.003239>.

Wu, Q. *et al.* (2018) 'Deep Learning Methods for Predicting Disease Status Using Genomic Data.', *Journal of biometrics & biostatistics*, 9(5). Available at: <http://www.ncbi.nlm.nih.gov/pubmed/31131151><http://www.pubmedcentral.nih.gov/articlerender.fcgi?artid=PMC6530791>.

Wu, S., Zhao, W., Rowson, B., *et al.* (2019) 'A network-based response feature matrix as a brain injury metric', *Biomech Model Mechanobiol*. Springer Berlin Heidelberg, (0123456789). doi: 10.1007/s10237-019-01261-y.

Wu, S., Zhao, W., Ghazi, K., *et al.* (2019) 'Convolutional neural network for efficient estimation of regional brain strains', *Scientific Reports*. Springer US, 9(1), pp. 1–11. doi: 10.1038/s41598-019-53551-1.

Wu, S. *et al.* (2020) 'A network-based response feature matrix as a brain injury metric', *Biomech Model Mechanobiol*, 19(3), pp. 927–942. doi: <https://doi.org/10.1007/s10237-019-01261-y>.

Yanaoka, T., Dokko, Y. and Takahashi, Y. (2015) 'Investigation on an Injury Criterion Related to Traumatic Brain Injury Primarily Induced by Head Rotation', *SAE Technical Paper*, pp. 2015-01–1439. doi: 10.4271/2015-01-1439. Copyright.

Yang, B. *et al.* (2014) 'Development of a Finite Element Head Model for the Study of Impact Head Injury', *BioMed Research International*, 2014, pp. 1–14. doi: 10.1155/2014/408278.

Yang, K. *et al.* (2011) 'Modeling of the Brain for Injury Prevention', in Bilston, L. E. (ed.) *Studies in Mechanobiology, Tissue Engineering and Biomaterials*. Springer-Verlag Berlin Heidelberg, pp. 69–120.

Yang, K. H. *et al.* (2006) 'Development of numerical models for injury biomechanics research: a

review of 50 years of publications in the Stapp Car Crash Conference', *Stapp Car Crash Journal*, 50, pp. 429–490. doi: 2006-22-0017 [pii].

Zeng, W. and Liu, G. R. (2018) 'Smoothed Finite Element Methods (S-FEM): An Overview and Recent Developments', *Archives of Computational Methods in Engineering*. Springer Netherlands, 25(2), pp. 397–435. doi: 10.1007/s11831-016-9202-3.

Zhan, X. *et al.* (2020) 'Deep Learning Head Model for Real-time Estimation of Entire Brain Deformation in Concussion', pp. 1–12. Available at: <http://arxiv.org/abs/2010.08527>.

Zhang, L., Yang, K. H. and King, A. I. (2004) 'A Proposed Injury Threshold for Mild Traumatic Brain Injury', *Journal of Biomechanical Engineering*, 126(2), p. 226. doi: 10.1115/1.1691446.

Zhao, W. *et al.* (2016) 'White Matter Injury Susceptibility via Fiber Strain Evaluation Using Whole-Brain Tractography', *Journal of Neurotrauma*, 33(20), pp. 1834–1847. doi: 10.1089/neu.2015.4239.

Zhao, W., Cai, Y., *et al.* (2017a) 'Injury prediction and vulnerability assessment using strain and susceptibility measures of the deep white matter', *Biomechanics and Modeling in Mechanobiology*. Springer Berlin Heidelberg, 16(5), pp. 1709–1727. doi: 10.1007/s10237-017-0915-5.

Zhao, W., Cai, Y., *et al.* (2017b) 'Injury prediction and vulnerability assessment using strain and susceptibility measures of the deep white matter', *Biomechanics and Modeling in Mechanobiology*. Springer Berlin Heidelberg, 16(5), pp. 1709–1727. doi: 10.1007/s10237-017-0915-5.

Zhao, W., Kuo, C., *et al.* (2017a) 'Performance evaluation of a pre-computed brain response atlas in dummy head impacts', *Annals of biomedical engineering*, 45(10), pp. 2437–2450. doi: DOI: 10.1007/s10439-017-1888-3.

Zhao, W., Kuo, C., *et al.* (2017b) 'Performance Evaluation of a Pre-computed Brain Response Atlas in Dummy Head Impacts', *Annals of Biomedical Engineering*, 45(10), pp. 2437–2450. doi: 10.1007/s10439-017-1888-3.

Zhao, W. *et al.* (2019) 'Regional Brain Injury Vulnerability in Football from Two Finite Element Models of the Human Head', in *IRCOBI*. Florence, Italy, pp. 619–621.

Zhao, W., Choate, B. and Ji, S. (2018) 'Material properties of the brain in injury-relevant conditions – Experiments and computational modeling', *Journal of the Mechanical Behavior of Biomedical Materials*. Elsevier Ltd, 80(February), pp. 222–234. doi: 10.1016/j.jmbbm.2018.02.005.

Zhao, W. and Ji, S. (2015) 'Parametric investigation of regional brain strain responses via a pre-computed atlas', *IRCOBI Conference*, (603), pp. 208–220.

Zhao, W. and Ji, S. (2017) 'Brain strain uncertainty due to shape variation in and simplification of head angular velocity profiles', *Biomechanics and Modeling in Mechanobiology*. Springer Berlin Heidelberg, 16(2), pp. 449–461. doi: 10.1007/s10237-016-0829-7.

Zhao, W. and Ji, S. (2018) 'White matter anisotropy for impact simulation and response sampling in traumatic brain injury', *J. Neurotrauma*, p. in press. doi: 10.1089/neu.2018.5634.

Zhao, W. and Ji, S. (2019a) 'Mesh Convergence Behavior and the Effect of Element Integration of a Human Head Injury Model', *Annals of Biomedical Engineering*, 47(2), pp. 475–486. doi: 10.1007/s10439-018-02159-z.

Zhao, W. and Ji, S. (2019b) 'Mesh convergence behavior and the effect of element integration of a human head injury model', *Annals of Biomedical Engineering*. Springer US, 47(2), pp. 475–486. doi: 10.1007/s10439-018-02159-z.

- Zhao, W. and Ji, S. (2019c) 'White matter anisotropy for impact simulation and response sampling in traumatic brain injury', *J. Neurotrauma*, 36(2), pp. 250–263. doi: 10.1089/neu.2018.5634.
- Zhao, W. and Ji, S. (2020a) 'Displacement- and Strain-Based Discrimination of Head Injury Models across a Wide Range of Blunt Conditions', *Annals of Biomedical Engineering*. doi: 10.1007/s10439-020-02496-y.
- Zhao, W. and Ji, S. (2020b) 'Displacement- and Strain-Based Discrimination of Head Injury Models across a Wide Range of Blunt Conditions', *Annals of Biomedical Engineering*, 48(6), pp. 1661–1677. doi: 10.1007/s10439-020-02496-y.
- Zhao, W. and Ji, S. (2020c) 'Incorporation of vasculature in a head injury model lowers local mechanical strains in dynamic impact', *J. Biomech.*
- Zhou, Z., Li, X. and Kleiven, S. (2018) 'Fluid–structure interaction simulation of the brain–skull interface for acute subdural haematoma prediction', *Biomechanics and Modeling in Mechanobiology*. Springer Berlin Heidelberg, pp. 1–19. doi: 10.1007/s10237-018-1074-z.
- Zhou, Z., Li, X. and Kleiven, S. (2019a) 'Biomechanics of Acute Subdural Hematoma in the Elderly: A Fluid-Structure Interaction Study', *Journal of Neurotrauma*, 36(13), pp. 2099–2108. doi: 10.1089/neu.2018.6143.
- Zhou, Z., Li, X. and Kleiven, S. (2019b) 'Biomechanics of periventricular injury', *J Neurotrauma*, pp. 1–41. doi: 10.1089/neu.2019.6634.
- Zhu, F., Gatti, D. L. and Yang, K. H. (2016) 'Nodal versus Total Axonal Strain and the Role of Cholesterol in Traumatic Brain Injury', *Journal of Neurotrauma*, 33(9), pp. 859–870. doi: 10.1089/neu.2015.4007.

